Technische Universität München
TUM Campus Straubing für Biotechnologie und Nachhaltigkeit

Development of enhanced site and infiltration assessment strategies: Augmenting Managed Aquifer Recharge to mitigate increasing groundwater scarcity

Rebecca Sultana

Vollständiger Abdruck der vom TUM Campus Straubing für Biotechnologie und Nachhaltigkeit der Technischen Universität München zur Erlangung einer

Doktorin der Naturwissenschaften (Dr. rer. nat)

genehmigten Dissertation.

Vorsitz: Prof. Dr. Henrike Niederholtmeyer

Prüfende der Dissertation:

1. Prof. Dr. Thomas Vienken
2. Prof. Dr. Florian Einsiedl

Die Dissertation wurde am 17.01.2024 bei der Technischen Universität München eingereicht und durch den TUM Campus Straubing für Biotechnologie und Nachhaltigkeit am 06.06.2024 angenommen.

Summary

Managed Aquifer Recharge (MAR) is a promising approach to replenish depleted aquifers, thus improving the water supply's security and responding to the impacts of climate change. Economic uncertainty, site-specific hydrogeological challenges, and land use conflict hinder MAR implementation. Hence, this research aims to promote the adoption of MAR by developing improved site and infiltration assessment techniques to address water scarcity.

To contribute to this goal, MAR site feasibility was evaluated by integrating adaptive site characterization to optimize infiltration rate estimation, leading to economically viable surface spreading methods. This approach, applied to a MAR site, combines high-resolution, cross-scale subsurface data. It enables a better understanding of the MAR sites located in fluvial deposits compared to conventional site investigation methods and offers alternative land use opportunities.

Furthermore, a novel MAR technique incorporating a subsurface irrigation system (SIS) was developed and assessed using numerical simulations and laboratory experiments to mitigate land use conflict. Nevertheless, the SIS implementation in line source arrangement demonstrated limited feasibility compared to the surface spreading method. Hence, SIS prototypes were designed to enhance the technology's competitiveness, followed by numerical modeling and field experiments to determine their technical efficiency. The results showed that SIS prototype infiltration was notably lower than trench infiltration, indicating a higher levelized cost. However, the diverse land use applications provided by SIS prototypes can compensate for the high levelized cost contributing to environmental sustainability.

In conclusion, this research has made a significant step towards amplifying the MAR uptake as a solution to water scarcity by integrating enhanced site characterization and infiltration assessment approach and simultaneously expanding the scope for multipurpose land utilization.

Zusammenfassung

Die künstliche Grundwasseranreicherung (Managed Aquifer Recharge - MAR) ist ein vielversprechender Ansatz zur Ertüchtigung überbeanspruchter Grundwasserleiter, um die Wasserversorgungssicherheit zu verbessern und auf die Herausforderungen des Klimawandels zu reagieren. Ökonomische Unsicherheiten, standortspezifische hydrogeologische Herausforderungen und Landnutzungskonflikte limitieren jedoch die Umsetzbarkeit von MAR. Das Ziel dieser Forschungsarbeit ist daher, die Verbreitung von MAR durch die Entwicklung verbesserter Methoden zur Standort- und Infiltrationsbewertung zu fördern und somit der voranschreitenden Wasserknappheit entgegenzuwirken.

Unter dieser Zielsetzung wurde eine adaptive Standortcharakterisierung in die Bewertung der Eignung von MAR-Standorten integriert, um präzise Abschätzungen der Infiltrationsrate und eine wirtschaftlich tragfähige Oberflächeninfiltration zu ermöglichen. Dieser Ansatz, angewendet auf einen MAR-Standort, kombiniert hochauflösende, skalenübergreifende Untergrunddaten. Dies ermöglicht ein verbessertes Verständnis von MAR-Standorten in Bereichen fluviatiler Ablagerungen gegenüber herkömmlichen Standortuntersuchungsmethoden und gleichzeitig alternative Landnutzungsmöglichkeiten.

Weiterhin wurde, aufbauend auf einem unterirdischen Bewässerungssystem (Subsurface Irrigation System-SIS), eine neue MAR-Methodik zur Vermeidung von Landnutzungskonflikten entwickelt und mittels numerischer Simulationen und Laborversuchen bewertet. Die Implementierung des SIS in einer Linienanordnung erwies sich jedoch im Vergleich zur Oberflächeninfiltration als nur begrenzt praktikabel. Daher wurden SIS-Prototypen entwickelt, um die Wettbewerbsfähigkeit zu verbessern. Die technische Effizienz dieser Prototypen wurde durch numerische Modellierungen und einen Feldversuch evaluiert. Die Ergebnisse zeigten eine deutlich geringere Infiltrationsleistung der SIS-Prototypen im Vergleich zur Grabeninfiltration und somit erhöhte Kosten. Die vielfältigen Landnutzungsmöglichkeiten der SIS-Prototypen können jedoch die höheren Kosten kompensieren und somit zur ökologischen Nachhaltigkeit beitragen.

Zusammenfassend stellt diese Forschungsarbeit einen Fortschritt für die breite Etablierung von MAR als Antwort auf die zunehmende Wasserknappheit dar, indem sie verbesserte Standortcharakterisierung und Infiltrationsbewertungsmethoden integriert und gleichzeitig den Raum für eine vielseitige Landnutzung erweitert.

Acknowledgment

As I write this acknowledgment, I feel grateful for the support I received during my PhD journey. Reflecting on my path from Bangladesh to Germany, I recognize that this experience has been transformative, and I am thankful for the people who have contributed to its accomplishment.

First, I thank my supervisors, Prof. Dr. Thomas Vienken and Dr. Ulrike Werban, for their tremendous mentoring, guidance, and kindness. Our meetings, which sometimes lasted for hours, often sparked my ideas. Prof. Thomas, your insightful feedback and guidance have been instrumental in molding my research endeavors. Dr. Ulrike, your support and advice in preparing the laboratory and field experiments at the UFZ and your encouragement in difficult times were invaluable. Both of your attention to details that I overlooked have made this thesis more worthwhile than I can remember.

I am thankful to my colleagues Maria Chiara, Nele, Carmen, Solveig, and Susan for all the moments we shared and the comfort when things did not go according to plan. The laboratory and field work, an integral part of my research work, would not have been possible without the enthusiastic participation of Julius, Marco, Andreas, Helko, Manuel, and Matteo. I also want to acknowledge Wasserversorgung Rheinhessen-Pfalz GmbH's support for conducting one of the significant field experiments of my research work.

I would like to extend my gratitude to my parents, who taught me the values of hard work and persistence and always had faith in my dreams despite them taking me thousands of miles away from home. I have nothing but admiration for my sister, Jhuma, for her endless encouragement. I thank Uncle Ahmed for inspiring me to dream bigger, work for it, and trust the Almighty to care for the rest. And to my friends Maha, Pritha, Baseerat, and Mehreen, who embraced me with open arms in Germany.

I sincerely appreciate the MARSoluT project for funding the research and giving me the invaluable opportunity to work with a remarkable group of young MAR researchers. This thesis is the result of all that interaction, support, shared moments, and kindness. Thank you all for being a part of my PhD tale.

Table of Contents

List of Figures

List of Tables

List of Abbreviations

2D	Two-dimensional
3D	Three-dimensional
% AF	Percentage area of fluorescence
ASR	Aquifer storage and recovery
ASTR	Aquifer storage transfer and recovery
bgl	Below ground level
BCs	Boundary conditions
CRF	Capital recovery factor
CV	Coefficient of variation
DPT	Direct push technique
DP EC	Direct push electrical conductivity
DP	Direct push
EC	Electrical conductivity
EMI	Electromagnetic induction
EC_a	Apparent electrical conductivity
FAO	Food and Agriculture Organization
FIA	Forest infiltration area
GDP	Gross domestic product
GWT	Ground water table
HPT	Hydraulic profiling tool
IBF	Induced bank filtration
K_s	Saturated hydraulic conductivity
LED	Light emitting diode
LCUs	Local currency units
MAR	Managed Aquifer Recharge
NAPL	Non-aqueous phase liquid
NPV	Net present value
OIP	Optical image profiler
O & M	Operation and maintenance

R^2	Coefficient of determination
RE	Richards Equation
RMSE	Root mean square error
RBF	River bank filtration
RWH	Rainwater Harvesting
SAT	Soil aquifer treatment
SIS	Subsurface irrigation system
TDR	Time domain reflectometry
UN	United Nations
US$	US dollars
WVR	Wasserversorgung Rheinhessen-Pfalz GmbH
VWC	Volumetric water content

1 Introduction

1.1 Water scarcity

Humanity faces many challenges today, including water scarcity, which is concerning because water resources have been severely stressed in recent decades. Water scarcity is the unavailability of sufficient amounts of water for both human and ecosystem demands (Bond et al., 2018; White, 2014). Rapid population growth, intensive agricultural and industrial activities, climate change, and high water demand are among the many causes of water scarcity (DeNicola et al., 2015; Petronici et al., 2019). According to Ritchie & Roser 2018, global freshwater consumption rose from 1.22 trillion cubic meters (m^3) in 1950 to 4 trillion m^3 in 2014 (Figure 1).

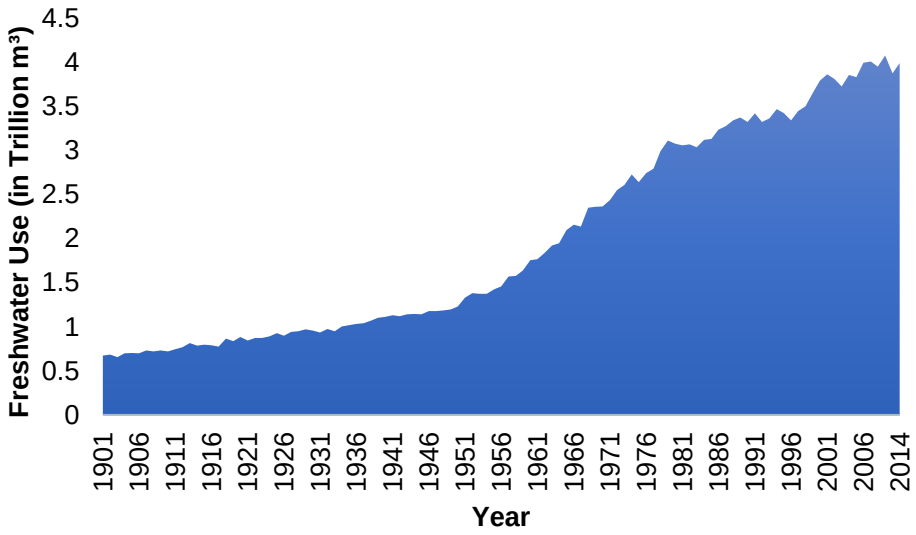

Figure 1 Worldwide freshwater consumption for domestic, agricultural, and industrial use (Modified from Ritchie and Roser, 2018).

Worldwide, residential, commercial, industrial, and agricultural water users are negatively affected by the current water scarcity (Mishra et al., 2021; Vollmer & Harrison, 2021), even though it is included in the UN 2030 Agenda for Sustainable Global Development (UN, 2015). Currently, an estimated 3.6 billion people, which is almost 50% of the world's population, live in areas where there is a risk of water scarcity for at least one month of

the year, and this number is expected to increase to around 4.8 to 5.7 billion by 2050 (UN-Water, 2018).

Groundwater is the second largest freshwater resource on earth (Swain et al., 2022), which plays a critical role in safeguarding human livelihoods and global food supplies by providing drinking water and supporting irrigated agricultural production (Mukherjee et al., 2021). Groundwater accounts for 49% of the water withdrawn globally for domestic use and around 25% of the water used for irrigation, benefiting 38% of the world's irrigated land (UN-Water, 2022). The annual per capita use of groundwater increased by 22.6 percent, from 124 m^3 in 1950 to 152 m^3 in 2021 (Loaiciga & Doh, 2023). Groundwater withdrawal during 2017 in different parts of the world was reported in the United Nations (UN) World Water Development Report 2022, shown in Figure 2.

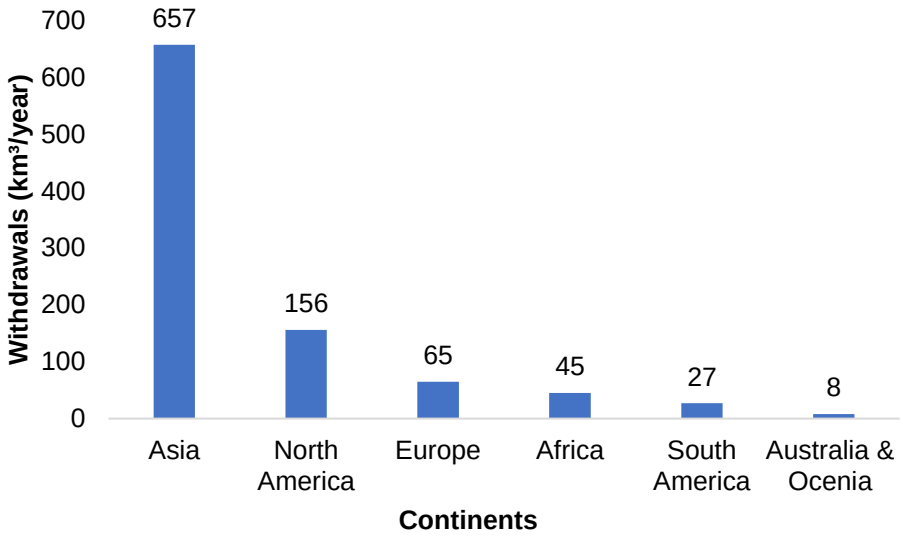

Figure 2 Groundwater abstraction in different continents in 2017 (UN-Water, 2022).

The total groundwater abstracted in 2017 was 959 cubic kilometers (km^3), of which 68.5% was withdrawn in Asia. North America ranked second with an extracted amount of 156 km^3. Despite Africa's 1.7 billion population, it only accounts for 4.7% of global groundwater withdrawals. Australia and Oceania also demonstrate minimal reliance on groundwater resources (UN-Water, 2022). Population and economic development in most Asian countries contribute to higher water abstraction and use, given that groundwater is a non-renewable resource in most locations. By 2030, water consumption

in Asian countries is anticipated to be double the amount currently in supply, which will significantly impact their development (Shan et al., 2020). It is also projected that worldwide groundwater abstraction will rise to 1530 km^3 by 2050, leading to a groundwater decline of 887 km^3. This prediction indicates that the undesirable effects of abstracted groundwater are likely to worsen, further exacerbated by climatic changes (Loaiciga & Doh, 2023).

The climate change effect will lead to rising temperatures, resulting in increased evapotranspiration. Combined with decreased rainfall, this will reduce groundwater recharge and increase water demand, negatively impacting sustainability (Mendieta-Mendoza et al., 2021). Portmann et al., 2013 examined how climate change will impact groundwater resources, mainly recharge. The study shows that by 2080, there will be a more than 10% reduction in global groundwater recharge from the baseline volume of 13,404 km^3. Furthermore, it is predicted that arid to semi-arid areas will encounter a 30% decrease in recharge in the forthcoming years. Also, the rise in temperature resulting from climate change will augment the water requirements for farming during the cultivation period (Peng et al., 2023). The Food and Agriculture Organization (FAO) has reported that water withdrawals for agricultural purposes will be 6% higher in 2050 compared to 2007 (Alexandratos & Bruinsma, 2012).

Excessive exploitation of groundwater systems can threaten water availability in the future if the groundwater pumping rate exceeds the aquifer recharge rate. One-third of the primary aquifer systems in the world are in distress, and this is an issue of global concern (Ingrao et al., 2023). According to economists, water shortage is a cost function, with higher water depletion rates indicating a higher price of obtaining or living without it (Zetland, 2021). The problems associated with groundwater are not confined to specific sectors, provinces, or national territories; they are a matter of humanitarian concern. Because of the complicated nature of aquifer systems and their growing significance as a primary water source, it is widely recognized that efficient, sustainable, and holistic groundwater management is crucial (Jakeman et al., 2016). Commonly, surface reservoirs are utilized to store water to combat water scarcity. However, they are susceptible to contamination, have high evaporation rates, require a large amount of land,

and naturally accumulate sediment (Maliva et al., 2006; Minsley et al., 2011). When water is abundant or low in demand, it can be stored in the subsurface for future consumption during water shortages instead of surface reservoirs (Minsley et al., 2011), and Managed Aquifer Recharge (MAR) is one such sustainable technology (Bouwer, 2002).

1.2 Managed Aquifer Recharge

MAR is an effective approach used in various conditions to replenish overexploited groundwater resources in stressed aquifers. This technique involves intentionally recharging aquifers from different sources, e.g., surface water, rainwater, storm runoff, and treated effluent (Bouwer, 2002; Dillon et al., 2009; Gale et al., 2002). It is most commonly used in conjunction with engineered treatment systems either as a pre-treatment before recharge or post-treatment after recovery. It relies on natural subsurface processes such as mechanical filtering, sorption, and biodegradation (Sprenger et al., 2017). It has the potential to contribute to the security of the water supply, address some of the consequences of climate change, and, in general, manage the groundwater quantity and quality (Casanova et al., 2016).

1.2.1 Managed Aquifer Recharge history and advancement

The extensive history of MAR is documented in various peer-reviewed documents explaining the MAR prototype and the experience gained from its implementation (Zhang et al., 2020). In China, during the period of the Warring States (475 to 221 BC), canals were constructed to allow surface water infiltration into the ground, thus improving the quality of the groundwater and reducing the salinity of the soil (Wang et al., 2014). Afterward, "Amunas," an infiltration canal (Gammie & Bievre, 2015), was used from 500 to 1000 AD by the pre-Incan Wari civilization in Peru (Akter, 2022). Then, in the 11th century, in Spain, “Careos”, a system of infiltration channels, was invented (Martín Civantos, 2010). In the 19th century, Europe's increasing population posed a significant challenge for water suppliers as industrialization progressed. The use of surface water as a traditional water supply was adversely affected by increasing contamination from emerging industries and insufficient sanitation. As a result, MAR became a viable solution between 1850 and 1950 (Zhang et al., 2020). After the Second World War, post-war

reconstruction and urbanization necessitated prioritizing water supply in quantity and quality. The practice of MAR was prevalent between 1950 and 1990 to fulfill the post-war requirement (Akter, 2022).

Since 1990, MAR has contributed to water conservation in both the developed and developing world, considering climatic change, rising population, and environmental and ecological demands. A 50-year study shows that MAR capacity grew from 1029 to 9945 Mm^3/year between 1965 and 2015 (Figure 3). In 1965, 15 countries had reliable data, and those 15 countries accounted for 34% of global groundwater use in 2010 (Dillon et al., 2019).

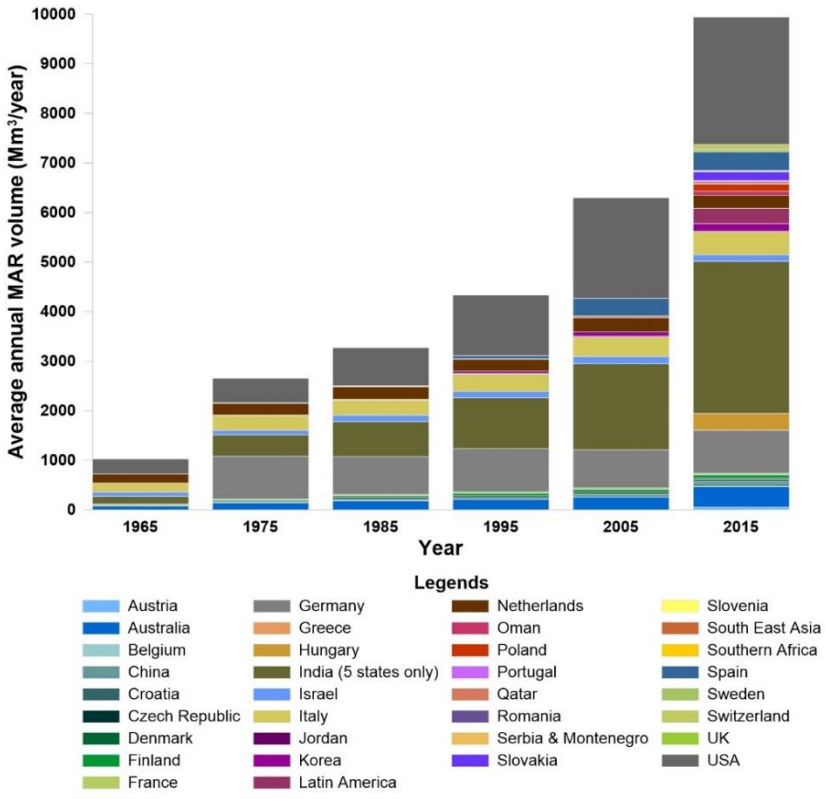

Figure 3 Average annual MAR volume in 15 countries from 1965 to 2015 (Modified from Dillon et al., 2019).

India and the USA account for the majority of the reported world's MAR capacity, with 31% and 26%, respectively. Germany is in third place with 9%, mainly using riverbank filtration (RBF) for municipal water supplies, which has been in application before the

1870s. Other European countries and Australia also make a modest contribution to the global capacity of MAR. The highest reported volumes of MAR occur in Asia, Europe, and North America, but MAR uptake within regions varies greatly. While India and the USA have a high level of groundwater consumption, this also applies to China, Latin America, and Southeast Asia, where the implementation of MAR is not yet well advanced, indicating enormous potential for the adoption of MAR in such countries for sustainable water resource management (Dillon et al., 2019). Developed countries in Europe, America, and other regions emphasized on the compilation of technical specifications from case studies. In contrast, developing countries such as India, South Africa, and China prioritized the planning and formulating of macro-strategies (Zhang et al., 2020). The evolution of MAR shows the emergence and expansion of the MAR initiative in different countries and highlights the possibilities for MAR application in several regions where it remains limited. Different types of MAR techniques applied in developing and developed countries for sustainable groundwater management are described below.

1.2.2 Managed Aquifer Recharge types

A MAR scheme can be developed by involving various techniques, e.g., surface spreading methods, in-channel modification, induced bank filtration (IBF), well, shaft, or borehole recharge; and rainwater and runoff harvesting (Bouwer, 2002; Ringleb et al., 2016; Russo et al., 2015).

The surface spreading method is considered the easiest and most commonly used method for MAR (Sprenger et al., 2017). It involves recharging an aquifer by distributing water over the land surface, usually on agricultural fields or infiltration basins where the water infiltrates through a permeable vadose zone into the unconfined aquifer (Figure 4a). Infiltration trenches, soil aquifer treatment (SAT), vegetated drained ditches, reservoir pavements, and recharge pits are also included in this category. Through this technique, water can be treated by the soil, which can remove pathogenic organisms and potentially harmful organic and inorganic compounds (Casanova et al., 2016). It is also possible to infiltrate large quantities of surface water at lower expenses. The disadvantage is that it requires a large area of unconfined aquifer for infiltration, which may only be available in some cases (IGRAC 2007).

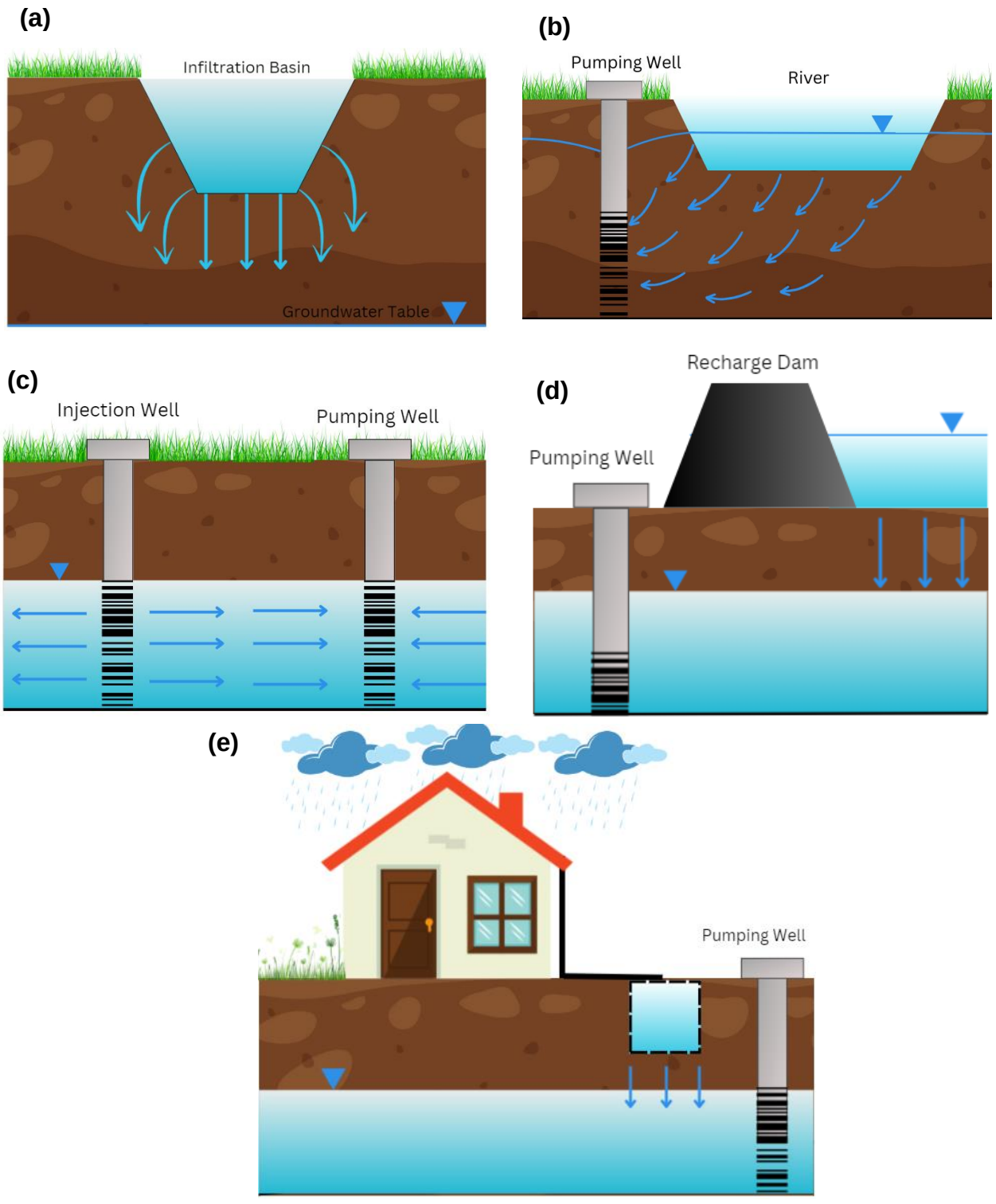

Figure 4 Managed Aquifer Recharge types: (a) Surface spreading method (b) Induced bank filtration (c) Well, shaft or borehole recharge (d) In-channel modification (e) Rainwater harvesting.

Induced bank filtration (IBF) is a technique where water is pumped from wells located near lakes, rivers, or catchments to infiltrate surface water (Figure 4b) (Hiscock & Grischek, 2002; Rossetto et al., 2020). This method reduces the need for expensive water treatment by treating surface water to remove turbidity, microbes, and chemicals. The amount of contamination that is removed depends on several factors, including the location of the wells, the source of the water, the pumping rate, etc. (Ray et al., 2011; Rossetto et al., 2020). European communities have had safe drinking water provided by these natural filtration systems for more than a century, while in the United States for more than fifty years (Ray et al., 2011).

Well, shaft and borehole recharge techniques include recharging directly into the aquifer, frequently overlain by low hydraulic conductivity strata (Figure 4c) (Sprenger et al., 2017). This technique allows deeper aquifers to retain recharge water by bypassing thick impermeable layers that are injected into parts of the aquifer that are more permeable (Murray & Tredoux, 1998). Several injection techniques exist, including Aquifer storage and recovery (ASR) and Aquifer storage transfer and recovery (ASTR) (Sprenger et al., 2017). Further information regarding different types of well injection techniques is provided by National Research Council, 1994; Pyne, 2005 and Zhang et al., 2020.

In-channel modifications aim to improve the aquifer recharge by modifying the streams, rivers, or canals to store water (Figure 4d). The goal is to improve groundwater recharge by storing flood events and releasing them slowly to allow for better infiltration into the subsurface. In-channel modifications are implemented primarily through the use of dams, which include sand storage dams, subsurface dams, recharge dams, and channel widening (Lasage et al., 2008; Mozzi et al., 2021; Standen et al., 2020).

When rainfall is adequate, groundwater supplies are inadequate, and surface water resources are scarce or inadequate, rainwater harvesting (RWH) offers a solution (Abdulla et al., 2021). Rainwater and runoff harvesting involve collecting rainwater and reserving it in deep pits where it can percolate and later be reused or recharged into the aquifer to replenish groundwater (Figure 4e). Natural filtration of rainwater to aquifers can

be enhanced by this process (Zhang et al., 2020). Collecting and storing rainwater in urban areas can reduce pressure on water supply systems (Parimalarenganayaki, 2021).

While there is a wide range of MAR techniques, surface infiltration has gained popularity for several reasons. Injection wells are effective for aquifer recharge. However, installation and maintenance costs are much higher (Mawer, 2014). Clogging is common in both well and surface infiltration systems but is costlier to remove from the well. Bouwer, 2002 emphasized on the requirement for higher water quality for well injection compared to surface infiltration, leading to complicated operation. The potential risk of dam failure causing significant damage downstream and its potential to cause surface water-related waterborne diseases raises concern about in-channel modification systems. While IBF has many advantages, it can also have some limitations, such as complicated design, construction, maintenance, and operation, high level of monitoring, and high risk of clogging the wells (IGRAC 2007). Moreover, short flow paths, high levels of heterogeneity, high hydraulic gradients, and associated high flow velocities can affect the effectiveness of RBF in removing microbial pollutants (Schijven & Berger, 2003).

The cost of constructing permanent RWH storage facilities is high, and water storage during long periods of drought is necessary due to the limited amount of rainwater available (Abdulla et al., 2021). In addition, semi-arid regions in developing countries may have a limited financial budget, which can be an obstacle to the implementation of MAR. Due to funding limitations, developing countries rely on a cost-effective MAR system, such as the surface spreading method, which requires minimal or no water treatment (Fathi et al., 2021; Seidl et al., 2024). Therefore, this research focuses on the surface spreading techniques for groundwater recharge. Despite the potential of MAR to alleviate water scarcity, its uptake still needs to be accelerated. In the following section, challenges associated with MAR implementation are discussed.

1.3 Managed Aquifer Recharge implementation challenges

Implementation of MAR sites may be hindered by a number of challenges, such as clogging, water contamination risks, appropriate site selection, determination of suitable MAR types based on hydrogeology, ensuring long-term finance, land acquisition,

groundwater resource modeling, socioeconomic challenges, and public acceptance (Ajjur & Baalousha, 2021; Alam et al., 2021; Zheng et al., 2023). The most relevant challenges are discussed in the following.

1.3.1 Economics of Managed Aquifer Recharge

The expenses involved in MAR projects are capital, operation, and maintenance costs. Capital costs are defined as fixed and one-time expenditures related to designing and constructing the MAR facility. Capital costs include land purchase, feasibility studies, testing expenses, consultancy fees for design, permitting and construction supervision, construction costs, and regulatory testing necessities involved in the installation and operational phases (Maliva, 2014). The operation and maintenance expenditures are the cost of maintaining and operating a MAR system. These costs are expressed in euros as a yearly and recurring cost (Maréchal et al., 2020).

As described in Ross & Hasnain, 2018, levelized cost estimates are typically employed for estimating MAR scheme costs. Levelized costs for a water supply project are calculated as a constant annual income required to cover all capital, operation, and maintenance costs over a project's lifetime, divided by the annual volume of water supplied. It offers an efficient way of comparing the cost of water from multiple projects (Dillon et al., 2009). Many hydrogeological, socioeconomic, legislative, and institutional factors influence the cost of MAR systems (Maréchal et al., 2020; Ross & Hasnain, 2018). The geology of the aquifer and the properties of the soil, for example, influence the rate of aquifer recharge and recovery. In contrast, socioeconomic circumstances influence both the availability and the price of labor and finance, and the regulatory framework determines the cost of establishing a project (Dillon et al., 2009; Ross & Hasnain, 2018).

Ross & Hasnain, 2018 investigated the factors affecting the cost of 21 MAR infrastructures in Australia, the United States, New Zealand, the Netherlands, and India. The presented data showed that surface spreading methods have lower costs for recharging per m^3 of water than recharge wells. The average cost of recharging natural water with an infiltration basin was 0.19 US$/$m^3$, compared to 1.46 US$/m^3 with recharge wells. Vanderzalm et al., 2022 also reported the cost of 10 MAR sites in Northern

Australia, which varied from 0.04 to 0.36 US$/$m^3$, and also highlighted the lower cost of schemes involving surface spreading methods.

Ross, 2021 presented another study in which he analyzed cost data from 24 MAR schemes in 18 countries, including capital and operation costs and levelized costs per cubic meter of recharged and recovered water. Using recycled water has a levelized cost of 0.75 US$/$m^3$, much higher than using natural water, 0.16 US$/$m^3$ for infiltration basins and wells, and 0.10 US$/$m^3$ for RBF. Tap water from selected large municipal water systems in the US costs between 2.68 US$/$m^3$ and 6.07 US$/$m^3$ (Statistica, 2021). Based on the cost data, it is evident that MAR can be a long-term solution for enhancing water resources in regions where conventional water sources present difficulties. People will use MAR water more often if they perceive that the costs involved in using it are affordable (Hasan et al., 2019).

The lack of economic analysis of MAR projects is one of the challenges associated with MAR implementation (Ajjur & Baalousha, 2021; Maliva, 2014; Palma Nava et al., 2022; Ross & Hasnain, 2018), and there are several reasons. In developing countries, MAR has potential that is both financially beneficial and would enhance people's quality of life, but it needs more financial support. In many cases, water sector development projects face competition for constrained budgets against other sectors, for example, health and transport, which also offer significant social benefits. Finances are incredibly scarce in impoverished regions of developing nations (Maliva, 2014). When assessing the viability of MAR systems, the emphasis tends to be on technical issues such as water suitability, infiltration rates, water mounding and movement, purification, and plant siting and specification (Brand, 2022). In addition, economic analysis of MAR projects requires a detailed assessment of costs and benefits, including the willingness to pay and socioeconomic risks of implementation (Halytsia et al., 2022). MAR has not been widely adopted because decision-makers, including water utility managers, officials of water management agencies, and political leaders, have yet to be presented with economically compelling and convincing arguments for investing in it (Maliva, 2014). In addition, perceived costs were identified as a significant barrier to consuming water derived from MAR compared to other sources (Hasan et al., 2019). It is essential to assess the

economic potential of a MAR facility before any investment is made in its development. A thorough economic assessment during the feasibility phase can contribute to the identification of the most promising alternative and provide vital information on optimizing the scheme size, phasing, and operation of the system (Brand, 2022).

1.3.2 Site suitability

A leading technical aspect that challenges MAR planning, execution, and operation is site suitability (Ajjur & Baalousha, 2021; Crites et al., 2006). Many factors must be considered to choose suitable sites for MAR that vary from area to area. Uncertainty in site hydrogeology is one of the factors hampering the implementation and operation of MAR in developing countries like Bangladesh (Ahmed et al., 2021). Unexpected hydrogeological conditions and site selection drawbacks contributed to MAR sites' failure or poor performance (Javadi et al., 2021; Maliva et al., 2006; Naik et al., 2017). In the Nile River basin, RBF facilities still need to meet their anticipated water delivery targets after being put into operation due to an insufficient understanding of hydrogeological properties (Ghodeif et al., 2016). Therefore, a critical aspect of sustainable MAR design and implementation is the proper knowledge of subsurface properties to optimize system design and performance considering the local hydrogeological conditions (Maliva et al., 2015).

Estimating infiltration rates and performance of MAR infrastructure is often done during the conceptual project phase using numerical models (Ringleb et al., 2016). Predicting the performance of the MAR system involves groundwater modeling, which relies on accurate model conceptualization and information on the hydraulic and transport characteristics of the aquifer (Maliva et al., 2015). MAR sites have been constructed mainly at sites with river water accessibility for recharging purposes (Alam et al., 2021; Standen et al., 2020). Hydraulic conductivity patterns are highly complex in alluvial or fluvial deposits due to their history of erosion and deposition (Dara et al., 2019). Collecting adequate hydrogeological data using conventional approaches to properly determine the alluvial aquifer’s spatial distribution and hydraulic conditions is often challenging, time-intensive, and costly (Vogelgesang et al., 2020). Thus, data for site characterization are obtained at a few selected points in many cases, which may need to provide information

regarding the variability of subsurface conditions representative of the entire investigated site (Binley et al., 2015; Kalbus et al., 2006). Since inadequate data are available to reliably represent subsurface heterogeneity (de Marsily et al., 2005; Koltermann & Gorelick, 1996) on a larger scale, numerical models often have to simplify or upscale heterogeneity (Maples et al., 2020), which makes it challenging to predict the performance of MAR schemes accurately.

During the operation of a basin or trench, it is usual to estimate infiltration rates ex-post based on water budgets or inflow measurements (Mastrocicco et al., 2016; Heilweil & Watt, 2011). More relevant for MAR is that characterization at greater depths is usually not practical with traditional techniques because a large volume of the vadose zone will be disturbed (Maliva, 2014). Additionally, the hydrogeological setting of the MAR site influences the MAR scheme cost (Ross & Hasnain, 2018; Vanderzalm et al., 2022). Different studies have demonstrated spatial variations in infiltration rates due to subsurface heterogeneity (Becker et al., 2013; Ganot et al., 2017; Medina et al., 2020; Racz et al., 2012; Uhlemann et al., 2022), yet these investigations have not addressed the contribution of site characterization to reduced MAR costs. Project managers have to make strategic decisions about the optimal budget allocation. They must decide which combination of tools and methods will produce the most relevant data within the available budget. Therefore, detailed hydrogeological characterization is required before constructing a full-scale MAR system (Maliva et al., 2016), which is fundamental for the MAR project's success (Seidl et al., 2024). Nevertheless, acquiring the spatial variation of data necessary for infiltration rate characterization continues to be a cost-intensive initiative, underscoring the necessity for a comprehensive approach. In this research, an advanced site characterization approach incorporating state-of-the-art techniques will demonstrate the achievement of this trade-off, resulting in relevant data for optimized MAR planning and design, thereby reducing costs.

1.3.3 Land use

MAR projects have been a source of conflict in terms of land use planning. MAR operations indirectly affect the allocation of resources by potentially restricting other land-use activities (Laukka et al., 2021). According to Ulibarri et al., 2021, California had 42

projects using agricultural land, including six on abandoned or fallowed farms; 30 were basin or injection wells that required land conversion. MAR infiltration basins are constructed on land dedicated to a specific application (Levintal et al., 2023). Surface infiltration requires more land than well recharge for recharge operations, and land availability often drives site selection (Parker et al., 2022). The basin construction and land costs incur a large part of the overall cost of the infiltration scheme. MAR infrastructures with lower costs receive land free from the local government, but schemes with higher costs incorporate the land expense (Ross & Hasnain, 2018). However, there are challenges associated with obtaining suitable land for MAR (Crites et al., 2006).

Limiting land use to MAR purposes only can lead to resistance from stakeholders, particularly farmers. Farmers may refuse to give up arable land for MAR initiatives (Walters, 2019). Concerns about ensuring sufficient compensation for lost agricultural potentials exacerbate this problem (Brunner et al., 2014). The difficulties of securing suitable land and the costs associated with land acquisition pose significant obstacles to adopting MAR approaches on a global scale, particularly in developing countries (Sasidharan et al., 2021).

Conversely, MAR has the potential to generate income when integrated with other land use options. One example is the Schiavon forest infiltration area (FIA) in the Veneto region of Italy. This particular site is intentionally forested to facilitate natural surface water infiltration. In addition to its primary purpose, this land can be used for many other purposes, such as producing woody biomass for renewable energy generation. In addition, planting trees as part of the system allows farmers to earn additional revenue from their land. These additional economic benefits contribute to the project's viability and sustainability (Filippi et al., 2016). Hence, optimization of MAR planning is essential to provide opportunities for potential land use to reduce cost and ensure the uptake of MAR. Developing innovative approaches to integrating MAR into existing land uses will be crucial in meeting this challenge.

1.4 Research objectives

The existing research indicates that reducing the MAR project costs is essential to ensure widespread MAR adoption. Further, addressing the uncertainties surrounding site conditions, which pose significant obstacles to planning, implementing, and operating MAR initiatives, is imperative. These uncertainties can significantly affect the selection of sites for MAR projects, which may result in poor performance and increase the associated expenses. Lastly, large-scale MAR efforts must consider activities like agriculture before the land is solely dedicated to MAR. Therefore, this research aims to promote MAR uptake by developing improved site and infiltration evaluation techniques in the context of the water scarcity challenge. To achieve this goal, three specific objectives have been formulated, which are in the following:

1. To develop an innovative methodology for evaluating MAR site suitability by incorporating adaptive site investigation technique enabling optimized infiltration rate assessment and cost-effective implementation of surface spreading techniques;
2. To develop and assess a novel MAR approach by employing a subsurface irrigation system (SIS) for diversified land use purposes;
3. To evaluate the performance and effectiveness of the developed SIS approach on a field scale for determining the competitiveness with the surface spreading method.

In order to achieve the first objective, a solution was demonstrated to the problem of the limited data availability in the early stages of MAR planning. The approach integrated adaptive site characterization with cross-scale exploratory techniques at multiple scales to identify the spatial variation of infiltration rates at a MAR site in Schiavon, Italy. This method improved data accessibility, thus providing multiple land use opportunities and reducing MAR planning uncertainty and costs.

The second objective was accomplished through a two-step process. Initially, numerical simulation was conducted to understand how the innovative MAR system operates with regard to water infiltration. The evaluation of the modeling results involved a comparison

of predicted soil moisture content data with the results obtained from a soil tank experiment. The aim of the laboratory experiment was to determine SIS's infiltration rate and moisture content distribution. Additionally, water percolation velocity was determined using an innovative tracing technique in this experiment. Finally, the effectiveness of the SIS in line source arrangement was evaluated based on the findings of the evaluated model.

The third objective involved designing the SIS prototypes for field application. The infiltration rates and wetting pattern distribution of the SIS prototypes were simulated using a numerical model, leading to the design of the field experiment. The goal of the field experiment was to evaluate the feasibility of this innovative MAR technique from both technical and economic perspectives in a study area in Guntersblum, Germany. Further, the technical and economic performance of the SIS prototypes were assessed to determine their competitiveness with the surface spreading method. This study will systematically address the methodologies applied to fulfill the research objectives in Section 2, followed by Sections 3, 4, and 5, presenting an overview of how these objectives were approached and detailed results.

2 Methodology

This chapter describes the basic principles of the methods encompassing field investigations, laboratory experiments, and numerical simulations applied throughout the research to achieve the objectives. Various techniques were applied across different scales, incorporating surface geophysics, direct push (DP) techniques, and soil sampling. In addition, this study also comprised hydraulic conductivity determination, infiltration rate estimation, and economic analysis.

2.1 Geophysical investigation

It has already been stated that the optimization of MAR site selection is constrained by the limited number of available subsurface data and the high cost of obtaining additional information through conventional direct techniques such as drilling. This issue is further complicated by the variable data scales and investigation depth required based on

specific MAR project features and subsurface properties. Surface spreading schemes, e.g., infiltration basins or trenches, can have a large project area and may require characterization of a larger site at greater depth (Parker et al., 2022).

Unlike boreholes, surface geophysics assesses the subsurface without generating physical disturbances and provides volumetric measurements (Demanet et al., 2001). This method allows large areas to be covered more rapidly than conventional drilling at a lower cost (Behroozmand et al., 2019; Parker et al., 2022). Geophysical surveys are helpful in the identification of locations to be strategically targeted for detailed investigation, thus eliminating the need for relatively expensive 'trial and error' drilling methods (Utom, 2019). Therefore, in this study, geophysical surveys were applied as a strategic and economical approach to identify the spatial variation of the subsurface by measuring the variations in the electrical conductivity (EC) of subsurface materials (McDowell et al., 2002).

The application of geophysical methods as a cost-effective means of sediment type characterization to implement MAR, including surface spreading technique, has gained importance over the past decade. In this research, an electromagnetic induction (EMI) survey was performed as the first step of an adaptive site investigation methodology to accomplish the first research objective. It is a method of determining soil apparent electrical conductivity (EC_a), which measures the cumulative relative contribution of the soil's bulk conductivity to a particular depth of distinct layers (Doolittle & Brevik, 2014). Most electromagnetic instruments consist of two coils: the transmitter and receiver coils (McNeill, 1980). The transmitter coil produces a primary electromagnetic field at a specific frequency (Figure 5). It induces electrical currents known as eddy currents in conductive materials in the subsurface. It results in the generation of a secondary magnetic field that the receiver coil detects. The receiver coil detects the induced secondary and primary fields (Nabighian & Macnae, 1991), which estimate EC_a (Doolittle & Brevik, 2014). EMI surveys are advantageous for measuring lateral variations in soil parameters at spatial scales because of their non-invasive and rapid operation (Saey et al., 2009).

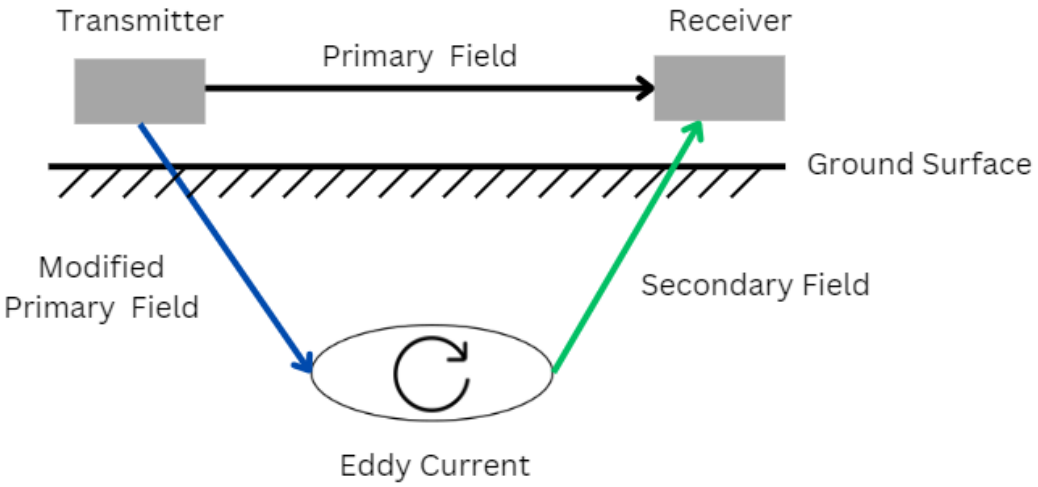

Figure 5 Electromagnetic Induction Survey Principle.

The measurement indicates the weighted integral of conductivity across a given depth as its sensitivity decreases with depth. The soil EC_a is determined by several parameters, including porosity, moisture content, soil temperature, dissolved electrolyte concentration, and colloid content (McNeill, 1980). Moisture and clay content are the primary drivers of soil conductivity in nonsaline soils (Kitchen et al., 1999). Different soil compositions have varying EC values. Soils with high salinity or clay content tend to have high EC_a values (Heil & Schmidhalter, 2012). Sand and gravel, on the other hand, have a low EC_a value. Although surface geophysics enables intermediate-scale characterization, providing the opportunity to resolve missing information between points (Briggs et al., 2016), the vertical resolution reduces with increasing depth (Dietrich & Leven, 2006). Since EC_a determined by the EMI surveys is a weighted average of the EC across the entire investigation depth (McNeill, 1980), obtaining high-resolution information on the vertical variation of subsurface characteristics is essential.

2.2 Direct push technologies

Direct push technique (DPT) is an essential tool for carrying out field investigations to obtain detailed information about the vertical composition of the subsurface and to overcome the constraints associated with surface geophysics (Dietrich & Leven, 2006). The primary objective was identifying clay layers at MAR sites that could impede water

infiltration. In recent years, DPT has become increasingly popular for subsurface exploration, providing centimeter-scale resolution information on subsurface conditions in the vertical direction (Figure 6). This method provides various advantages over conventional techniques, including faster advancement into the subsurface, cheaper costs, real-time inquiry, and minimum subsurface disturbance (Butler, 2002; Morgan, 1996). As a minimally invasive technique, this method provides depth-accurate in-situ information (Schmidt et al., 2019) in contrast to drilling techniques by avoiding soil compaction (Hausmann et al., 2018). However, DPT does not provide direct information on the abundance of clay. Instead, it indicates the presence of clay-rich material based on EC measurement. An increase in soil EC often correlates with the increased abundance of clay minerals (Vitharana et al., 2006).

Figure 6 Application of DPT in Guntersblum, Germany.

In this approach, steel rods are driven, shoved, or vibrated into the subsoil (EPA, 1997). Various probes attached to the rod string end can capture real-time hydrogeological,

hydrological, geophysical, chemical, and geotechnical data (Dietrich & Leven, 2006). DPT can also be used to install small-diameter groundwater monitoring wells. There are limitations and challenges involved with DP-based data acquired along one-dimensional vertical profiles. Lateral information is missing between two DP profiles, like conventional drilling. Combining geophysical surveys with DP techniques is thus beneficial for delineating complex subsurface features. Such a combination of methodologies offers significant potential for investigating scale-related problems in the heterogeneous subsurface (Utom, 2019), which is critical for MAR site planning. In addition to the usual field application of DPT, it was used in a laboratory experiment to determine water percolation velocity. The following sections detail various DP tools used in this research to determine high-resolution vertical profiles of subsurface conditions and water percolation velocity.

2.2.1 Direct push electrical conductivity logging

Direct push electrical conductivity (DP EC) logging is one of the most common DP applications to investigate sediment stratigraphy variation based on the EC (Schulmeister et al., 2003). We performed DP EC profiling using Geoprobe SC 500 probes configured in Wenner mode. The EC probe has a diameter of 3.8 cm. The DP EC probe has four-point electrodes with a spacing of 2 cm (Figure 7), generating high-resolution depth-relevant EC value (Schulmeister et al., 2003).

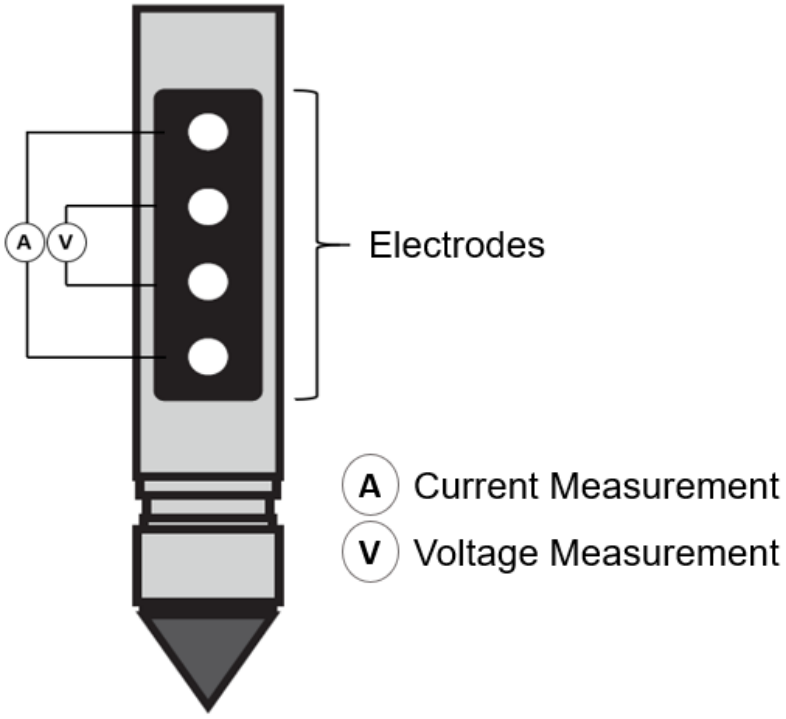

Figure 7 Schematic representation of DP EC probe.

This research employed DP EC to delineate the presence of thin confining layers that may impede water percolation through the vadose zone and, hence, groundwater recharge in the context of the MAR site investigation. Further information on DP EC profiling is provided by Beck et al., 2000 and Sellwood et al., 2005.

2.2.2 Optical image profiler

An optical image profiler (OIP) is utilized to detect non-aqueous phase liquid (NAPL) hydrocarbon fuels, oils, and tars in the subsurface (Geoprobe, 2019). It is hydraulically driven into the subsurface at 0.5 cm/sec speed (Verhegge & Delvoie, 2021). An OIP probe (model OP6560, Geoprobe Systems) has dimensions of approximately 52.71 cm long and about 5.08 cm in diameter. Its configuration incorporates a tapered square body design, which optimizes contact between the probe and the geological formation. It has an EC dipole array situated near the probe bottom, which measures the bulk EC of the soil, providing information regarding formation lithology (McCall et al., 2018), and an OIP unit located at the center of the probe (Figure 8).

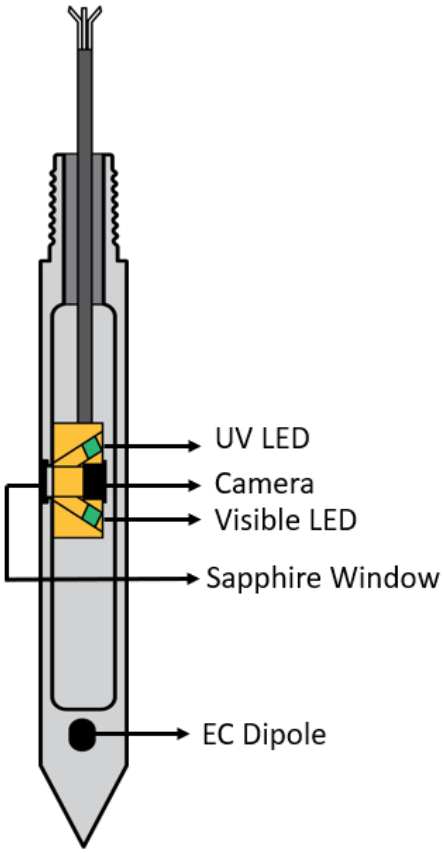

Figure 8 Schematic image of DP OIP probe.

The device involves two light sources for generating light – a UV light emitting diode (LED) that emits light with the wavelength required for inducing fluorescence and a secondary LED that emits visible or infrared light. Light illuminates the adjacent soil and liquids through a 0.2 cm thick sapphire window measuring 1.27 cm in diameter (Reischer et al., 2020). An internal camera captures the fluorescence generated by the UV light source. The images captured at every 1.5 cm interval are 0.9 cm × 0.75 cm. The area of fluorescence is then determined by analyzing the captured image. The percentage area of fluorescence (%AF) within the fluorescence image indicates the presence of NAPL hydrocarbon fuel, oil, or tar (Geoprobe, 2019). OIP is not only effective for the in-situ determination of hydrocarbon contamination in the soil, it has proved to be effective in detecting the presence of fluorescent tracers in soil (Reischer et al., 2020). This research utilizes the unique feature of OIP for accurately determining water percolation velocity by detecting uranine tracer in the unsaturated zone rather than the traditional use of OIP in the field.

2.2.3 Hydraulic profiling tool

The DP hydraulic profiling tool (HPT) is developed to investigate in situ variations in vertical hydraulic conductivity at a resolution of 1.5 cm in unconsolidated sediments (Zhao et al., 2023). The HPT probe has a maximum diameter of 4.45 cm and measures 54.61 cm long. With a diameter of about 0.77 cm, the HPT injection port is covered in stainless steel mesh (Figure 9). Water is injected into the formation at a regulated flow rate through the port during the advancement of the probe (McCall, 2011). The probe's design keeps the formation in good contact with the screen face, reducing the chance of clogging. The screened port can be replaced in the field. It is 40.64 cm above the probe's tip and prevents clogging (McCall & Christy, 2020). An HPT probe is driven into the ground at 2 cm/s speed, and a downhole transducer measures the pressure needed to inject water into the subsurface. In contrast, a flow controller placed at the surface measures the injection flow (McCall, 2011).

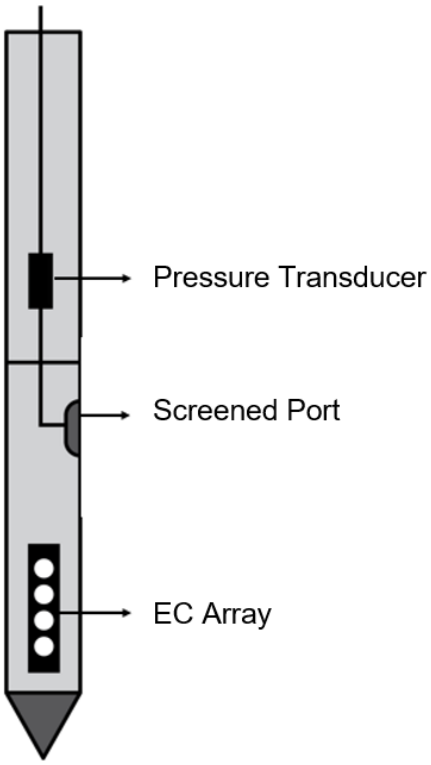

Figure 9 Schematic diagram of DP HPT.

Formation permeability can be assessed using this injection pressure log. HPT flow and pressure ratio changes indicate soil permeability and sediment variations, while low-pressure response indicates large grain sizes and high water transmission ability (McCall et al., 2014; McCall & Christy, 2020). An EC array is also included in the HPT probe for simultaneous measurements of EC in bulk formations (Figure 9). EC logs can provide valuable information about lithology in freshwater environments (Schulmeister et al., 2003). An increased EC often implies a decrease in permeability and an increase in clay content under nonsaline conditions.

While the log runs, the HPT pressure response, flow rate, and EC of the surrounding material are measured with depth and displayed on the computer screen (McCall et al., 2009). The combination of these three parameters can be a good indicator of hydrogeological properties. A single HPT-EC log can guide sampling, groundwater well installation location, or contaminant remediation activities based on the information regarding sediment type and permeability over depth. In general, a combination of HPT profiles in a transect or a grid can provide high-resolution hydrostratigraphy detail faster and at a lower cost than previously possible (McCall & Christy, 2020). HPT was used in this work to determine the feasibility of a potential MAR site by acquiring high-resolution K information, which subsequently assisted with the field installation of the innovative SIS approach in addressing the third research objective.

2.2.4 Soil sample collection

DP sampling instruments are designed to acquire soil samples from distinct depths without removing the topsoil. Samplers with varying diameters and lengths allow for volume sampling. In this technique, the probe is driven into the subsurface by the weight of the mobile platform to collect soil samples (Dietrich & Leven, 2006). DP soil samplers are classified as single-tube or dual-tube systems. Dual tube soil sampling devices are favored for soil sampling because the outer casing shields the borehole during operations. It is possible to conduct rapid continuous sampling above and below the water table using dual tube systems (ASTM, 2015). Soil samples are obtained using the DP technique for determining the saturated hydraulic conductivity (K_s) of soil, leading to the estimation of infiltration rates.

2.3 Saturated hydraulic conductivity measurement

Constant head permeameter tests were performed to determine the K_s of soil samples (Figure 10). K_s of the soil samples was determined using a KSAT device (METER Group AG, 2016). The measurement range of this device varies from 1.16×10^{-09} m/sec to 5.79×10^{-04} m/sec.

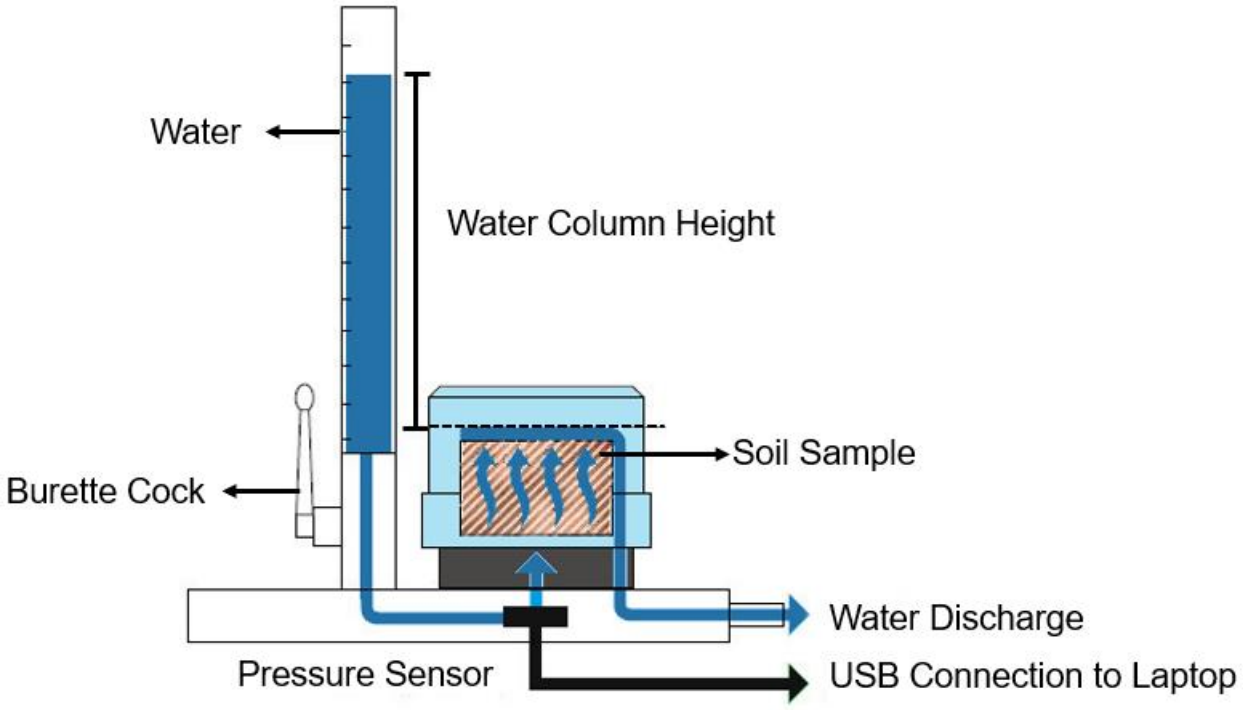

Figure 10 Schematic set-up of the experiment for K_s measurement (Modified from METER Group AG, 2016).

Each soil sample was homogenized and filled in the 250 cm^3 sample ring. Then, it was compacted and saturated with water. After saturating the soil sample, the assembly was mounted on the measurement device and fixed with a screwed cap. Once the burette cock was opened, water started flowing from it vertically upward through the sample. The burette's water level was higher than the water level of the outlet. Based on the pressure head change data recorded by the permeameter, the percolation velocity of water is automatically calculated based on this data. K_s was estimated using Darcy's law (Darcy, 1856).

$$q = \frac{Q}{A} = \frac{V}{At} = -K_s \frac{\Delta h}{\Delta z} \quad (1)$$

Where Q = flow through the soil sample, A = cross-sectional area of the soil sample, V= water volume, t = time, K_s= the saturated hydraulic conductivity (m/s), Δz = soil sample length, and Δh = difference of hydraulic head.

2.4 Laboratory analysis of sampling material and infiltration rate estimation

Following the constant head permeameter tests to determine the K_s, the infiltration rate was estimated using the following equation for a canal with a deep groundwater table in an isotropic homogeneous porous medium (Swamee et al., 2000).

$$q_i = K_s F_t \quad (2)$$

Where q_i = the infiltration rate per unit length of the trench (m^2/s), and F_t is the seepage function dependent on the geometry of the trench (dimensionless). For a trapezoidal channel, the seepage function can be expressed as:

$$F_t = [\{(4\pi - \pi^2)^{1.3} + (2m)^{1.3}\}^{\frac{0.77+0.462m}{1.3+0.6m}} + (\frac{b_w}{y_w})^{\frac{1+0.6m}{1.3+0.6m}}]^{\frac{1.3+0.6m}{1+0.6m}} \quad (3)$$

Where m = the side slope of the trench, b_w = the trench bottom width, and y_w = water level in the trench (m).

2.5 Numerical simulation for infiltration rates and wetting front distribution determination

MAR processes and operational plans can be assessed using modeling, such as scenario analysis and future prediction. Due to their flexibility, model-based preliminary assessments are frequently recommended prior to on-site pilot investigations (Ringleb et al., 2016). HYDRUS-2D/3D is an advanced modeling tool that offers both two-dimensional (2D) and three-dimensional (3D) simulation capabilities for analyzing the flow of water, heat, and solutes in porous media (Kandelous & Šimůnek, 2010; Šimůnek et al., 2016). It is widely used to determine the amount of recharge and discharge to and from

groundwater (Eltarabily et al., 2021), to evaluate infiltration rate and wetting pattern distribution of irrigation systems (Cai et al., 2019; Gupta et al., 2009; Kanda et al., 2020), to estimate recharge from cultivated croplands (Ganot & Dahlke, 2021; Post et al., 2022; Wang et al., 2021). Various soil types have been studied using this software to simulate hydrologic processes in the unsaturated zone, nutrient leaching, salinization, and plant growth (Bali et al., 2023). Thus, HYDRUS-2D/3D software was utilized in this study to simulate the infiltration rate and wetting pattern distribution of a novel MAR technique by using SIS in an unsaturated zone. The simulation results were utilized to determine the placement depth of SIS and location of the observation points for monitoring wetting pattern distribution in order to perform a soil tank experiment. It was also used for planning a field experiment that provided insights into the distribution of the wetting front of an advanced SIS prototype, thereby guiding the decision-making in determining the optimum excavation depth and interval between the prototypes.

In a porous medium, uniformly and variably saturated movement of water can be described by the Richards Equation (RE) (Richards, 2004), which is solved by HYDRUS-2D/3D numerically.

$$\frac{\partial \theta}{\partial t} = \frac{1}{r}\frac{\partial}{\partial r}\left(rK(h)\frac{\partial h}{\partial r}\right) + \frac{\partial}{\partial z}\left(k(h)\frac{\partial h}{\partial z}\right) + \frac{\partial k(h)}{\partial z} \quad (4)$$

Where θ represents volumetric water content (cm^3/cm^3); t is the time (hr); r is the radial axis and z is the vertical axis, K (h) is the unsaturated hydraulic conductivity (cm/hr); h is the soil water potential (cm).

The van Genuchten-Mualem constitutive relationships can be used to estimate the soil water retention curve as well as the unsaturated hydraulic conductivity function (Mualem, 1976; Van Genuchten, 1980).

$$\theta(h) = \begin{cases} \theta_r + \dfrac{\theta_s - \theta_r}{(1 + |\alpha h|^n)^m} & h < 0 \\ \theta_s & h \geq 0 \end{cases} \quad (5)$$

$$K(h) = K_s S_e^l [1 - (1 - S_e^{\frac{1}{m}})^m]^2 \quad (6)$$

$$S_e = \frac{\theta - \theta_r}{\theta_r - \theta_s}; m = 1 - \frac{1}{n} \quad (7)$$

Where θ_r = residual soil water content (cm^3/cm^3), θ_s = saturated soil water content (cm^3/cm^3); S_e = effective saturation; α, m, n, and l = empirical coefficients which influence the hydraulic functions shape parameters, and K_s = saturated hydraulic conductivity of soil (cm/hr).

2.6 Economic analysis

Financial cost data, including capital, operation, and maintenance (O & M) costs, were obtained for MAR sites in local currency units (LCUs). The capital and operating costs of the MAR system correspond to different periods. Therefore, to standardize the MAR project's declared capital and operation costs, they were multiplied by a gross domestic product (GDP) deflator, which tracks price fluctuations for all produced goods and services domestically, to express costs in LCUs valued at the year 2022. Afterward, capital and operation costs in LCU were converted to US dollars (US$) for standardization. MAR scheme operation life (n) of 30 years and a discount rate (r) of 3% was assumed for estimating the capital recovery factor (CRF). In addition, the cost estimate was based on the assumption that all infiltrated water contributes to recharging the aquifer. MAR scheme operation period depends on several factors, such as the site condition, scheme types, drought conditions, and maintenance constraints. Hence, a 200-day operation period was assumed for estimating the MAR expense, considering these factors. The cost estimate can be adjusted according to the site-specific MAR operating period. The focus of this study was on the comparison of levelized costs. The levelized cost was estimated using the following equations (Ross & Hasnain, 2018):

$$\mathrm{CRF} = \frac{\mathrm{r}(1+\mathrm{r})^{\mathrm{n}}}{(1+\mathrm{r})^{\mathrm{n}}-1} \quad (8)$$

$$\text{Levelized cost} = \frac{(\text{capital cost} \times \text{CRF}) + \text{annual O \& M cost} + \text{recharge \& recovery cost}}{\text{average annual water recharged or recovered in m}^3} \quad (9)$$

Due to data limitations, the exact levelized costs for the MAR schemes investigated in this research could not be determined; however, an approximate levelized cost could be

derived for each system. More details regarding the levelized cost estimation of the MAR scheme are provided by Ross, 2022; Ross & Hasnain, 2018 and Vanderzalm et al., 2022.

3 Evaluation of MAR site suitability by incorporating adaptive site investigation technique enabling optimized infiltration rate assessment and cost-effective implementation of surface spreading techniques

This section describes how to overcome data scarcity during the conceptual MAR planning phase. This involves employing an adaptive site characterization method to optimize the infiltration rates estimation, leading to economically viable surface spreading method implementation. As part of this research, a specific MAR site located in the Schiavon municipality of Vicenza, Veneto, Italy, near an agricultural region, was studied. The alluvial aquifer in this area was an important site to investigate due to the heterogeneous nature of its subsurface properties.

3.1 Study area

The MAR site is close to an agricultural area in Schiavon municipality in the Province of Vicenza, Veneto, Italy (Figure 11) (Filippi et al., 2016). One of the vital water supply systems in the Eastern Alps hydrographic zone is the Vicenza upper plain aquifer, a relatively undifferentiated aquifer located in the pre-Alpine foothills, which is why this land is strategically important to all the residents living in this area. As in recent years, over-exploitation of groundwater, climate change, and land use have caused the reduction of water levels in this aquifer of Brenta megafan (Baruffi et al., 2012; Pasini et al., 2012). In the Veneto region, the progressive groundwater level depletion has shortened the water availability for agricultural, industrial, and collective use (Sottani et al., 2014), and MAR schemes could have great potential to address the issue of groundwater depletion (Passadore et al., 2012).

Figure 11 The location of Schiavon FIA.

The Schiavon MAR site, an FIA, covers an area of 1.1-hectare, applying furrow irrigation to recharge the unconfined aquifer (Figure 12). A canal feeds the trenches with a connection to the irrigation network of the area, which is diverted from the Brenta River (Mastrocicco et al., 2015). It comprises nine infiltration trenches with a distance of 7.5 m. Each trench has a trapezoidal cross-section (0.7-0.8 m top width and 0.3-0.4 m bottom width) with a length of 163 m, which is a total length of 1467 m (Figure 13). The trenches are 0.7-0.8 m deep (Filippi et al., 2016), and the surface water is distributed among the infiltration channels by a level control system (Sottani et al., 2014) to recharge the groundwater at about 19 m below ground surface (Mastrocicco et al., 2015).

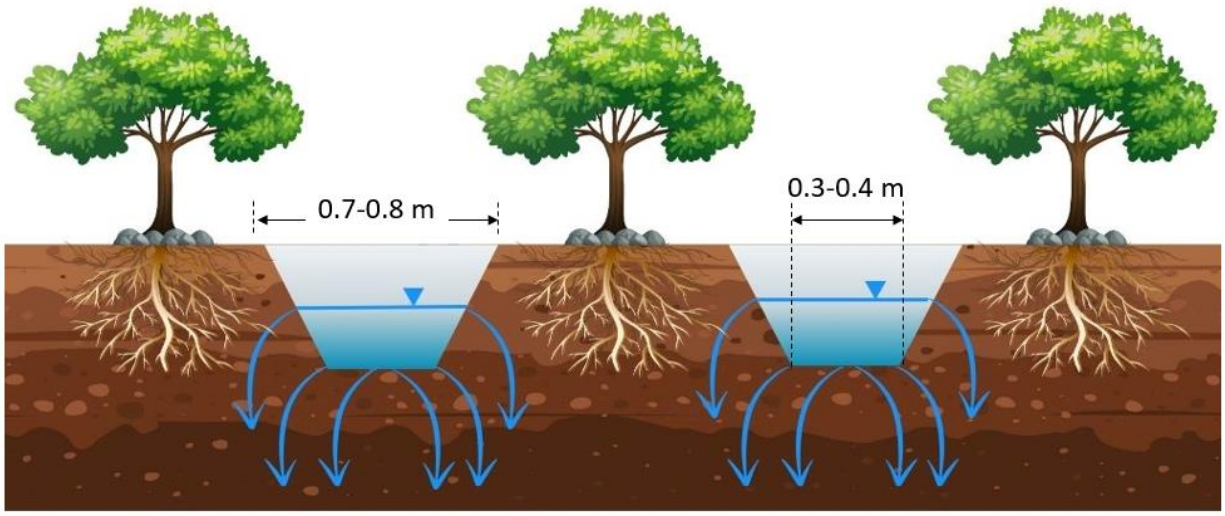

Figure 12 Schematic diagram of the infiltration trenches at Schiavon FIA (Picture not to scale).

At this infiltration site, trees and shrubs (1400 plants/ha) are grown between the ditches (Figure 13) in a short-rotation forestry scheme for five years to limit water evaporation and provide additional biomass to compensate for land costs and eventually reduce the cost of recharged water.

Figure 13 Infiltration trenches at Schiavon FIA.

Mastrocicco et al., 2015 provided an overview of the site stratigraphy based on conventional hydrogeological site characterization. Excavation of two trenches was conducted within the site up to a depth of 2.5 m below ground level (bgl). Three horizons were identified in the excavated trenches. The topsoil, horizon 1 extending from 0 to 0.35 m bgl, shows the influence of tillage and plant root growth and has a sandy, loamy structure with 20% gravel content. Two soil profiles (0.35-0.45 m bgl and 0.45-0.75 m bgl) in the middle horizon reveal sandy clay loam and sandy loam texture within a coarse-grained gravel (55%) skeleton. The horizon 3 (0.75-1.2 m bgl) is inconsistent and has a sandy texture with a 60% coarse gravel skeleton. The K_s at these horizons was determined by a Guelph Permeameter and varied over several orders of magnitude between 6.6×10^{-05} m/sec and 1.7×10^{-02} m/sec. This broad range shows the relevance of proper knowledge of subsurface conditions within the heterogeneous deposits of the Brenta River megafan to reduce uncertainty regarding site conditions.

Furthermore, in many cases, land cost contributes significantly to the overall expenditure of the MAR schemes (Hutchinson et al., 2017; Itani et al., 2022; Sasidharan et al., 2021), which poses challenges to MAR uptake. This highlights the importance of developing an innovative approach for strategic planning in the application of MAR schemes enabling optimized land use. Hence, in this research, the MAR site suitability was evaluated by integrating adaptive site investigation techniques, leading to cost-effective MAR planning and design.

3.2 Schiavon forested infiltration area site investigation

The aim of the site investigation was to characterize the infiltration site's subsurface properties and map variability in alluvial sediment properties. This was done with a particular focus on the hydrogeological properties at shallow depths relevant to the infiltration using an adaptive site investigation concept. This approach was established several years ago for the characterization of large contaminated sites due to its advantage in terms of data reliability, ability to obtain data across different scales, and rapid data acquisition (Schuetze et al., 2012; Utom et al., 2019). While years ago, e.g., during the planning of the investigated MAR site, the chosen site investigation approach was beyond state of the art, it is an important and established approach in complex hydrogeological

site investigation today. Hence, we obtained high-resolution subsurface data that is unrivaled by traditional site investigation approaches, which often provide limited information when used for complex subsurface characterization. The methodological approach applied in this study incorporated an EMI survey, direct push (DP) electrical profiling, DP-based soil sampling, and laboratory analysis of collected samples.

As a first step in the site investigation, the potential spatial variation of soil properties in the shallow subsurface was investigated using rapid and non-invasive EMI measurements. The EMI focuses on characterizing the spatial variability of soil EC_a since an increase in soil EC under nonsaline conditions commonly corresponds to an increase in clay mineral abundance (Vitharana et al., 2006). The higher proportion of fines can inhibit infiltration, locally reducing infiltration rates. Following the identification of areas of interest, representative points were chosen to conduct minimally invasive DP logging and soil sampling to gain high-resolution vertical profiles of the relevant subsurface features with depth. Ultimately, K_s were determined on selected samples to calculate infiltration rates. The applied methods of the site characterization are explained in the following.

3.2.1 Electromagnetic induction measurements

EMI surveys were conducted between the infiltration trenches, which aimed to rapidly characterize the shallow unsaturated zone in terms of sedimentary areal zonation using the EM38DD electromagnetic induction sensor (Geonics Ltd., ON, Canada). The EM38DD comprises two EM38 sensors, which are positioned perpendicular to each other. Both of the sensors have a transmitter and a receiver coil with a fixed spacing of 1 m. Simultaneous measurement of EC_a is performed in two orientations with different depth response profiles. The horizontally oriented sensors receive the response from the uppermost top 0.75 m of soil and are mainly influenced by the characteristics of the topsoil (Callegary et al., 2012; McNeill, 1980). The focus was on the vertical dipole mode with a depth of investigation up to 1.5 m bgl.

Ten parallel profiles between the infiltration trenches were measured with a sampling interval of 0.2 sec (Figure 14) to obtain dense information regarding EC_a. A differential GPS (smart antenna A100, Hemisphere GNSS) was used for positioning. The spatial

mapping obtained by EM38DD, with a 1.5 m penetration depth, exhibits a zonation of the soil EC_a across the test site.

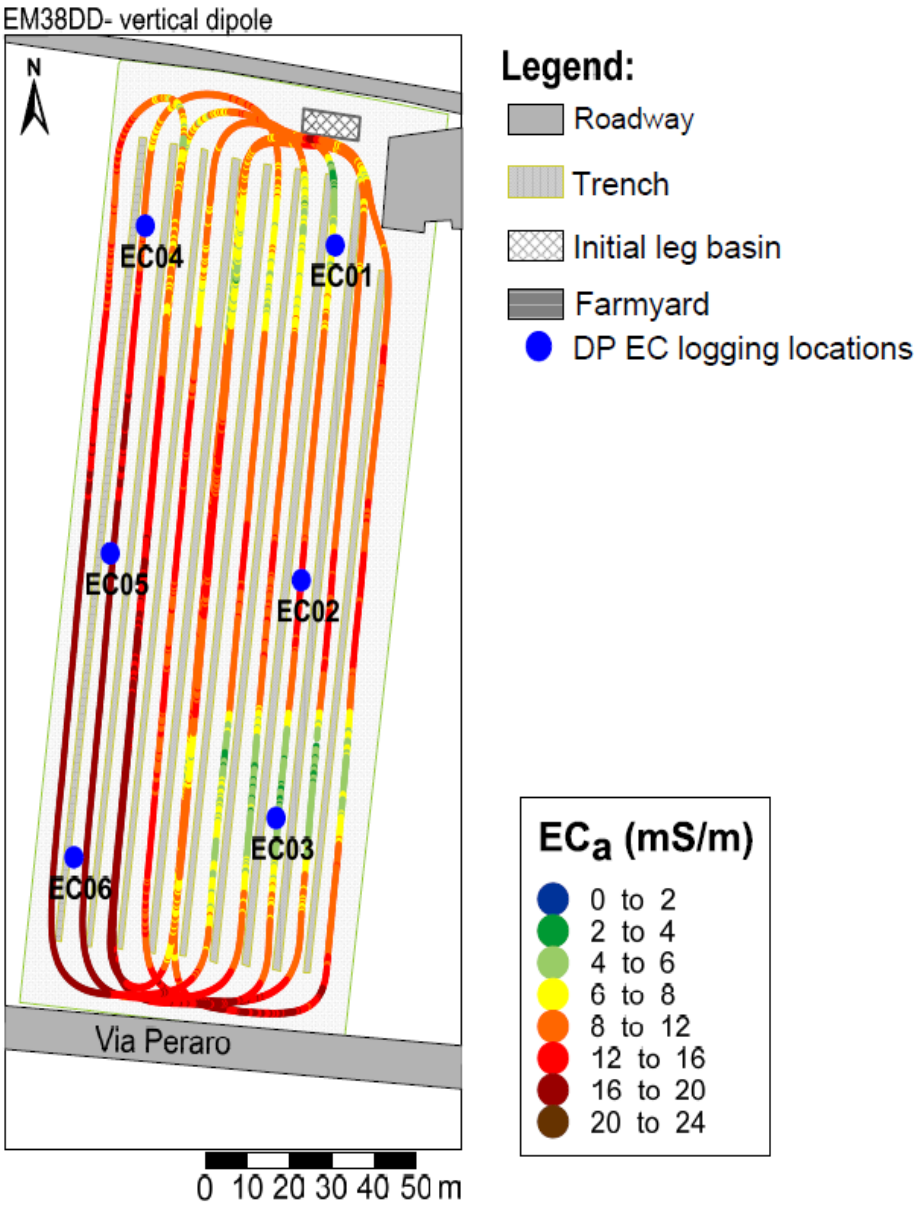

Figure 14 Results of the electromagnetic survey, EM38DD, with 1.5 m penetration depth and location of six direct push investigation points are represented by closed blue circles at the MAR site.

The EC_a measured at the site varies from 2.4 to 24 mS/m, as presented in Figure 14. There are three zones identified:

1. EC_a values are low in an isolated area north of the test site.
2. EC_a values are low to moderate in an isolated area southeast of the site.
3. EC_a values are higher in the rest of the area.

As previously stated, an increase in EC_a is anticipated to be correlated with an increase in the mineral content of clay, which will cause a decrease in hydraulic conductivity and a consequent decrease in recharge rates. The results mentioned above depict that an EMI survey can effectively obtain the delineation of the lateral variation in soil properties. However, the EC_a measured by the EMI is an average weighted conductivity measurement of a vertical soil column up to a certain depth (McNeill, 1980), which in this case is 1.5 m. As a result, DP EC logging and soil sampling were performed at the identified zones to acquire in situ high-resolution data on the vertical variation of EC and sediment properties.

3.2.2 Direct push electrical conductivity logging and soil sampling

Six DP EC probing points were chosen based on the EMI survey results (Figure 14) to identify possible confining layers that might impede water infiltration (Figure 15).

Figure 15 DP EC logging at Schiavon FIA.

Figure 16 presents the high-resolution vertical DP logging profiles from the six locations (EC 01 to EC 06). These points were positioned to reflect the various EMI zonation and to provide a good representation of the entire site. The DP profiling supports the main finding of the EMI survey, as generally low EC values in the upper 1.5 m bgl are encountered at probing locations EC 01 and EC 03 positioned in the isolated low zones of low soil EC_a. The most important individual features that are observed in the logging profiles are described below.

Profile EC 01 exhibits the most substantial deviations from all other logging profiles, although the EC values for EC 01 ranged from 0.01 to 42.5 mS/m. The profile is characterized by low EC values except for two horizons with increased EC values at 0.4 to 0.6 m bgl and starting at 8.20 m bgl. EC load tests were performed before and after each DP EC profile, which confirms that the used equipment worked properly. The most likely reason is that the sensors were not coupled to the surrounding soil material because of the presence of dry sand and gravel.

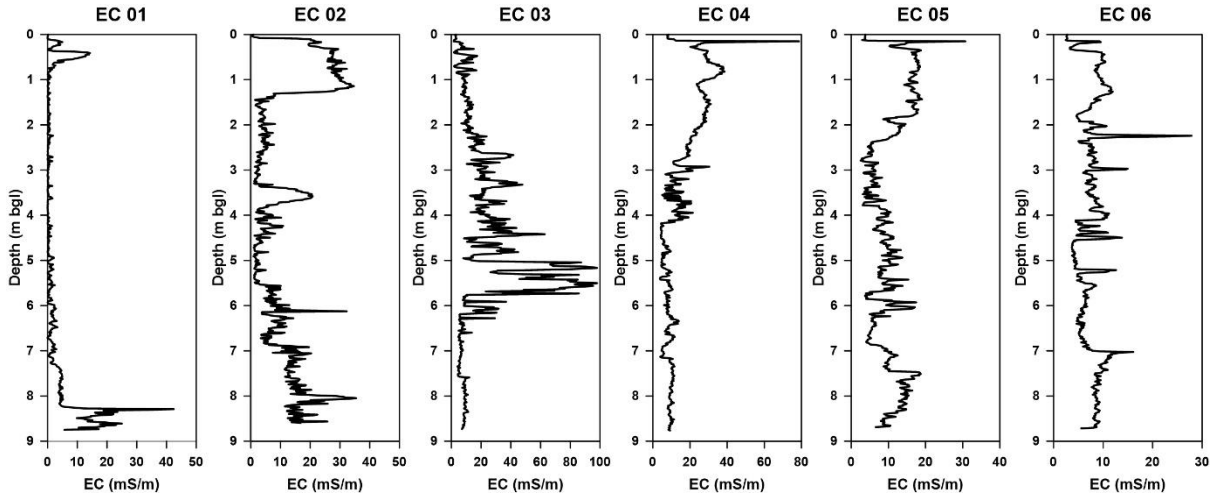

Figure 16 Vertical variation in EC at six DP EC logging profiles up to 9 m depth bgl. Please note the individual scaling of x-axes.

There is a prominent layer of increased EC up to 1.25 m at EC 02. Importantly, this distinct area of elevated EC, indicative of higher clay mineral content, is located below the bottom of the trenches. EC 03 does not have a near-surface zone of high EC values. On the other hand, at a depth of 5-6 m, an isolated interval of high EC values up to 100 mS/m is present, indicating the strong presence of clay minerals. The values recorded at EC 04 and EC 05 again show higher EC values in the top 1.8 m of soil. An interesting observation is that the logging profile measured at EC 06 shows only a slight variation in the distribution of EC values in the vertical direction, in contrast to the substantial EC variation observed at EC 01 to EC 05 logs.

The compilation of the DP EC logging results revealed a significant variation in measured EC values, underlining the high degree of subsurface variability at the site. A significant vertical variation in EC values was observed at positions EC 01 to EC 05, with EC 06 being an exception. Additionally, a pronounced lateral variation between the logs can be detected, as reflected in the discontinuous nature of most of the isolated features, indicating clayey lenses rather than continuous confining layers, particularly at greater depths. The lenses of increased EC are discontinuous and, therefore, are not expected to affect the overall infiltration rate at the site. However, this is different for the high EC zones near the surface. The trenches are located on low hydraulic conductivity material, which immediately impedes infiltration in these zones.

Further information was needed to quantify the effects of surface-near variation in EC values on the infiltration rates. Accordingly, soil samples were collected to compare the grain size distribution with the EC values and, as a third step, to measure K_s to determine the infiltration rates at the selected sampling points. In total, 15 soil samples were collected at four locations: EC 01, EC 02, EC 03, and EC 05. The sampling locations and depths were selected based on differences in the DP EC logging data.

3.2.3 Laboratory analyses of soil samples

After collecting the soil samples, grain size analyses were performed to determine to which degree the increase in EC translates into an increase in the abundance of clay content. As previously stated, the soil analysis was focused on samples obtained in the upper 2 m bgl. Figure 17 illustrates the results of the grain size analysis.

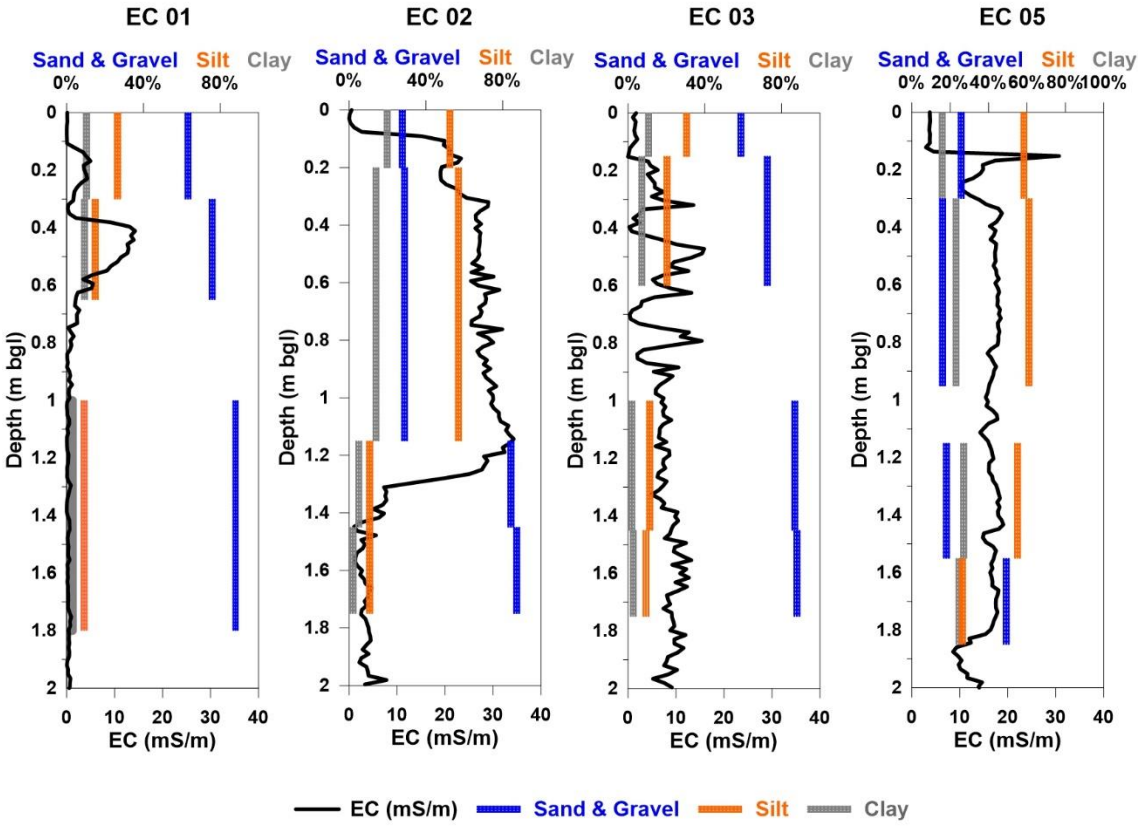

Figure 17 Combined representation of EC profiles and sand and gravel, silt, and clay percentages at four probing points up to 2 m bgl.

The results at EC 01 and EC 02 support the hypothesis that fine materials, specifically clay range particles, increase with increasing EC. This is mainly observed by comparing grain size fraction with EC distribution at EC 02.

EC 02 probing location shows higher percentages of clay (14%) and silt (57%) at 0.2-1.15 m depth, which is also evidenced by high EC values in logs. Sand and gravel are present in 58.8% and 72.6% abundances at the EC 03 location at 0-0.15 m bgl depth and 0.15-0.6 m bgl depth, respectively. At these depths, clay material accounts for 10.7% and 7.2%, respectively, while clay amount was lower at 1-1.45 m bgl and 1.45-1.75 m bgl. The EC values at EC 05 are approximately 15 mS/m with slight variations between 0.4 and 1.8 m bgl. There is an increase in clay content in sediment samples, ranging between 23% and 28% of the material sampled at the same depth interval. It is essential to mention that the amount of clay found at EC 05 results in a measured EC of 15 mS/m, while EC 02 has a much higher EC of around 30 mS/m due to half as much clay content (14%), which occurs over a depth interval of 0.2-1.15 m bgl.

Individual discrepancies between the DP measured EC and the grain size analysis results are also apparent. At EC 01, the difference between the grain size composition change and variation in EC values over two consecutive depth intervals (0.15-0.25 m and 0.4-0.55 m) is noticeable. The probable reason for this mismatch may be the insufficient electrical coupling of the DP EC probe in shallow depths or the remaining uncertainty regarding the exact soil sampling depth and sample disturbance. As a result, at this particular site, it is not possible to deduce a general relationship between EC and clay content in the samples, and further investigation is required. Furthermore, other parameters besides fine grain content also impact hydraulic conductivity and, ultimately, infiltration capability. These include packing density, porosity, and tortuosity. Further information on these factors is provided by Cherif Taiba et al., 2019 Ghanbarian et al., 2013 and Vienken & Dietrich, 2011. Hence, K_s were directly determined on selected samples. Seven out of the fifteen soil samples were selected to determine K_s. Three measurements were obtained for each soil sample, and the arithmetic average of the results was calculated to determine the K_s of each soil sample (Table 1).

Table 1 K_s of soil samples at different depths

Sample Location	Depth (m bgl)	K_s (m/sec)			
		1st measured value	2nd measured value	3rd measured value	Mean value
EC 01	1-1.8	2.58×10^{-04}	2.70×10^{-04}	2.91×10^{-04}	2.73×10^{-04}
EC 02	0.2-1.15	4.65×10^{-07}	4.65×10^{-07}	3.49×10^{-07}	4.26×10^{-07}
EC 02	1.15-1.45	1.31×10^{-04}	1.44×10^{-04}	1.21×10^{-04}	1.32×10^{-04}
EC 03	0.15-0.6	2.40×10^{-05}	1.89×10^{-05}	1.88×10^{-05}	2.06×10^{-05}
EC 03	1-1.45	3.80×10^{-04}	3.55×10^{-04}	3.65×10^{-04}	3.67×10^{-04}
EC 05	0.3-0.95	1.05×10^{-06}	9.30×10^{-07}	6.98×10^{-07}	8.93×10^{-07}
EC 05	1.15-1.55	1.86×10^{-06}	1.63×10^{-06}	1.51×10^{-06}	1.67×10^{-06}
EC 05	1.55-1.85	7.21×10^{-06}	9.07×10^{-06}	1.12×10^{-05}	9.16×10^{-06}

Figure 18 indicates the sampling intervals and compares the vertical variation of EC and K_s at four DP EC locations.

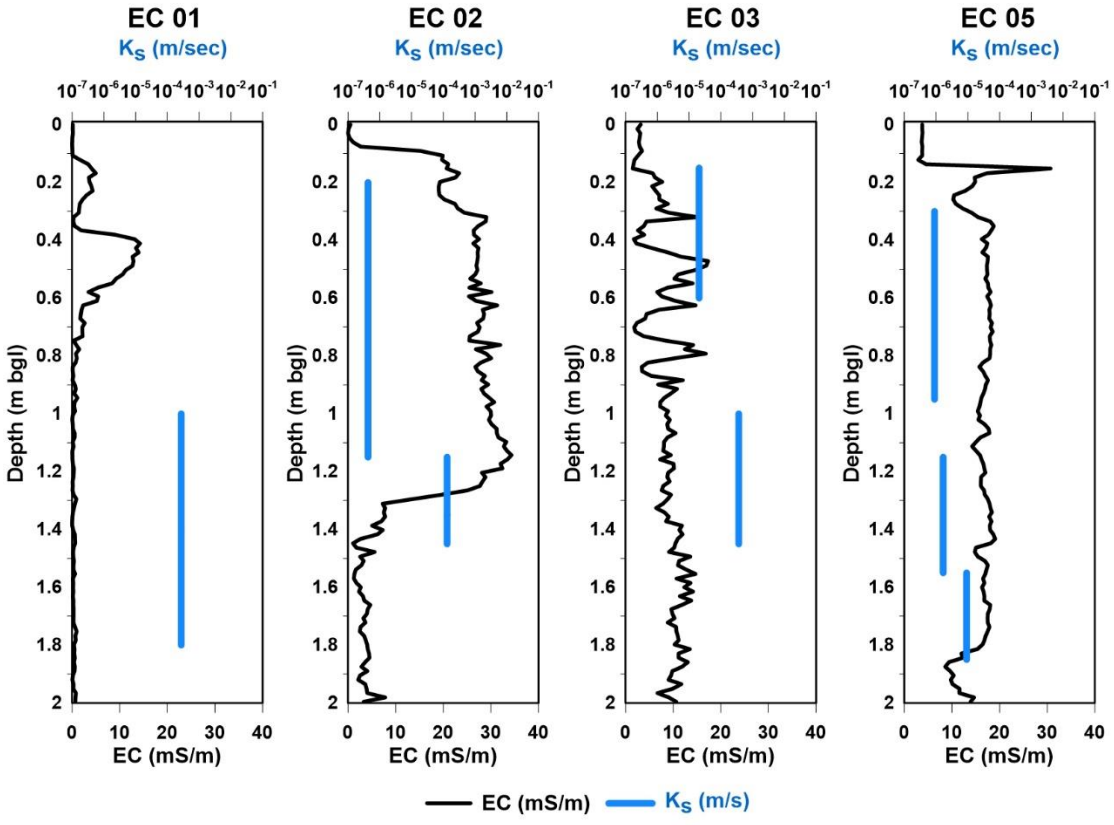

Figure 18 DP EC logs and depth-dependent K_s at four EC logging points up to 2 m below the land surface. It shows that the high EC translates into low K and vice versa.

The measured K_s values vary over three orders of magnitude between 4.26×10^{-07} m/sec and 3.67×10^{-04} m/sec. At EC 01, the K_s at 1-1.8 m bgl depth revealed by the constant head permeameter test was high with 2.73×10^{-04} m/sec, which indicated sand and gravel dominated deposit. It can also be seen that the low hydraulic conductivity of 4.26×10^{-07} m/sec at EC 02 was reflected in the grain size composition and high EC values at EC 02 point. When the lithology transformed from silt and clay to sand and gravel, observed in the EC value at a depth of 1.45 m bgl, the K_s increased to 1.32×10^{-04} m/sec. The constant head permeameter tests conducted on the samples obtained at the EC 05 location revealed a moderate variation of measured K_s at different depths. K_s of the soil materials present at 0.3-0.95 m bgl were determined to be 8.93×10^{-07} m/s and 9.16×10^{-06} m/s between 1.55 and 1.85 m bgl. In contrast to the differences in measured K_s, no significant variation in EC was measured at the respective depths.

A particular limitation in this study was encountered in the determination of K_s. The constant head permeameter was operated using a small sample of 250 cm^3 under controlled conditions using one-dimensional flow. The value of data obtained from laboratory measurement, hence, always depends on the sample's representativeness and avoidance of sample disturbance, especially under non-isotropic soil conditions. Disturbance of the sample was, however, unavoidable in this case. In-situ measurements of K_s with a larger sample volume would be preferable. However, they could not be realized in the field as the work was performed in the unsaturated zone above the groundwater table, leaving only laboratory analyses. The collection of mixed soil samples did not reflect the clogging properties of soil; hence, in situ determination of soil hydraulic properties is recommended for future studies.

Grain size analysis and measured K_s results demonstrate that the subsurface properties vary at different points and over depth. Results further showcase how high-resolution DP EC logging can be utilized to identify confining layers and assess their lateral continuity. However, in this case, using EMI measurements, representative locations for DP investigations must be determined beforehand. Additionally, DP EC logging enabled the depth-specific identification of lithological changes and, hence, depth-oriented soil sampling for further laboratory analyses.

The eventual step in this research was to distinguish zones with different infiltration behavior and determine specific infiltration rates. The goal was to identify and locate zones of expected high infiltration rates, i.e., zones composed of coarse-dominated sedimentary deposits. Based on the results, the infiltration site was categorized into three zones (Figure 19) primarily based on the EC_a distribution obtained from the EMI survey.

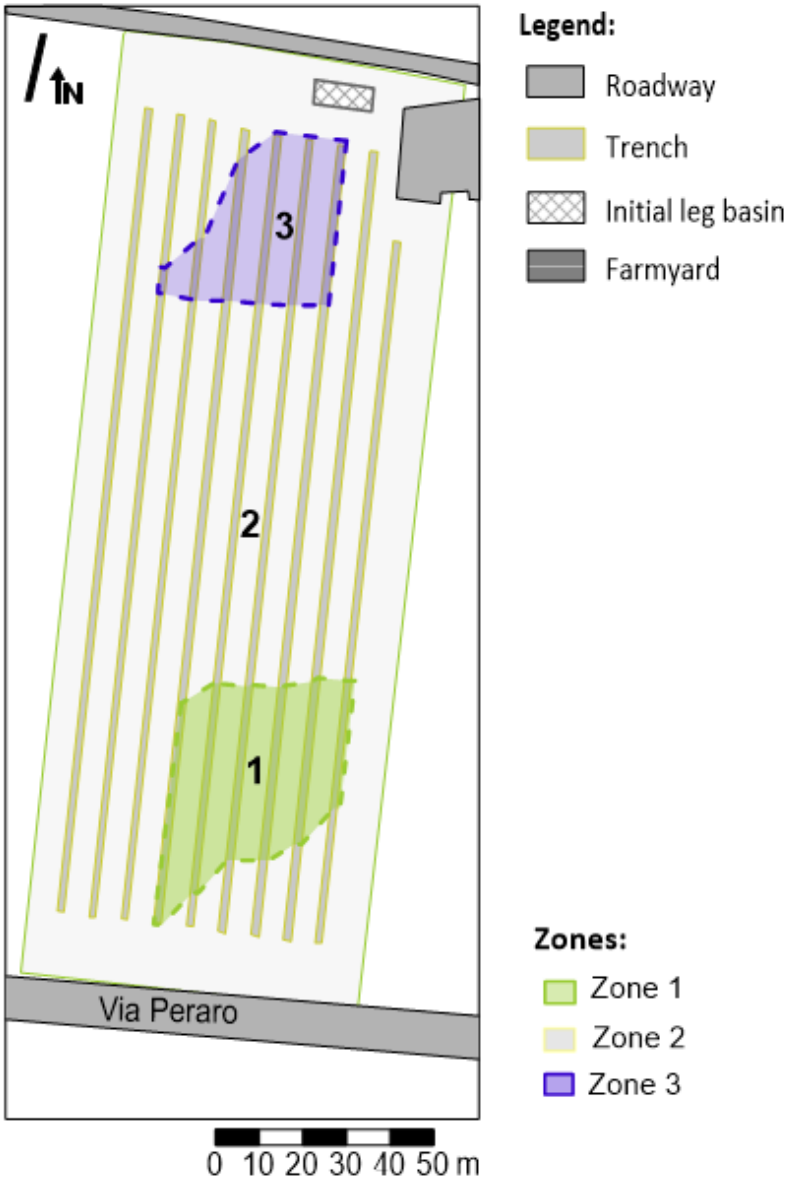

Figure 19 Three zones with different infiltration characteristics distinguished using EMI and DP techniques.

This approach is feasible as the DP probing and the soil analyses agree with the EMI results, i.e., that areas of increased electrical conductivity are characterized by reduced infiltration rates. An exception is found at probing location EC 06, where the EMI survey indicated comparably high EC_a values, while EC values obtained from DP profiling were comparably low. During the EMI measurement, surface water was present in that part of the test site, and it was assumed that it influenced the results by producing high EC_a values. However, because of the water remaining in the trenches, we consider the infiltration capacity of this area to be low. Hence, we attributed EC 06 to be part of the low conductive and low infiltration zone despite low DP EC values. Soil samples were unavailable, so no further investigation of the material was possible.

Infiltration rates were calculated for three zones using equation (2) based on the K_s. The average water height in the trenches was not available. Hence, the infiltration rate in the 0.7-0.8 m deep trenches was estimated by assuming an average water level of 0.4 m. Table 2 shows the estimated infiltration rates of the total length of the infiltration trenches within the three separate zones.

Table 2 Estimated infiltration rates of three zones identified from the EMI survey

Zones	Surface area of trenches (m^2)	Calculated maximum infiltration rates (l/sec)
Zone 1	148.26	124.58
Zone 2	887.98	1.02
Zone 3	103.90	65.01
Total	1140.14	190.61

According to the estimation, the infiltration rate at Schiavon FIA is 190.61 l/sec when the trenches are continuously filled to a height of 0.4 m from the trench bottom. However, there are noticeable discrepancies in the computed infiltration rates when comparing the individual infiltration rates at each zone. The maximum infiltration rate among all the zones is 124.58 l/sec, found in Zone 1. Zone 2 has the largest infiltration area and the lowest infiltration rate of 1.02 l/sec. The second highest rate of surface water infiltration is observed in Zone 3, at 65.01 l/sec.

Mastrocicco et al., 2015 monitored the hydrological performance of Schiavon FIA from May 2011 to May 2014. In their study, the amount of surface water infiltration was 25.4 l/sec. This case study's calculated infiltration rate is higher than the measured value at Schiavon FIA. However, several factors possibly explain the differences in potential maximum and actual monitored infiltration rates during operation. At the Schiavon FIA, the inflow canal section had limited capacity to convey water. The equation for calculating the infiltration rate depends on the trench geometry, water level depth in the trench, and saturated hydraulic conductivity. Due to limited information, the trenches' water level was considered 0.4 m for our calculations. Further analysis shows that linear variation in water level (0.1 m to 0.6 m) increases the infiltration rates linearly from 86.1 l/sec to 256.61 l/sec. Additionally, varying inflow rates, evaporation from the trenches, and temporal variation of water level in the trenches during actual operation were not considered in our calculations of the infiltration capacity.

The study's most significant finding is that, according to the survey, 99.5% of the surface water diverted from the Brenta River is anticipated to be infiltrated through zones 1 and 3. Zone 2 has the largest surface area; however, it is estimated that just 0.5% of surface water infiltration occurs here. Conversely, this suggests that the size of the MAR site can be reduced by 77% and used for other purposes, such as agriculture, if the infiltration site is reduced to zones 1 and 3 and a loss of infiltration capability of 0.5% is acceptable.

3.2.4 Economic analysis of Schiavon FIA

The MAR site was established in 2009. Several cost metrics in local currency units (LCUs) were obtained from De Carli, 2015. Land acquisition cost for the year 2012 was obtained from Eurostat, 2017, as the information for 2009 was not available. Finally, the adaptive site investigation cost was obtained based on expert consultation at the Helmholtz Centre for Environmental Research-UFZ Leipzig. All the expenses in LCUs were then multiplied by a gross domestic product (GDP) deflator and an exchange rate of 1.07 to get the standardized cost in US dollars (US$) for 2022. GDP deflator values for 2009 and 2022 were 1.15 and 1.12, respectively. The capital, operating, and management costs and levelized costs of Schiavon FIA are demonstrated in Figure 20.

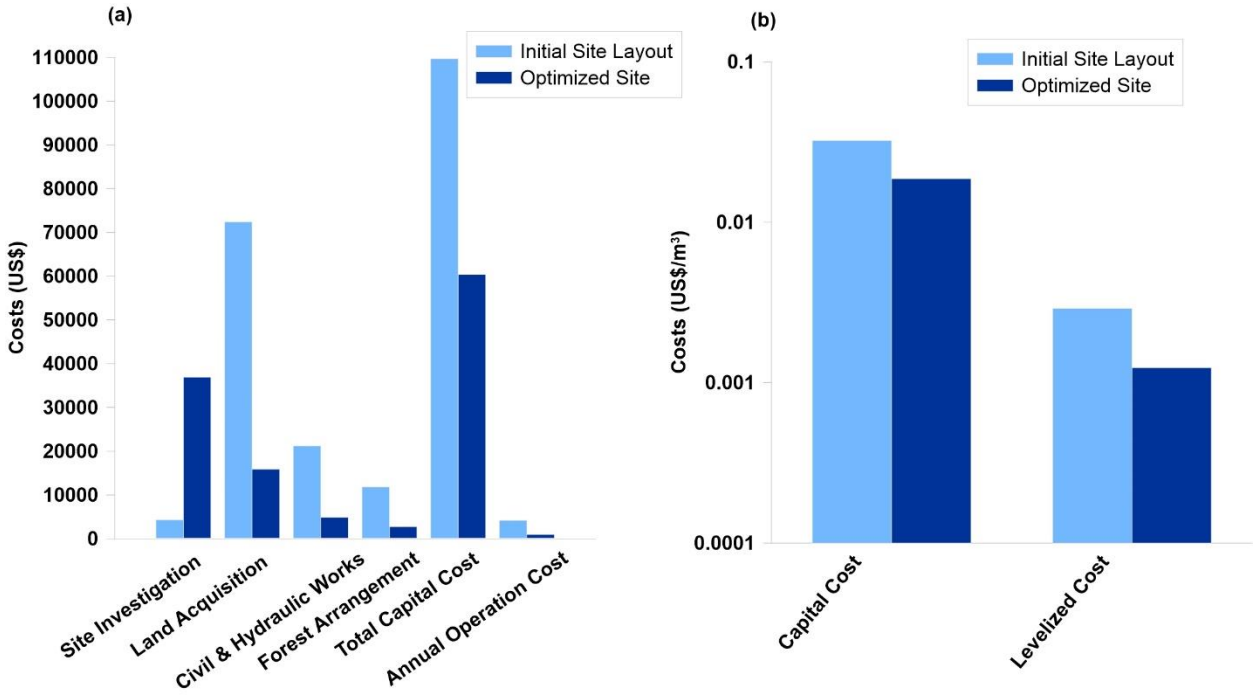

Figure 20 (a) Site investigation, land acquisition, civil & hydraulic works, forest arrangement, capital and operation cost (b) Capital and levelized cost per m^3 of recharged water for initial and optimized site layout of Schiavon FIA scheme

The initial expenses related to constructing an FIA of one hectare totaled 109,704.76 US$. According to Figure 20a, Schiavon FIA's initial annual operation and management cost was 4,149 US$, which equals 3.78% of the initial capital cost. During the economic analysis, we assumed that the FIA was built on agricultural land. In the Veneto region, the price of arable land in 2022 was 72,393 US$, which equals almost 65.9% of the declared investment cost. This demonstrates that the cost of land acquisition is a crucial factor for evaluating the costs of MAR projects when it is not provided for free. Detailed information regarding the cost analysis based on the initial and optimized layout of Schiavon FIA is provided in Table 3.

Table 3 Initial and recalculated cost of the Schiavon FIA scheme ([1]De Carli, 2015, [2]Eurostat, 2017)

Cost Items	Initial Layout		Optimized Layout	
	Cost in LCU (Euros)	Indexed cost for 2022 (US$)	Cost in LCU (Euros)	Indexed cost for 2022 (US$)
Site Investigation[1]	3,500	4,303	30,000	36,881
Land Acquisition[2]	57,954	72,393	13,329.42	15,888
Civil & Hydraulic Works[1]	17,250	21,207	3,967.5	4,878
Forest Arrangement[1]	9,600	11,802	2,208	2,714
Total Capital Cost	88,304	109,704.76	49,504.9	60,362
Annual Operation Cost[1]	3,375	4,149	776.25	954
Total estimated water recharged (m^3)	3.37×10^6		3.35×10^6	
Capital Cost/ m^3	0.026	0.033	0.015	0.018
Levelized cost/ m^3	0.0023	0.0029	0.001	0.0012

It was also assumed that the MAR scheme would be operated for 200 days in a year, and that all the surface water infiltrated through the trenches would contribute to groundwater recharge. The annual estimated recharge volume for the initial and optimized site layout is 3.37×10^6 m^3 and 3.35×10^6 m^3 respectively (Table 3). Based on the estimated recharge value, the initial FIA arrangement will infiltrate surface water at a capital cost of 0.033 US$ per m^3 and a levelized cost of 0.0029 US$ (Figure 20b, Table 3). As 0.23 hectares of area is favorable for infiltration, the land cost will be reduced to 15,888 US$ if the land use is

optimized for aquifer recharge. Although the adaptive site investigation cost is 8.5 times higher than the traditional investigation approach, it results in an overall levelized cost reduction of 58.4% of the estimated recharged water.

4 Development and assessment of a novel MAR concept by employing a subsurface irrigation system for land use diversification

The cost of land acquisition is one of the main determinants of the surface spreading scheme cost, influencing the adoption of MAR. Tailored site characterization can reduce the footprint of MAR systems, allowing for other land-use applications, especially agriculture. However, there could be circumstances when land use and cost reduction may not be possible by enhanced site characterization; therefore, exploring alternative solutions is essential. In this study, the focus is on the optimization of land use through the development of a novel MAR technique using a subsurface irrigation system (SIS), thereby generating an additional source of revenue.

In the first stage of fulfilling this aim, a numerical simulation was conducted to determine the SIS's infiltration rate and wetting pattern distribution. A soil tank experiment was then performed to evaluate the model's performance and determine percolation velocity with different techniques. Finally, the model was used to investigate the optimal installation depth and the cumulative infiltration rate of the SIS for a hypothetical scenario, resulting in an evaluation of the suitability of the SIS in a line-source configuration.

4.1 Subsurface irrigation system

A SIS involves installing perforated or open-jointed pipes or drip under the soil surface to provide plant water, reducing water loss and evaporation (Figure 21). Historically, common sub-surface irrigation was implemented by burying pots, pitchers, and porous pipes (Ashrafi et al., 2002; Kanda et al., 2018; Siyal et al., 2013). Porous pipes made of

clay, rubber, and polyethylene are the main types of porous irrigation systems (Gupta et al., 2009; Liang et al., 2009; Siyal et al., 2009).

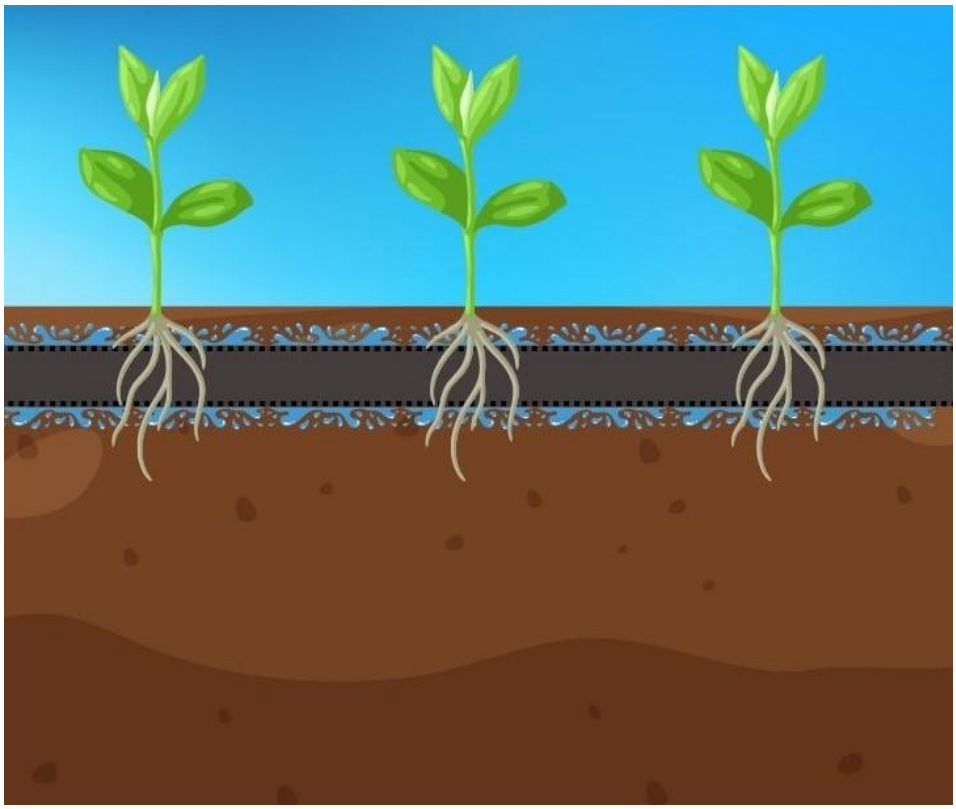

Figure 21 Schematic diagram of a perforated pipe installed underground for irrigation.

Micro-irrigation using porous pipes manufactured from recycled rubber tires and polyethylene particles is one of the most effective irrigation methods for dry climates (Liang et al., 2009). Depending on how large the emission pores are, they can be classified as microporous pipes or nanoporous pipes (Kanda et al., 2018). Water is released throughout the length of the porous pipe under pressure (Patel et al., 2011). This pipe serves as a conveyance and an emission water system for cultivation.

The SIS used in this study has been developed for the agricultural industry (Figure 22). According to the manufacturer, the novelty of this system is that it is the first permeable subterranean irrigation system with uniform water distribution up to 100 m (www.ecotube.eu).

Figure 22 SIS used for aquifer recharge (Source: Ecotube).

It has a microporous fabric made of recycled tire granulation mixed with polyethylene. The optimum pressure of the system is 0.6 bar. At this pressure, it distributes 1.3 L/h/m of water in the air. The pipe has a 17.5 mm outer diameter and a 12.5 mm inner diameter. With increasing operating pressure, the discharge of SIS also increases. When the pressure is higher, the flow rate at the beginning of the pipe will be higher. The flow rate tends to decrease with increasing pressure at the end of the pipe, resulting in a non-uniform flow rate. Therefore, optimum pressure application becomes more important to maintain uniform discharge when the SIS length increases. Also, the manufacturers stated that the discharge of the pipe at the beginning of the irrigation process is high due to the fabric properties of the pipe, which gradually becomes constant over time.

SIS for cultivation is mainly used for delivering sufficient water to the crops at a specific time. Water is mainly provided at the plant root zone for their growth and development. There have been several numerical models developed to understand the soil water dynamics of dripper or line-source irrigation systems to optimize their design and management for agriculture and prevent water percolation into groundwater (Cai et al., 2018; Kanda et al., 2020; Siyal et al., 2009). In contrast to agricultural applications, it is essential to ensure infiltration to the groundwater and minimize water loss to the surface

for SIS applications intended for aquifer recharge. It is also vital to determine the infiltration rate through this system, the optimum installation depth, and the lateral spacing between the SIS. As a first step in understanding the performance of SIS, a numerical simulation was performed to determine the performance of SIS in sandy soil as a MAR technique.

4.2 Numerical simulation to determine subsurface irrigation system's infiltration behavior

The HYDRUS-2D/3D software was used to predict the SIS infiltration rate and wetting pattern dimensions in sandy soil. The simulated result also provided information to determine the placement depth of SIS and the position of observation points for volumetric water content (VWC) measurement, leading to the design of a soil tank experiment. One of the objectives of the soil tank experiment was the evaluation of the model's prediction performance, which will be explained in section 4.3. The evaluated model was then used to obtain knowledge regarding the installation depth and spacing of SIS for feasibility assessment, considering a continuous operating period of 200 days in a year. The geometry and boundary conditions (BCs) for simulating the infiltration characteristics of SIS using HYDRUS-2D/3D software are described below.

4.2.1 Model domain and soil hydraulic parameters

The model domain was 45 cm by 100 cm, with the SIS system located 20 cm below the soil surface (Figure 23). The placement depth of SIS for the modeling purpose was chosen based on the studies performed with line source irrigation systems (Fan et al., 2018b; Kanda et al., 2020). The symmetric condition was considered in this study to reduce computational time. That is why one side was simulated to determine the SIS's infiltration rate and wetting pattern distribution. The model was discretized into 1602 nodes. The sandy soil was considered as a common MAR soil type and assumed to be homogeneous and isotropic.

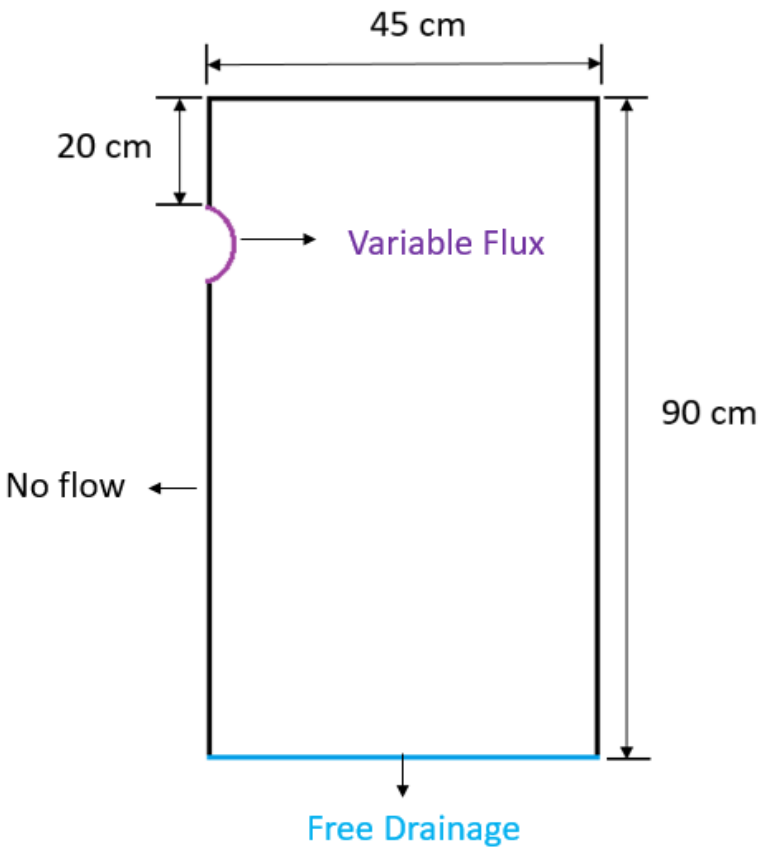

Figure 23 Schematic diagram to represent the SIS location, the transport domain, and BCs.

The HYDRUS-2D/3D model requires soil hydraulic parameters values such as residual water content (θ_r), saturated water content (θ_s), empirical co-efficient l, α, and n, along with the initial condition of the soil and BCs for simulating the infiltration characteristics of the SIS. The hydraulic characteristics of several soils have been incorporated into a soil catalog (Carsel & Parrish, 1988), which was helpful for obtaining these parameters for sandy soil. The model was further parameterized by incorporating the K_s value of the sandy soil, which was used in the soil tank experiment. The K_s value was determined by a constant head permeameter test and average value of 4.95×10^{-04} m/sec was obtained and was incorporated in the model to accurately represent the K_s value of sandy soil. For the simulation of water flow, an initial soil condition must be defined for the entire model domain before the simulation is initiated. The sandy soil's initial moisture content

was measured prior to the beginning of the soil tank experiment and an average value of 0.049 cm^3/cm^3 was integrated into the model.

4.2.2 Boundary conditions

Three BCs were used to simulate the infiltration characteristics of the SIS system. The primary objective of this modeling was to gain a comprehensive understanding of infiltration rate and wetting pattern distribution. This study did not include surface processes such as evaporation and precipitation. Simplifying the model by excluding these parameters allowed for an accurate and controlled investigation of the wetting front distribution, facilitating the identification of the SIS placement depth. That is why no flux BC was defined at the top boundary. No flux BC was also defined at the sides of the model domain. A free drainage boundary was applied at the lower boundary.

A special flux boundary named drip characteristics function was used to define variable flux boundary on the SIS. It is a system-dependent BC that incorporates the porous pipe properties, the inlet pressure, and the soil hydraulic properties while determining the source discharge (Lazarovitch et al., 2005). The equation for this special BC is expressed in Equation 10 (Simunek et al., 2012).

$$Q = Q_0(h_s - h_{in})^c \qquad (10)$$

Where Q [$L^3\ T^{-1}$] ([$L^2\ T^{-1}$] in 2D) is the source discharge for the pressure h_s, Q_o [$L^3\ T^{-1}$] ([$L^2\ T^{-1}$] in 2D) is the optimal flux or discharge of the source, h_s [L] is the pressure head at the source-soil interface (back pressure), h_{in} [L] is the inlet pressure and the back pressure is zero, and c [-] is the empirical constant for the emitter which represents the emitter flow characteristics.

For defining this special flux BC in the model, the respective parameter values were determined from the pressure-discharge relationship of the SIS. The experiment for determining the discharge characteristics of the SIS and the results are described in section 4.2.3.

4.2.3 Discharge characteristics of subsurface irrigation system

There are no existing guidelines or established standards for the ideal length to be used in determining the discharge characteristics of porous pipe (Kanda et al., 2018). For this experiment, a 50-meter-long SIS was divided into multiple 1-meter-long segments. Different 1-meter sections were used to obtain information about the discharge behavior with different pressures. The main reason for choosing a shorter length was to minimize the influence of friction losses on the accuracy of the discharge measurements. The range of pressure varied from 0.6 bar (6 m pressure head) to 1.5 bar (15 m pressure head), and the pressure variation was measured with a pressure gauge. The discharge was determined by measuring the water volume emitted in the air from the SIS at 15-minute intervals using a 1 L graduated cylinder. The discharge can be expressed as a function of pressure in the form of a power function shown in Equation 11.

$$Q = Kh_{in}^{c} \tag{11}$$

Where $Q =$ Discharge (L/h/m), $K =$ Emitter Constant, $h_{in} =$ Operating pressure (m), and $c =$ exponent of discharge.

Typically, emitter discharge exponents range from 0 to 1. A value of 0 represents a fully pressure-compensated emitter, 0.5 represents turbulent flow, and a value of 1 represents laminar flow (Amin et al., 1997). The determined parameters from the pressure-discharge relationship were used to define the special BC in HYDRUS-2D/3D for simulating the SIS's infiltration rate in sandy soil.

Figure 24 demonstrates the effect of pressure on the discharge rate of the SIS, shown on a linear scale. It shows maximum, minimum, and stabilized discharge rates and explains how pressure influences SIS flow characteristics.

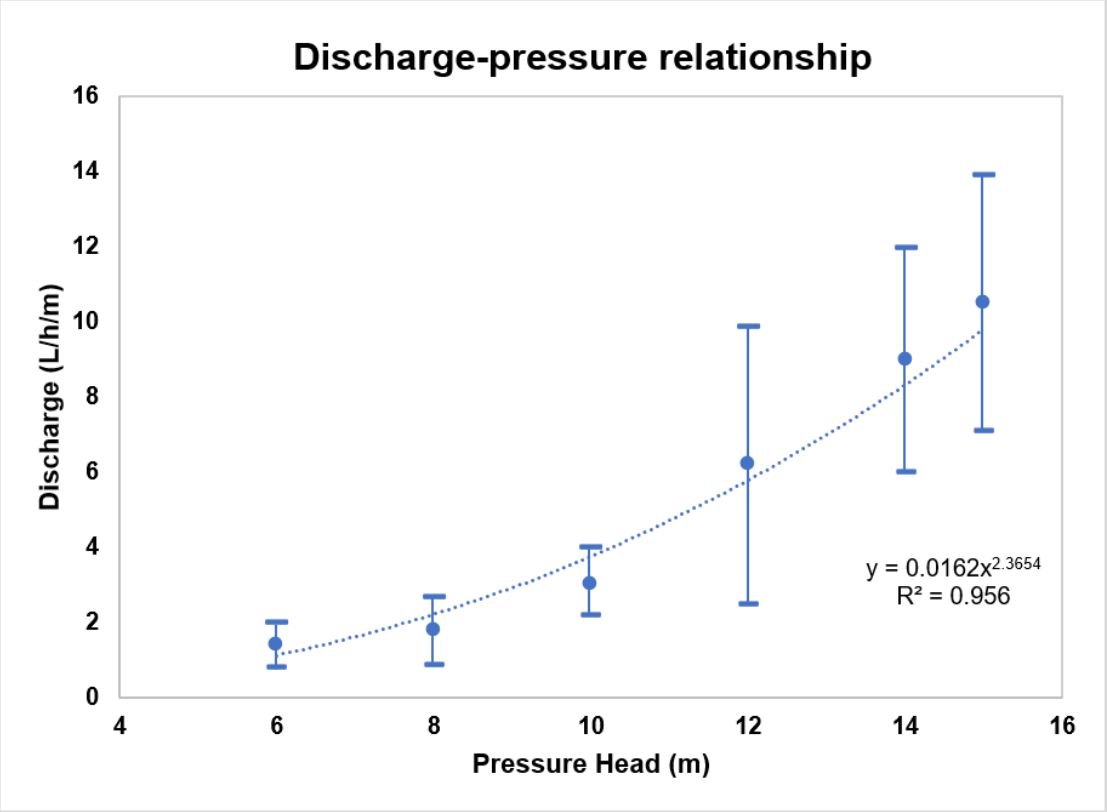

Figure 24 Effect of different pressures on the discharge of SIS.

The discharge from the SIS under varying pressure can be represented by a power function (R^2 = 0.956), as illustrated in Figure 24. The stabilized flow rate varies from 1.4 L/h/m at 6 m to 10.5 L/h/m at 15 m pressure head. The relationship is expressed in equation 12.

$$q = 0.0162x^{2.3654} \quad (12)$$

The emitter constant (k) and exponent (x) values determined from the power function are 0.0162 and 2.3654, respectively. In this study, the exponent of the porous pipe is greater than 1, meaning that the emission rate will significantly increase with the increase of operating pressure, which is like non-compensating emitters. The pipe allowed a faster flow through the pores, expanding their diameters and creating more efficient emission pores (Liang et al., 2009). These parameters were used in the HYDRUS-2D/3D software to define the special flux boundary, enabling the infiltration rate and wetting pattern distribution prediction. In the following section, the results of the model will be discussed in detail.

4.2.4 Numerical simulation result

The model was run for 13 hours to reflect the soil tank experiment duration. Figure 25 shows the simulated cumulative infiltration rate of the SIS. The figure shows that 15.26 L of water was infiltrated through the SIS in sandy soil for 13 hours.

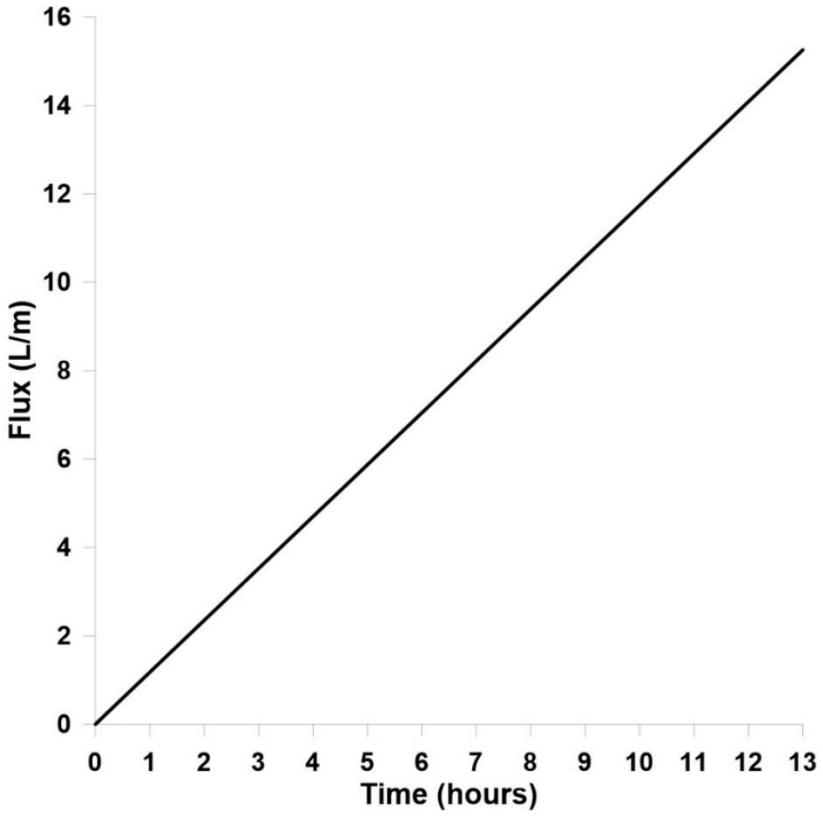

Figure 25 Cumulative infiltration rate of SIS in sandy soil.

The wetting pattern distribution of SIS in sandy soil is shown in Figure 26. The wetting dimension increased with time and discharge. Sandy soils are characterized by relatively large particles compared to silt and clay. These larger particles leave a greater amount of space between them, resulting in larger pores. As a result, there is a smaller surface area for water to adhere to, resulting in lower water retention capacity.

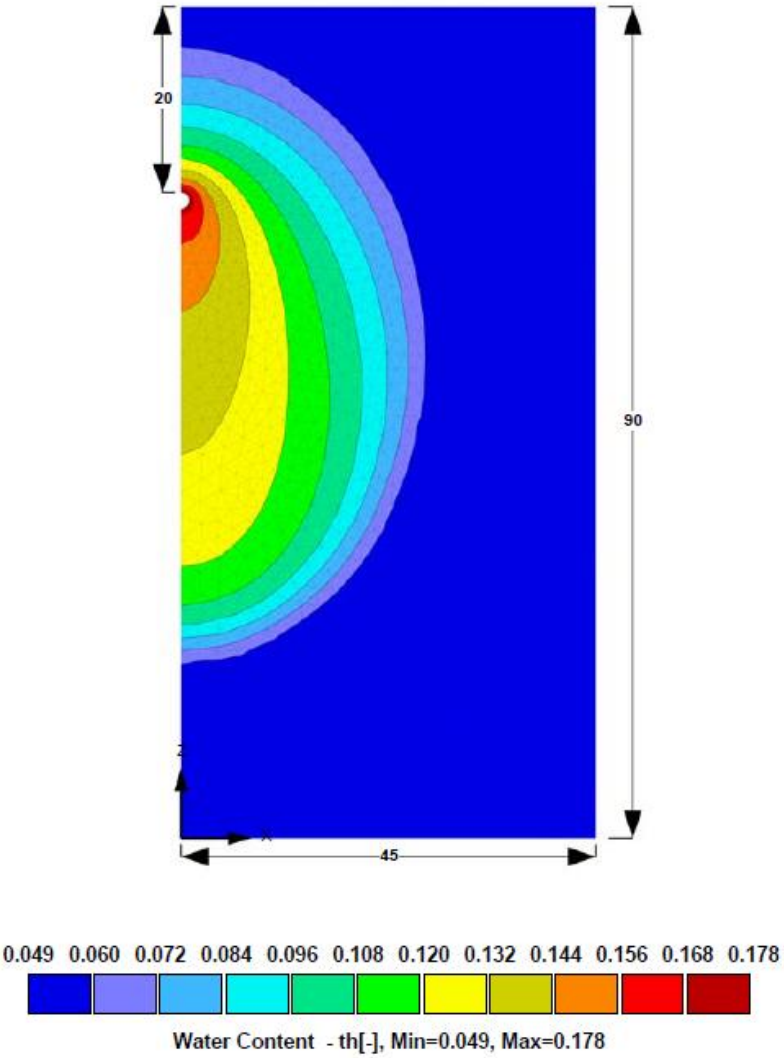

Figure 26 Wetting pattern distribution of SIS in sandy soil after 13 hours. The dimensions of the model domain is in cm.

During infiltration, water movement in the soil is also affected by both the matrix and gravitational potentials. Matrix potential has less effect on sandy soils than gravitational potential (Cai et al., 2019). As a result, the aspect ratio gradually increases, and the wetting front develops an ellipsoidal shape. The wetting front's downward vertical and lateral distances were 44.94 cm and 25.28 cm, respectively. In addition, it was observed from the modeling results that a depth of 20 cm was sufficient for 13 hours of water infiltration in sandy soil. The following section focuses on a soil tank experiment designed

to assess the infiltration characteristics of SIS, leading to an evaluation of model performance.

4.3 Soil tank experiment for HYDRUS-2D/3D model performance assessment and percolation velocity determination

A soil tank experiment was conducted to obtain a reference data set for assessing the numerical simulation outcome. The model performance was assessed by comparing the simulated and experimental VWC and determining the coefficient of determination (R^2) and root mean square error (RMSE). Additionally, different tracing methods, such as soil moisture sensor and direct push (DP) optical image profiler (OIP), were used to measure the percolation velocity in soil, as it is an important parameter that indicates the efficiency of recharging an aquifer (O'Geen et al., 2015). The following sections provide a detailed explanation of the performed experiment and associated results.

4.3.1 Soil tank experiment

The experimental setup comprised a soil tank, sandy soil, a garden pump, SIS, moisture sensors, DP OIP, uranine tracer, and a water barrel (Figure 27). The soil tank was 110 cm long, 90 cm wide, and 90 cm high, with a volume of 0.9 m^3. The sandy soil had particles ranging from 0.002 to 2 mm (2% clay, 4% silt, and 93% sand) and a 2.62 gm/cm^3 particle density. It was filled in the soil tank at 5 cm intervals and compacted with a rubber pad and hammer. Each layer was scraped after compaction in order to avoid stratification.

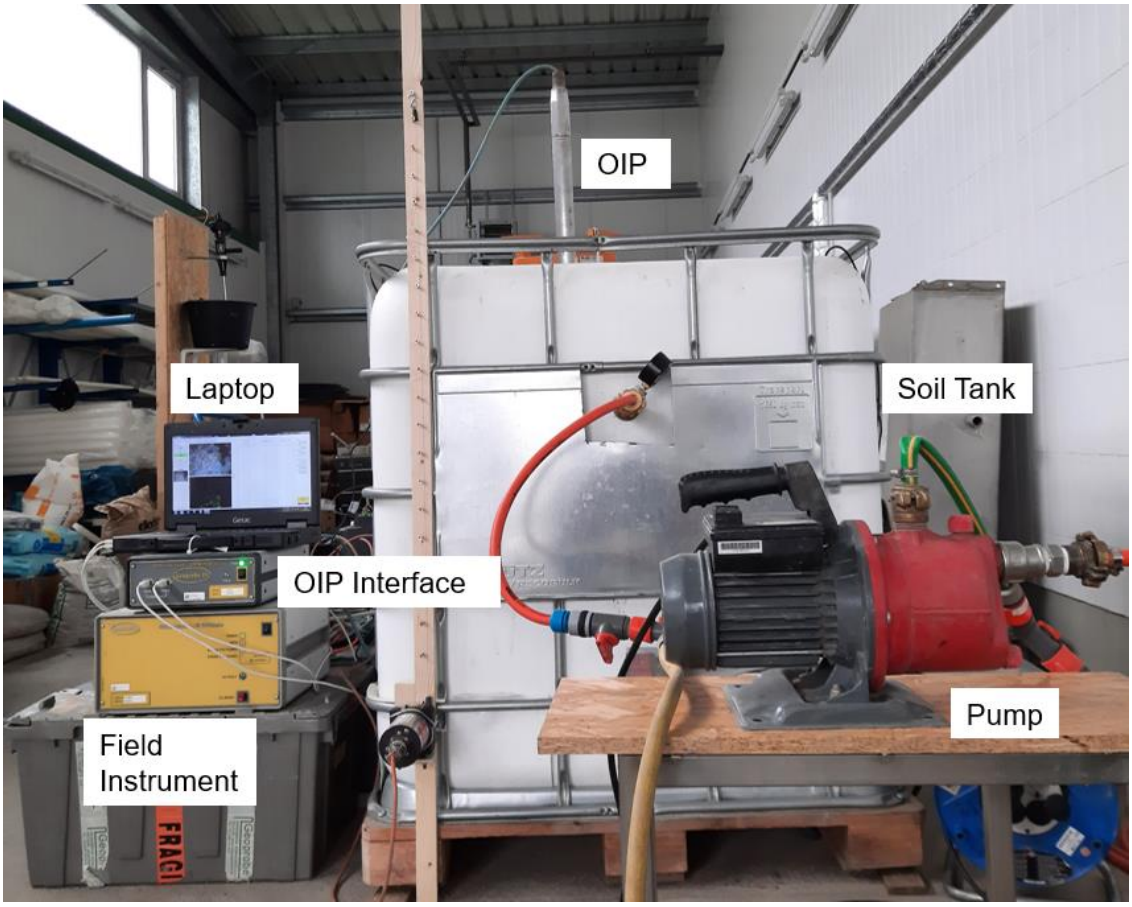

Figure 27 Setup of the soil tank experiment.

Commonly, time domain reflectometry (TDR) and capacitance sensors are used to continuously monitor the soil water content. The TDR technique measures the propagation rate of a high-frequency signal through waveguides in the sub-surface (Kirkham, 2014). TDRs have demonstrated high accuracy operating at the 1 GHz frequency, but high cost limits their application to more extensive networks (Kanso et al., 2020; Topp et al., 1980). The EC-5 uses capacitance/frequency domain technology to measure the dielectric constant of the medium. The sensors are designed to operate from -40 degrees to +50 degrees (Decagon Devices, Inc., 2014). Data can be sampled and recorded from the Decagon EC-5 sensors using several commercial data loggers with sampling times of 10 ms. With an accuracy of 3%, the EC-5 sensor measures VWC between 0% and 100%. A standard EC-5 sensor measures 9.9 cm in length, 1.8 cm in width, and 0.7 cm in height and has a measurement volume of 0.24 cm^3 (Jackisch et al., 2020). The sensors can be easily installed in soil (Parsons & Bandaranayake, 2009) and

connected to a close network that enables detailed spatial determination of the soil's VWC distribution. Hence, in this experiment, EC-5 sensors were used to measure VWC and were installed at varying depths (Figure 28a, 28b) for VWC measurements. The sensors were placed 10 cm apart to avoid magnetic interference between their fields (Figure 28a). The SIS with 100 cm length was placed 20 cm below the subsurface (Figure 28c).

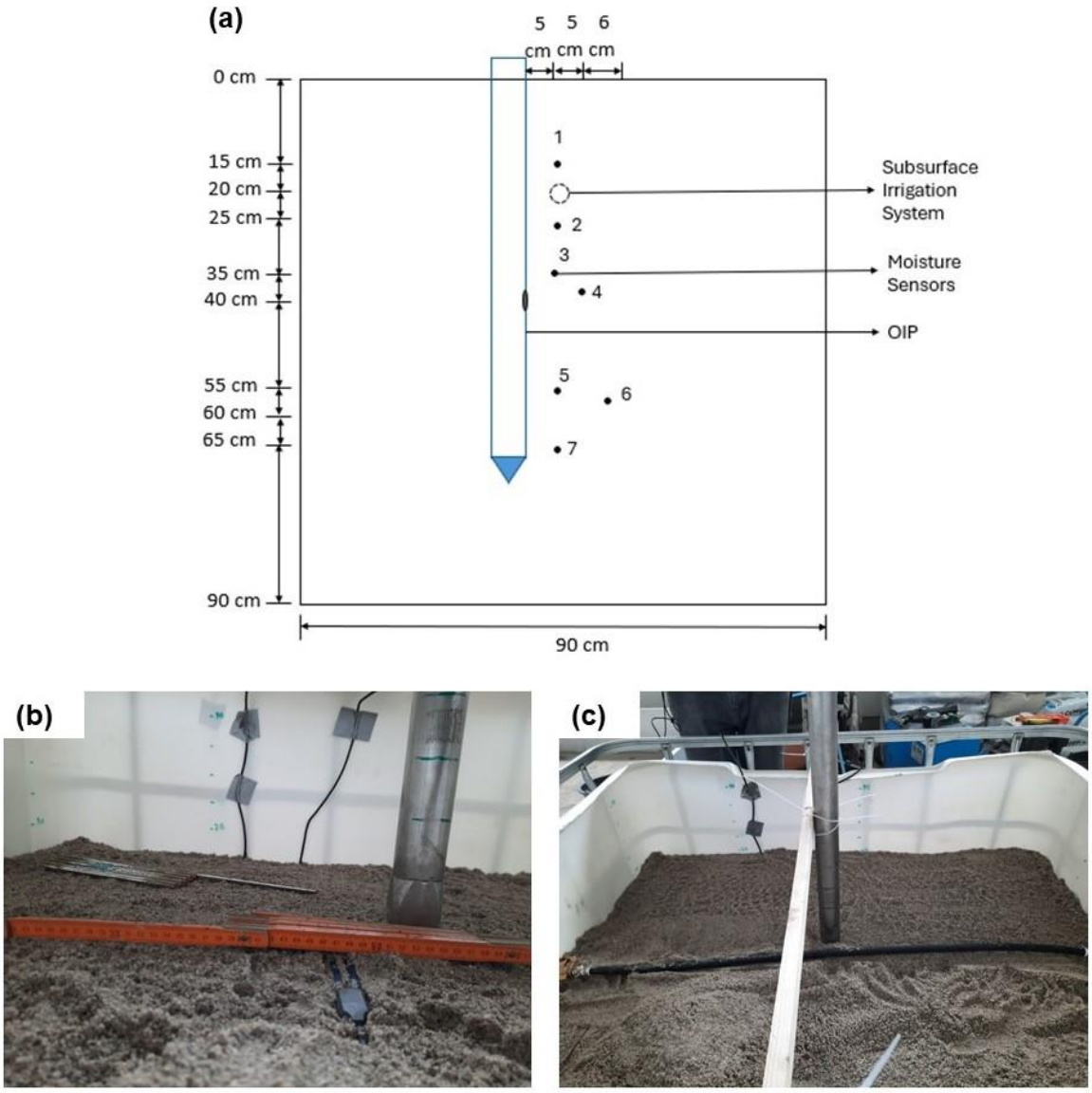

Figure 28 (a) Schematic diagram of the cross-section of the experiment representing the location of moisture sensors, SIS, and OIP (Picture not to scale) (b) Placement of soil moisture sensors (c) Placement of SIS in sandy soil at 20 cm depth from the surface.

Soil moisture sensors are also used to determine percolation velocity in soil (Hardie et al., 2013). However, the average moisture content is determined within a given soil volume around the sensor (Jackisch et al., 2020), leading to earlier detection of water or tracer arrival even though it has not reached the sensor's exact location. On the contrary, OIP estimates the percentage area of fluorescence (%AF) in the soil adjacent to the camera (Reischer et al., 2020). In this experiment, OIP was used to detect the presence of a fluorescent tracer instead of its standard use in the field. A uranine tracer was mixed in the water to determine percolation velocity by OIP as a reference measurement for identifying the integral volume influence of moisture sensors. In contrast to the usual deployment of the OIP system in the field (refer to Section 2.2.3), the probe was placed within a soil tank at a defined position (Figure 28a). The optical opening of the OIP probe was positioned 40 cm below the soil surface and at a horizontal distance of 5 cm from the SIS. After installing the OIP, the sand was refilled in the soil tank at every 5 cm interval. We avoided manually advancing the probe with hammer strikes as it would disrupt the soil compaction and influence the water flow path.

A Variolux V-GP 900 pump with a maximum conveying amount of 3600 l/h was used to supply water to the SIS. As the pump's capacity was high, the total flow rate of the pump was divided into three subflows using two bypasses. Two of the subflows were directed toward the water storage tank, ensuring the pump's flow rate was not significantly reduced. Finally, the third subflow flow was diverted to the SIS pipe to supply water at 0.6 bar for infiltration. The uranine tracer was mixed with water at a concentration of 20 mg/l to detect fluorescence by DP OIP.

The experiment was run for 13 hours at a constant 0.6 bar pressure. The fluorescence was detected in real-time with the DI acquisition software. In the following, the captured images and the %AF were used to assess the tracer breakthrough curve and to compare it with the moisture data recorded by EC 5 sensors. The %AF in a given image is computed based on the number of pixels in the image that detects fluorescence (Reischer et al., 2020). In this case, %AF indicates the presence of uranine tracer within the images.

4.3.2 Comparison of soil moisture sensor and direct push optical image profiler

The EC-5 moisture sensor and the OIP probe were placed at the same depth of 20 cm and 5 cm horizontally from the subsurface irrigation pipe (Figure 28a). Figure 29 reveals the variation of UV-induced fluorescence at different times during the experiment.

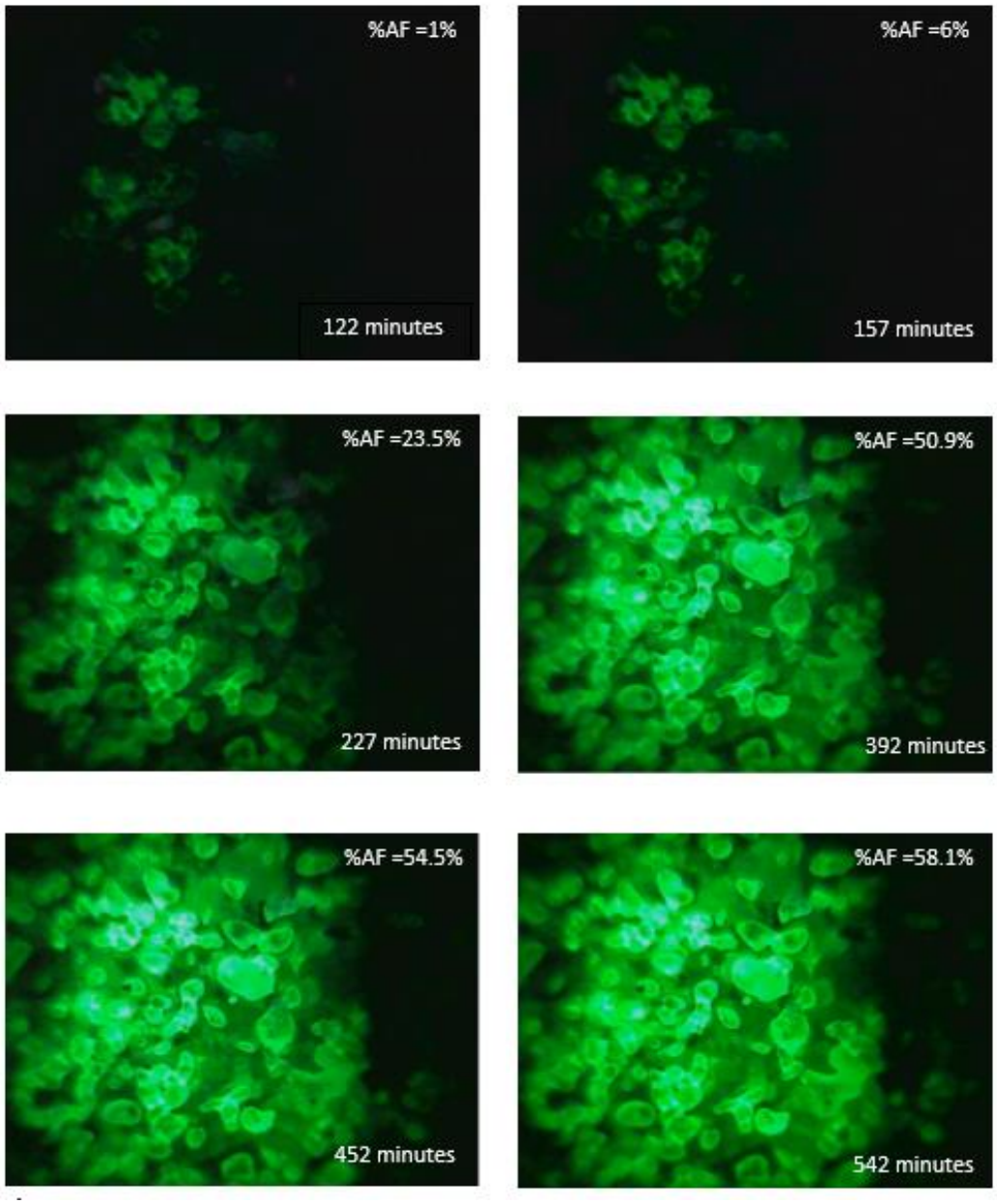

Figure 29 Variation of % AF at different time steps.

Additionally, Figure 30 represents the distribution of %AF determined by OIP and moisture content obtained by EC-5 sensor for 13 hours in sandy soil.

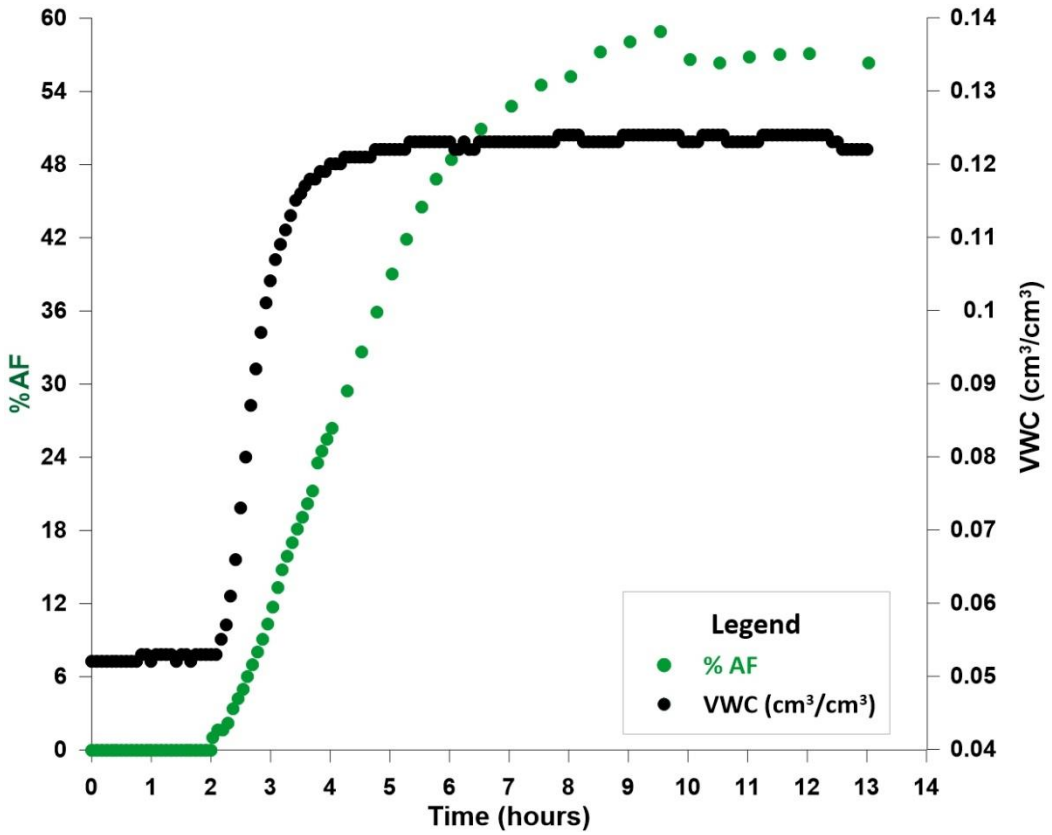

Figure 30 Detection of tracer arrival by OIP and EC-5 sensor.

It is visible from the figure that the presence of fluorescence was detected 122 minutes after the experiment began. As the VWC increased from 5.2%, it remained relatively constant after 210 minutes, varying between 12.1% and 12.4%. The %AF analyzed by the OIP increased up to 575 minutes and then stabilized at 56-57% after 600 minutes. The percolation velocity from SIS to the observation point was calculated to be 9.84 cm/h. After 130 minutes, the EC-5 moisture sensor measured a variation in VWC at observation point 4. The OIP probe detected the fluorescence, providing real-time information on tracer presence. The EC-5, on the other hand, measured the VWC at 5-minute intervals, though it had a frequency measurement of 10 ms. The interval values were chosen based on different studies conducted for VWC measurement (Dirwai et al., 2021; Sales et al., 2015; Thompson et al., 2007). Due to the selected time interval, the level of detail and the immediate nature of the information obtained were influenced, which made it difficult to compare the breakthrough curve. However, it is noticeable that the difference in the time for detecting the tracer's arrival was small, indicating the feasibility of using EC-5 sensors to determine the percolation velocity. Also, the measurement volume of the EC-5 sensor

is 240 cm^3 (Kanso et al., 2020), which is smaller compared to other soil moisture sensors, e.g., TDR, 5TM, 10HS, Trime Pico 64, etc. Further information regarding the measurement volume of these soil moisture sensors can be found in Jackisch et al., 2020. Moisture content changes within large integral volumes may influence the percolation velocity evaluation. In contrast, OIP provides more localized measurement by determining the percolation velocity when the tracer moves along the camera screen.

Additionally, soil moisture sensor installation at greater depths in the field can be complicated. The sensors can be installed in two ways: (i) by excavation of a trench or hole and horizontal installation of the sensors at various depths towards the crop root zone, or (ii) by using an auger or soil sampling probe to excavate a hole and vertical installation of the sensors down to the bottom of the hole. Special tools to secure sensors at greater depths during installation are required for the latter method (Sharma, 2018). Soil disturbance and the potential for soil compaction can occur when inserting soil moisture sensors into the subsurface (Fares & Polyakov, 2006). Also, soil-specific calibration of moisture sensors is necessary because sensors respond differently to changes in soil moisture depending on soil texture (Mochizuki & Sakaguchi, 2023; Silva et al., 2021). Moreover, it is time-consuming and labor-intensive to install wired sensors in the soil profile (Liao et al., 2021). Another advantage of the OIP is its ability to measure percolation velocity at greater depths without excavation. These advantages provided by OIP make it an effective tool for determining water percolation velocity in soil.

4.3.3 HYDRUS-2D/3D model's performance assessment

The results of VWC distribution with time in sandy soil at six observation nodes are presented in Figure 31. The observed upward and downward wetting front velocity was consistent with the simulated percolation velocity except at observation points 4 and 7. At observation 4, the model predicted the arrival of water 45 minutes later than the observed value. Based on the numerical simulation, water reached observation point 7 after 6.5 hours, whereas based on measurements, it reached after eight hours.

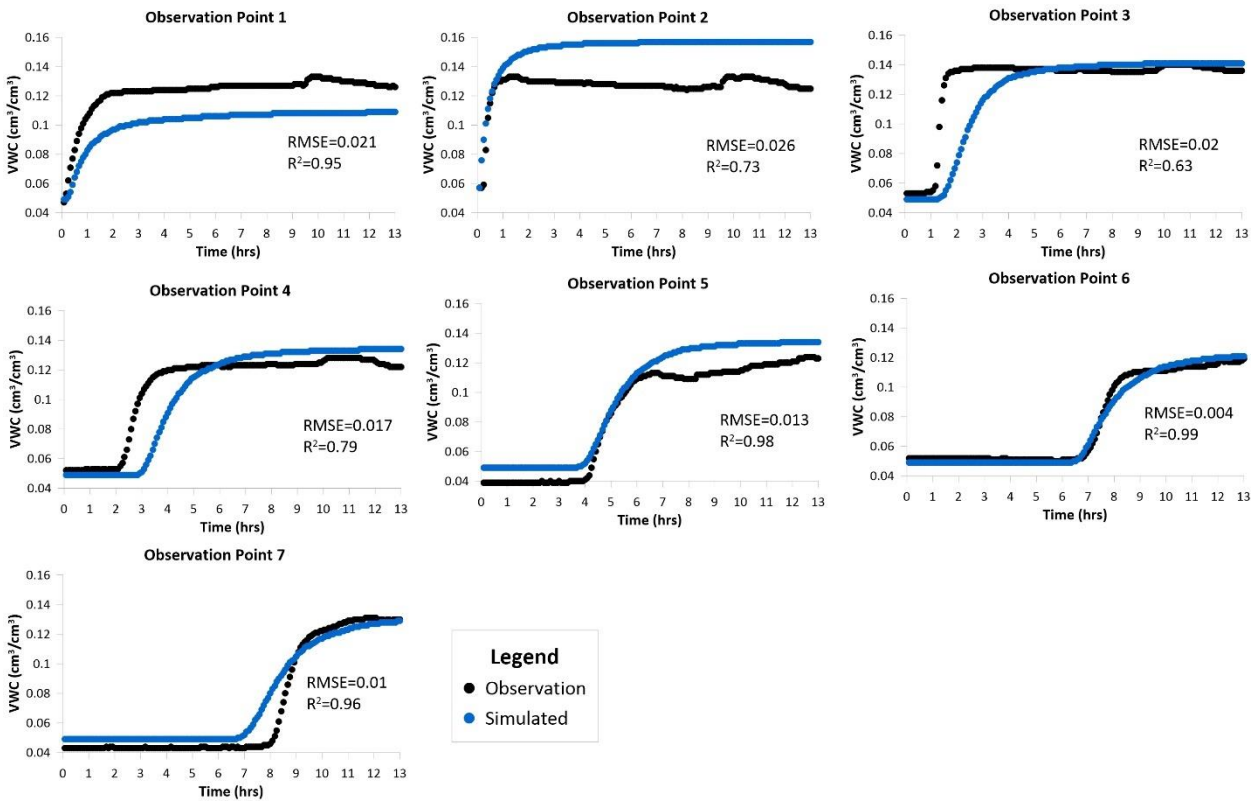

Figure 31 Observed and simulated VWC at seven observation points in sandy soil.

A difference between observed and predicted wetting front arrival at observation points 4 and 7 in the flow domain might be described by the influence of preferential water flow pathways and soil compaction at the observation nodes. In some observation nodes, VWC was different from simulated VWC. In our simulation, the hysteresis of the soil water characteristic curve was not incorporated, which may lead to the deviation between observed and predicted VWC.

The performance of the HYDRUS-2D/3D simulation was evaluated by the coefficient of determination (R^2) and root mean square error (RMSE). These parameters are expressed in the following equations.

$$RMSE = \sqrt{\frac{1}{n}\sum_{i=1}^{n}(Y_o - Y_s)^2} \quad (13)$$

$$R^2 = \left[\frac{n\sum(Y_o Y_s) - (\sum Y_o)(\sum Y_s)}{\sqrt{[n\sum Y_0^2 - (\sum Y_o)^2][n\sum Y_s^2 - (\sum Y_s)^2]}}\right]^2 \quad (14)$$

Where, Y_o is the observed parameter value, Y_s is the simulated parameter value, n is the total number of measured data, and i= numbers 1, 2, 3…. n.

A general estimation of the extent to which the observed data differs from numerical simulation predictions is provided by R^2. The numerical value zero indicates that the proposed numerical model does not improve the prediction. In contrast, the numerical value 1 shows that the model makes a perfect prediction compared to the average model. Based on RMSE, the goodness-of-fit between simulated and observed values can also be quantitatively compared. A lower RMSE value means a better fit to the model.

In this study, the RMSE value varied from 0.004 to 0.026, indicating a minimal spread in data between observed and predicted values. Moreover, the model is well fitted as the R^2 ranged between 0.63 and 0.99, which indicates that HYDRUS-2D/3D accurately predicts the infiltration behavior of SIS in sandy soil. Therefore, numerical simulations with HYDRUS-2D/3D will be carried out to determine the optimum installation depth of SIS.

4.4 Assessment of the feasibility of subsurface irrigation system

The evaluated model was upscaled and simulated with different installation depths of SIS to determine the optimum installation depth for a hypothetical case. The hypothetical scenario allowed, without the limitations of practical implementation, to investigate the system's behavior at different installation depths. The dimension of the model was 2 m × 2 m. Four cases were simulated with installation depths of 20, 30, 40, and 50 cm. The simulation was conducted to evaluate the distribution of the wetting front depending on the installation depth.

For agriculture, greater vertical distribution may not be preferred since water movement under the root zone can lead to water wastage, loss of nutrients, and groundwater contamination. Overlapping the wetted area under the irrigation system maximizes the amount of horizontal movement compared to vertical movement for a particular irrigation application (Skaggs et al., 2010). In groundwater recharge, avoiding overlap will foster a

more widespread distribution of recharge in the soil, with the potential to reach deeper depths for more efficient groundwater replenishment. Therefore, the maximum dimension of the wetting front in the horizontal direction is obtained from the model results, which allowed the determination of the distance between the SIS so that the overlapping of the wetting front is avoided. The model was simulated over an assumed MAR operation period of 200 days. The next step was to estimate the cumulative infiltration rate based on the appropriate number of SIS line sources. The SIS infiltration rate was compared with the observed rates in surface spreading methods to assess its competitiveness. The variation of wetting pattern dimension simulated for different installation depths after 200 days of operation is represented in Figure 32.

The wetting zone decreased with decreasing placement depth. The initial movement of the wetting front was faster. It gradually slowed down as the infiltration time increased. At constant depth, the horizontal wetting front was smaller than the vertical wetting front due to gravity. The SIS that was installed 20 cm deep took 24 hours for the wetting front to reach the soil surface. The SIS installed at a depth of 30 cm had the wetting front almost reaching the surface. After 200 days, the wetting front did not reach the soil surface for the SIS installed at 40 and 50 cm depths. As both of these installation depths prevent the wetting front from reaching the surface and consequently reduce evaporation loss, opting for the 40 cm depth may reduce the excavation costs compared to the 50 cm installation depth. The maximum distribution of the wetting front in the horizontal direction for the SIS installed at 40 cm is approximately 135 cm, indicating that at least 2.7 m distance should be maintained between the SIS.

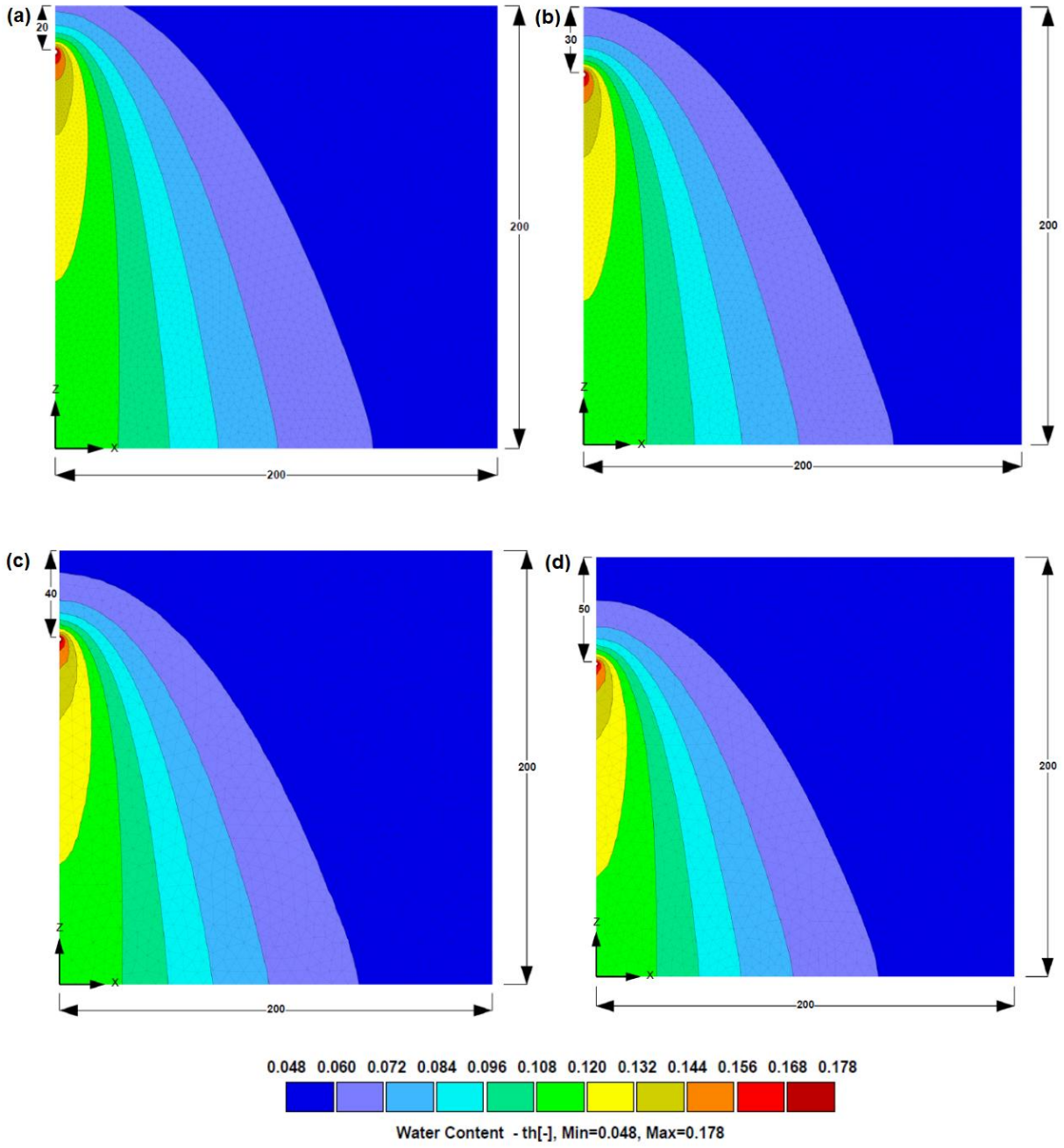

Figure 32 Wetting pattern distribution of SIS in sandy soil after 200 days with installation depths at (a) 20 cm, (b) 30 cm, (c) 40 cm, and (d) 50 cm

The approach we used in this study was a decision-making tool to assess the depth and the spacing of SIS in various operational scenarios, among which we considered 200 days operation of the system. By simulating scenarios and modes of operation, the model

assists in analyzing how the depth and spacing of installations can change over time. This considers instances of operational schemes and potential interruptions of the system.

According to Bouwer, 1999, typical infiltration rates of surface infiltration systems range from 0.3 to 3 m/day for river waters that are relatively clean and low in turbidity. Furthermore, other studies have calculated infiltration rates of infiltration basins, which range from 0.1 to 3 m/day (Beganskas et al., 2017; Hellauer et al., 2018; Mawer et al., 2016; Racz et al., 2012). If an infiltration pond has a surface area of 1.1-hectare and a maximum infiltration rate of 3 m per day, it will recharge 3.2×10^7 L/day of water through the vadose zone. Additionally, with a lower infiltration rate of 0.1 m/day, the total amount of water that will be infiltrated is 1×10^6 L/day. If SIS is used to infiltrate as a line source in a 1.1-hectare area (Length = 162 m, width = 66 m) composed of sandy soil, then 60-line sources with 66 m length can be installed with 2.7 m spacing. The total amount of infiltration through SIS will be 1.12×10^5 L/day. The SIS installation as a line source exhibits limited competitiveness compared to the infiltration basin. Therefore, it is important to explore several options for enhancing its functionality. One aspect of this could be the modification of the SIS in terms of design and installation, aiming to improve its performance.

5 Evaluation of the performance and effectiveness of the developed subsurface irrigation system approach for determining its competitiveness with the surface spreading method

This section describes the design and field assessment of modified SIS installation for groundwater recharge to determine its technical and economic competitiveness with traditional surface spreading techniques. Following the model and laboratory experiments of line source SIS, SIS prototypes were designed, and their infiltration characteristics were simulated using the HYDRUS-2D/3D software for planning a field recharge experiment. The field experiment was conducted in Guntersblum, Germany, to determine the infiltration rates of the prototypes. Furthermore, to assess the competitiveness of the

modified SIS design in comparison to surface spreading, an infiltration trench was simulated to investigate its technical potential. Finally, the technical potential and levelized costs were compared with the infiltration trench under a given area.

5.1 Design of subsurface irrigation system prototypes

The SIS faces challenges competing with other surface infiltration methods in its current form or configuration as a line source. This suggests that the approach needs to be more efficient at achieving increased infiltration rates. It is expected to install SIS straight in a line to supply water to plants. In order to optimize infiltration rates for a unit area, innovative designs have been implemented for recharging the aquifer with SIS. These designs are similar to structures known as geothermal energy baskets (Boughanmi et al., 2017). The conical configuration, with its increased surface area (Figure 33), can offer the possibility of accommodating longer lengths of SIS with efficient utilization of the space available.

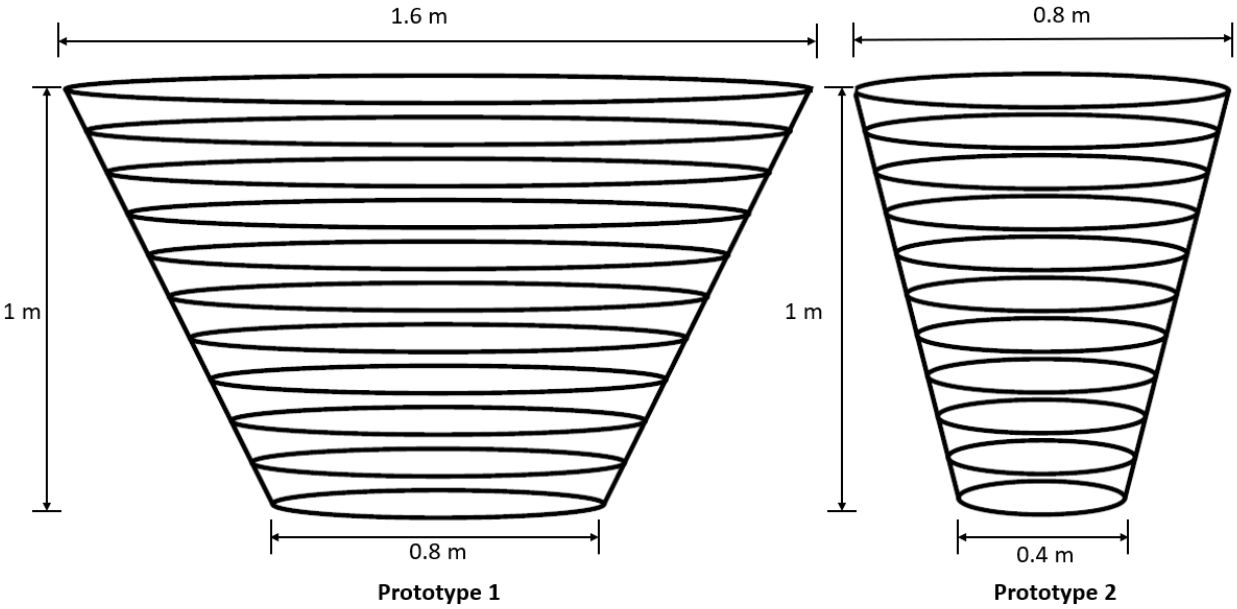

Figure 33 Designed prototypes for Field Experiment (Picture not to scale).

Two conical prototypes were designed with different dimensions to ensure the SIS would not require large installation areas. Prototype 1 had a top diameter of 1.6 m and a bottom diameter of 0.8 m, comprising a total length of 40 m. Prototype 2 measured 21 m in length,

with a 0.8 m top diameter and 0.4 m bottom diameter. Each prototype was 1 m in height (Figure 33).

5.2 Study area

The infiltration behavior of two prototypes was investigated at a site, which is a water pumping station located in Guntersblum, Germany (Figure 34). The site is owned by Wasserversorgung Rheinhessen-Pfalz GmbH (WVR), the second-largest drinking water supplier in Rhineland-Palatinate.

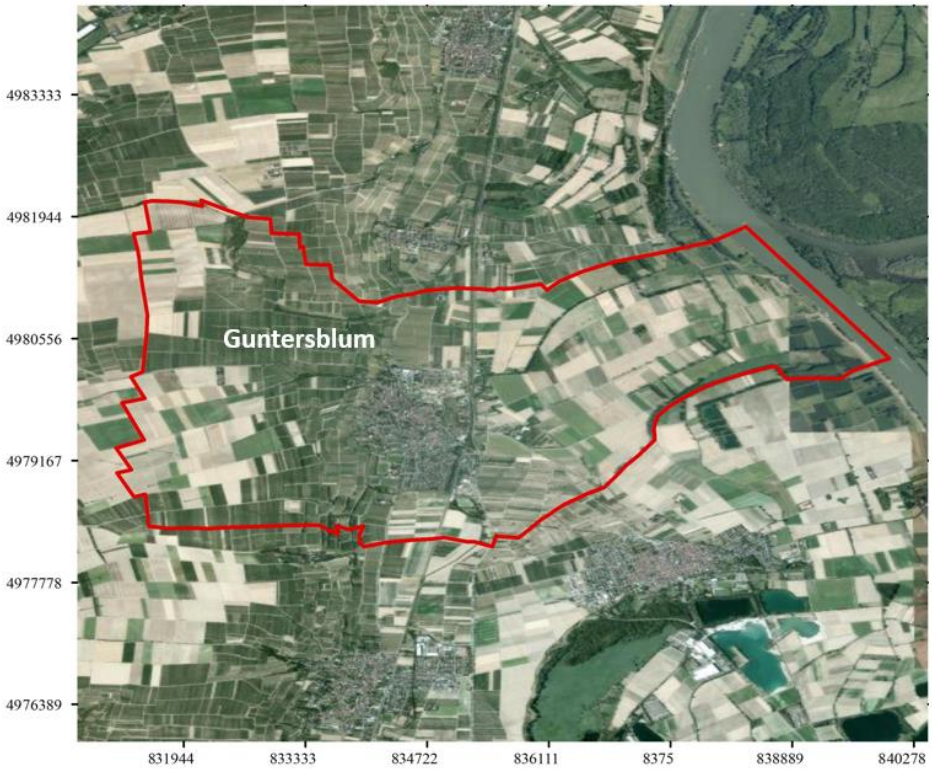

Figure 34 Location of Guntersblum in Germany.

Climate change is already impacting water resources in typically water-abundant regions such as Germany, where average water scarcity is minimal. However, prolonged and exceptional droughts have occurred in recent years due to hot and dry summers (Wriedt, 2019), causing groundwater declination. Due to a decrease in the recharge of groundwater and an increase in water demand during summer, regional water suppliers are being pushed to their capacity to meet the demands during dry periods. In the future, regions in Germany could face heightened conflicts over water distribution among

domestic, agricultural, and industrial uses (Philipp & Kraljevic, 2015). Furthermore, the recent drought and low precipitation rate have reduced water levels in the Rhine River (Brito & Kuhlicke, 2020; Gobert & Rudolf, 2023).

The test site's location near the Rhine River implies that variations in the river's water level may have consequences on groundwater levels and groundwater resources in the area. The study area exhibits a range of groundwater levels, from 4.5 to 6 m bgl. The height of the prototype was limited to 1 m to avoid costly excavation and potential installation close to the groundwater level due to the shallow water table in the study area. During periods of high demand, groundwater pumping can result in a reduction of groundwater level, which has implications for the reliability of water supplies. Therefore, a sustainable solution for recharging aquifers in the study area to meet future water demands was explored in collaboration with WVR. The company provided site stratigraphy information. Several boreholes are located in the area (Figure 35).

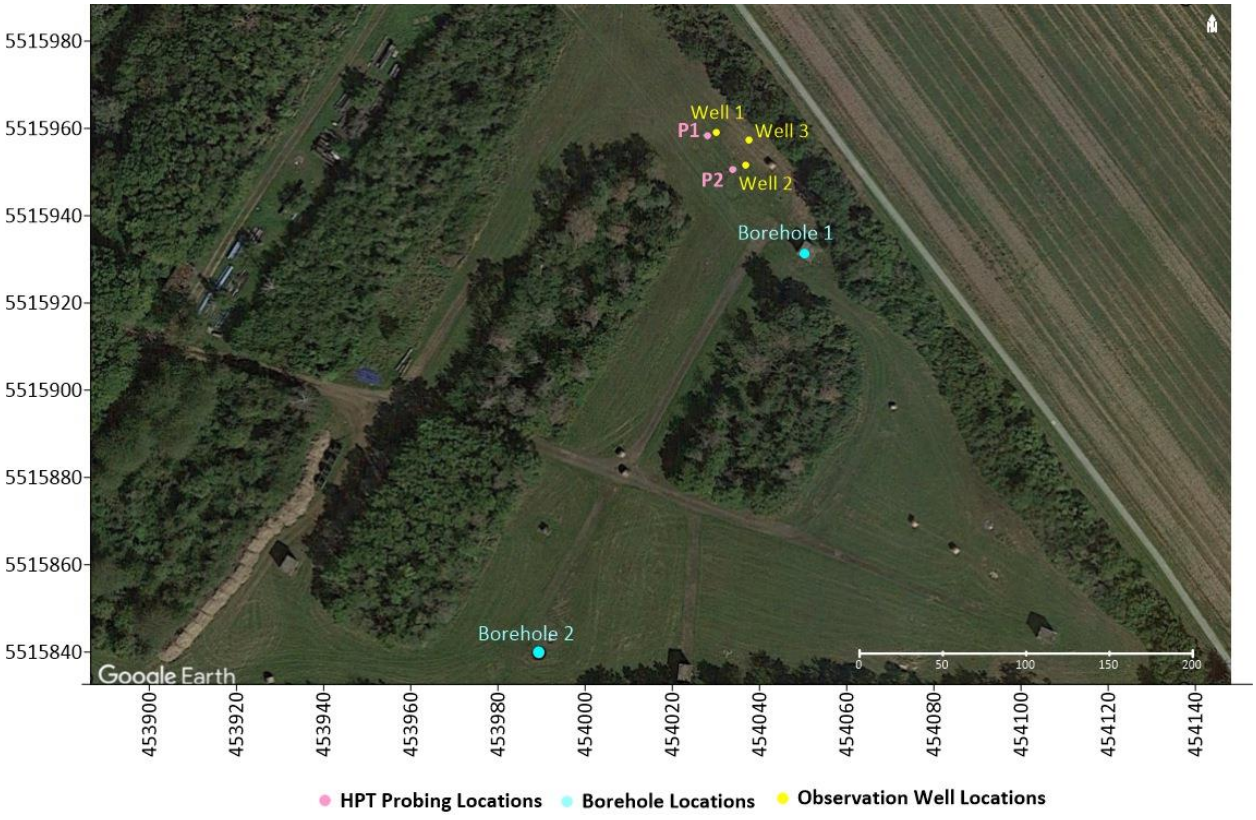

Figure 35 Locations of boreholes, HPT profiling, and monitoring wells in Guntersblum.

The stratigraphy of borehole 1 reveals that the soil up to 1 m bgl contains silt material. There is sand and gravel between 1 m and 48 m bgl indicates that the site is suitable for installing prototypes and has the potential to be one of the sites for MAR. At borehole 2, clayey sand is present up to 1.30 m bgl. Later, up to 13 m, the formation is a mixture of fine, medium gravels, medium to coarse sand, and fine sand. The stratigraphic data shows the variation in the depth of fine material in the study area.

Therefore, a site characterization was important to test the suitability of the prototype's installation points (P1 and P2). It was fundamental in identifying the required depths to be excavated at these specific locations, which depended on the characteristics of the soil encountered. While on-site investigations were essential to support on-site decision-making, understanding the minimal installation depth was also required to prevent evaporation losses and reduce excavation costs. In addition, for installing the prototypes in the field, the knowledge about the optimal distance between the SIS prototypes was vital for preventing any interference between them. Hence, numerical simulation was undertaken to determine these parameters for field experiment planning.

5.3 Numerical simulation for field experiment planning

Two separate models were set up using HYDRUS-2D/3D software for assessing the infiltration rates and the wetting pattern distribution of the SIS prototypes (Figure 36 & Figure 37). The models were set up in the axisymmetric domain to represent the conical shape of the prototypes. The models were conceptualized before the site characterization of the study area, and it was parameterized based on the information provided by WVR for designing the field experiment. The model domains consisted of 10 m by 14.5 m, with the SIS prototypes base located at 1.5 m below the soil surface. The model's dimension in the horizontal direction were selected in a way so that the right-side boundary does not have any impact on the model results. Each model was discretized into 24868 nodes with 0.1 m mesh size.

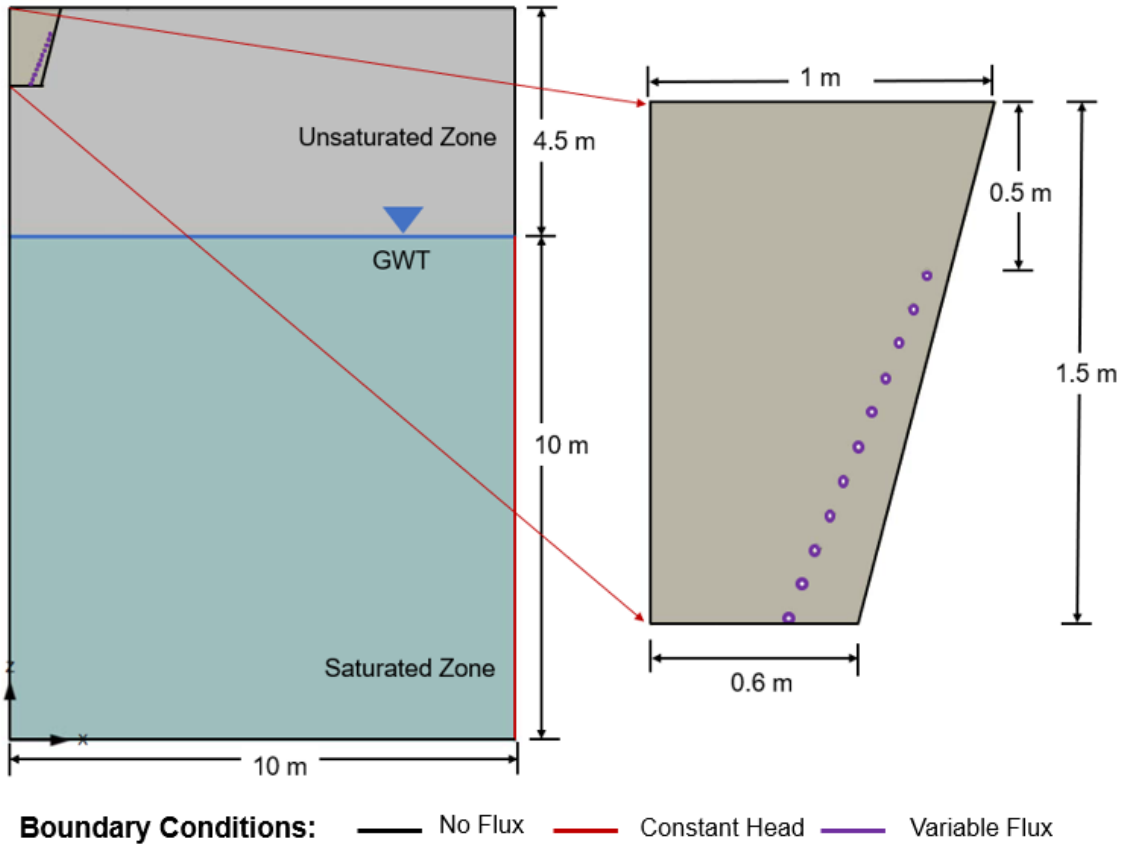

Figure 36 Schematic diagram of the conceptualization of the field model for Prototype 1. The circles represent the cross-section of the SIS prototypes.

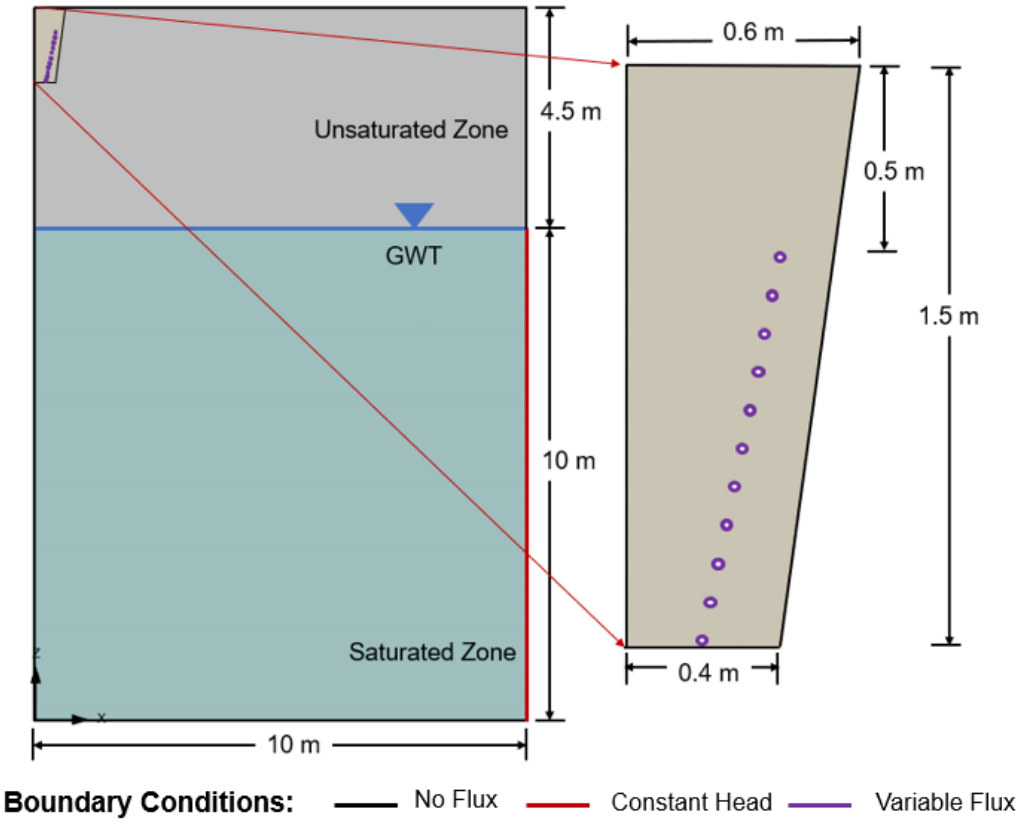

Figure 37 Schematic diagram of the conceptualization of the field model for Prototype 2. The circles represent the cross-section of the SIS prototypes.

As detailed soil profile information was unavailable at these locations, it was assumed that the unsaturated zone was composed of predominately sandy soil based on the overall information provided by the WVR. For the installation of the prototypes, the soil needs to be excavated, and the excavated area was considered trapezoidal in shape to provide soil stability during the installation of the prototypes. In the model for Prototype 1, the excavated area had a top width of 2 m, a bottom width of 1.2 m, and a height of 1.5 m. The excavation area for Prototype 2 model was 1.2 m in width at the top, 0.8 m in width at the bottom, and 1.5 m in height. Only half of the excavated area and prototype's diameter were defined in axisymmetrical domain since it represented radially symmetric condition.

For the backfilling of the excavation area, sandy soil was chosen to maintain consistency with the surrounding material. The soil materials were assumed to be homogeneous and

isotropic. Soil hydraulic properties were defined in a similar way according to the HYDRUS-2D/3D model of SIS in line source arrangement (Section 4.2.1). The K_s of the backfilled and surrounding sandy soils were determined by constant head permeameter test after collecting the soil samples from Guntersblum. Later, the model was refined with obtained values of 2.4×10^{-04} m/sec and 1.6×10^{-04} m/sec for backfilled and surrounding sandy soils respectively. Here, a saturated thickness of 10 m was considered, while an unsaturated zone was considered 4.5 m above. The pressure at the base of the saturated thickness was 10 m. It was linearly decreasing until it reached the WT, where the head was 0 m. For the vadose zone, a pressure head of -1 m was defined at the top, which then increased in a linear manner to 0 m towards the water table. The operating pressure of SIS prototypes was 0.8 bar in these two models. The models were simulated based on the planned experimental duration of 92 days.

5.3.1 Numerical simulation result of field-scale model

The simulated cumulative infiltration rate for both of the prototypes is shown in Figure 38.

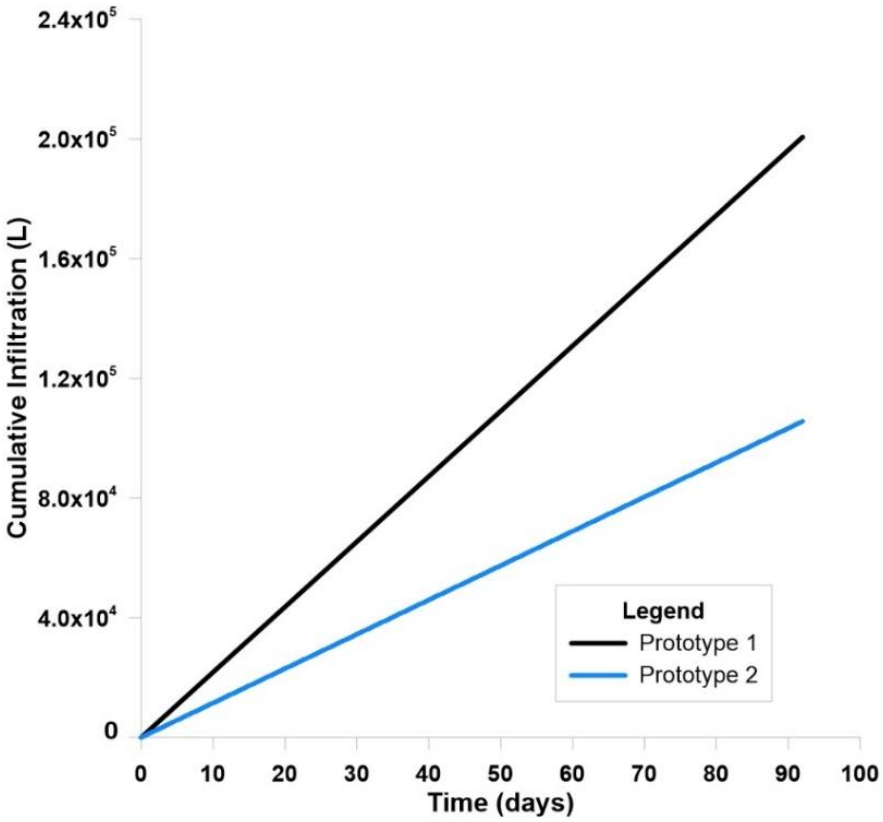

Figure 38 Cumulative infiltration rate of Prototype 1 and Prototype 2.

The simulated result demonstrated that Prototype 1 and Prototype 2 would infiltrate 2.01×10^5 L (5×10^3 L/m) and 1.1×10^5 L (5.2×10^3 L/m) of water in 92 days. Figure 39 shows the water content variation of Prototype 1 and Prototype 2 with time.

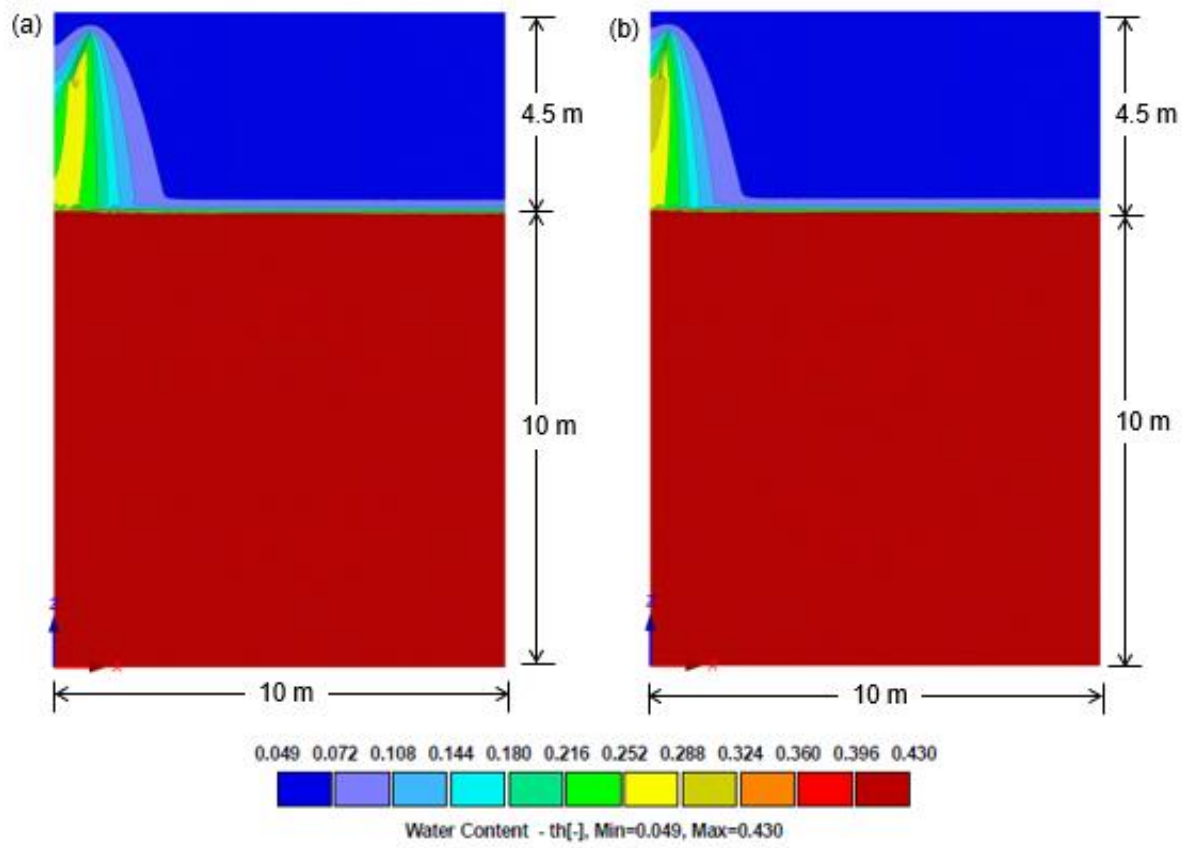

Figure 39 Wetting pattern distribution of Prototype 1 and Prototype 2 after 92 days.

The width and depth of the wetting front of both prototypes increased with time. After 92 days, the migration of the horizontal wetting pattern from the axis for both prototypes was 2.25 m and 2.1 m, respectively. As the radius of the prototypes was 0.8 m and 0.4 m respectively, the area of influence for each prototype was considered approximately 1.5 m. Hence, to avoid any interference, a minimum of 3 m distance should be maintained between the prototypes. Additionally, it was observed that the excavation depth of SIS prototypes at 1.5 m was sufficient to prevent evaporation loss and the discharge of water emerging on the surface. However, the excavation depth was dependent on the presence of high hydraulic conductivity material beyond this depth. Thus, a site investigation was carried out to assess the suitability of the prototype's installation points, providing

knowledge to make informed decisions regarding the excavation depth for the prototype installation. The details and outcome of the site investigation of the study area are elaborated in the next section.

5.4 Site characterization

Hydraulic profiling tool (HPT), a DP technique, was used to characterize the subsurface. In contrast to borehole information, HPT allows the identification of local small-scale confining layers with the combination of EC and pressure. In our study, HPT was used to ensure that there were no small-scale confining units beneath the prototypes that could potentially bias the infiltration experiment results. Also, the excavation depth for installing the prototypes was carefully selected using the information gained from this characterization.

Two HPT tests were conducted at P1 and P2 locations (Figure 35) up to a depth of 6 m. Tests and calibrations of HPT systems were performed with a pressure sensor. Deviation in pressure was found to be less than 10% which is acceptable for the proper functioning of HPT (McCall, 2011). Both HPT soundings directly assessed bulk formation EC, pressure response, and injection flow rate. The corrected HPT pressure (P_c) was obtained by subtracting hydrostatic and atmospheric pressures from the total HPT pressure. The Geoprobe® Direct Acquisition software was used to process and analyze HPT data. Figure 40 displays the EC variation, corrected pressure, and relative K in HPT soundings P1 and P2.

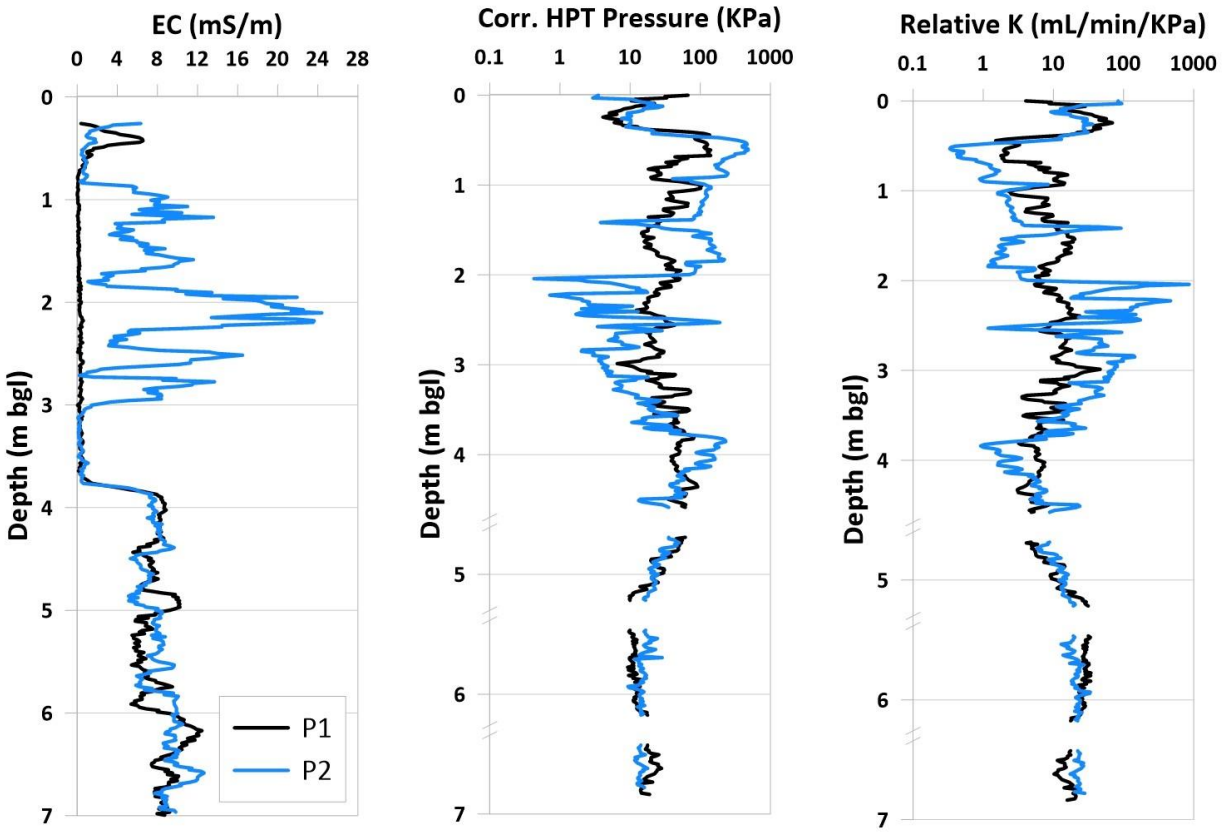

Figure 40 The variation in EC, corrected pressure, and relative K at P1 and P2 locations.

Figure 40 shows that at the P1 location, there was an increase in EC and pressure value from 0.3 m-0.6 m bgl, which indicated the presence of fine material. Additionally, from the field observation and core sample, it was visible that the soil material was compacted at around 0.5 m bgl and composed of sand and fine material. At 0.6-3.7 m bgl, the EC value varied from 0.01-0.78 mS/m, and the low EC value was due to the absence of electrical coupling between the EC sensors and surrounding material. The soil samples taken at this depth interval demonstrated that dry sand was present. Hence, there was no electrical coupling between the EC sensors and dry sand. At 3.73 m bgl, there was electrical coupling along with low EC values, indicating sand and gravel dominated formation. It was observed that, after 0.8 m, there was no fine material at this location. Hence, the excavation depth for installing prototype 1 was decided to be 1.5 m bgl. The groundwater table (GWT) at this location was measured at 4.52 m bgl.

Contrasting variations in EC could be seen by comparing the HPT logs at P2 with P1. Intermittent low conductivity layers, indicated by pressure variations, were observed between 0-3 m bgl. Soil sampling within this interval revealed a heterogeneous mix of sand, gravel, brick fragments, and fine materials. On-site observation suggested an artificial fill at this depth. It was difficult to identify the exact depth of the artificial fill due to the soil compaction in the core. This challenge in determining the depth of artificial fill highlights the importance of using HPT for field investigations. From 3 to 3.7 m bgl, the low EC value indicated the presence of dry sand. However, at around 3.7 m bgl, there is an increase in pressure and reduction in relative K, indicating the presence of a fine layer. Hence, a 4 m bgl excavation depth was chosen to reach the high hydraulic conductivity zone. The GWT measured at this location was 4.28 m bgl. HPT provided high-resolution data, allowing a detailed understanding of subsurface conditions, particularly where compacted or complex materials are present. HPT overcame the limitations of traditional core sampling, facilitating on-site decision-making to install two prototypes at these locations.

5.5 Technical potential evaluation of subsurface irrigation system prototypes

In this section, the field experiment to evaluate the technical potential of the prototypes and the findings are discussed. Additionally, the comparison between the simulated and observed cumulative infiltration rates is demonstrated.

5.5.1 Field experiment

Figure 41 shows the final installation layout of the SIS prototypes. A 0.9 m^3 water tank was used to supply water to the prototypes (Figure 41a). A pressure of 0.8 bar was maintained using two submersible pumps (Figure 41b) submerged in the water tank. This pressure, which is slightly higher than the initial optimum pressure, was selected for this experiment after corresponding with the manufacturer. Infiltration rates were measured using two Atrato flow meters (Figure 41c). Commonly, water flow meters are designed for higher flow rate measurements. Atrato flow meters measure lower flow rates ranging from

0.6 L/h to 102 L/h and have data logging features, making them ideal for the field experiment, where low flow rate measurement was important.

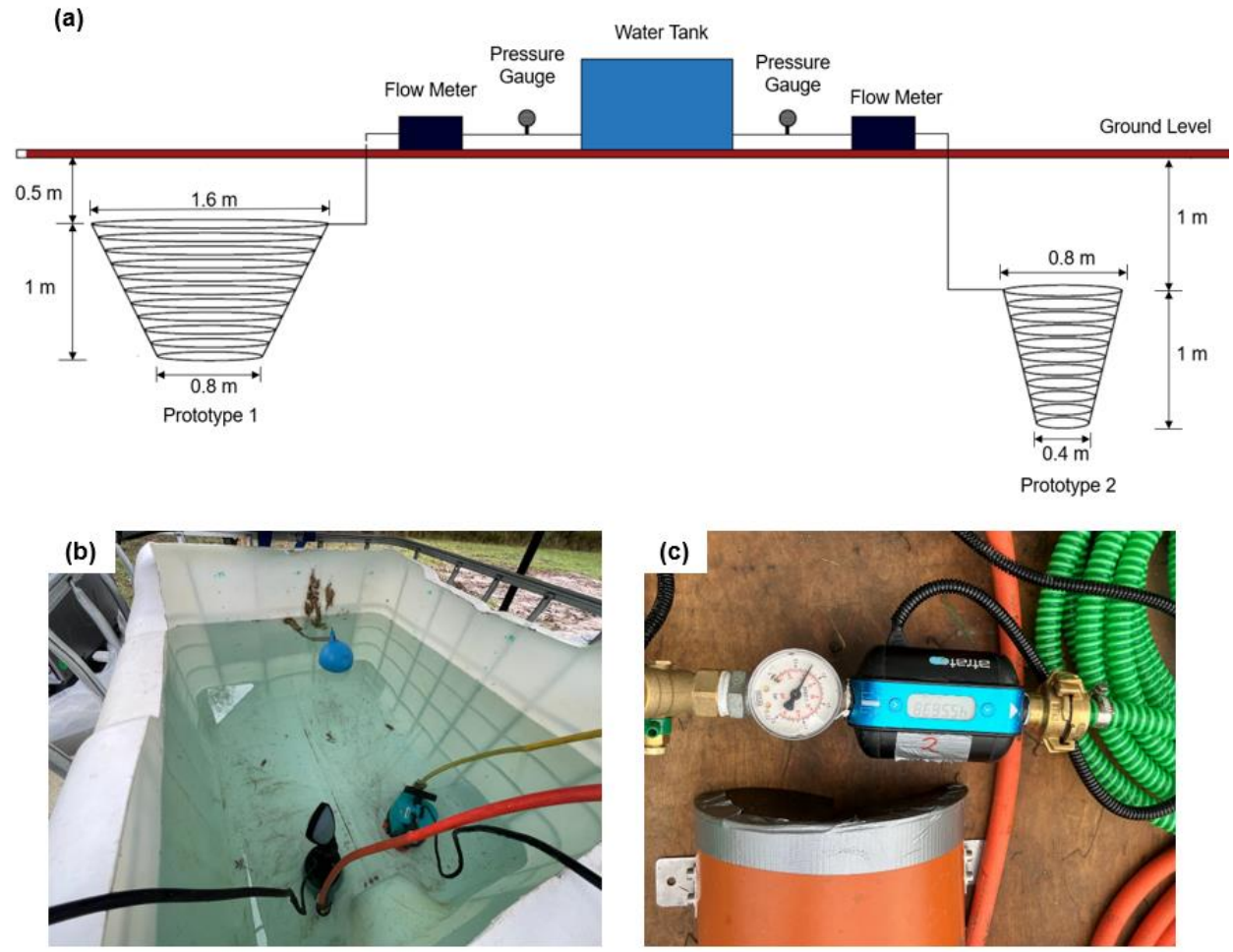

Figure 41 (a) Final installation layout of SIS prototypes (b) Submersible pumps (c) ATRATO flow meters.

Based on the site characterization result, excavation was conducted (Figure 42a) at P1 and P2 locations. At the P1 location, excavation was performed till 1.5 m bgl for Prototype 1 installation (Figure 42b). It was then filled with sand to reflect the aquifer's composition, with a hydraulic conductivity of 2.4×10^{-04} m/sec.

Figure 42 (a) Excavation of soil for prototypes installation (b) Installation of Prototype 1 at 1.5 m bgl.

At the P2 location, excavation was performed till 4 m bgl. Later, the excavated area was backfilled to a depth of 2 m to accommodate installing Prototype 2. This adjustment was

required because the width of the excavated trench decreased with depth and to avoid interference with the surrounding materials. It was then installed at 2 m bgl (Figure 43).

Figure 43 Installation of Prototype 2 at 2 m bgl.

Two monitoring wells (well 1 and 2) were installed 1 meter from the prototype to assess their influence on the groundwater level. In addition, a separate observation well (well 3) was installed at a distance of 7 meters from Prototype 1 to measure the baseline water level, which was not influenced by the infiltration of the prototypes. Groundwater levels can vary due to pumping activities, rainfall, or other environmental factors. These background variations can be distinguished from the variations caused by the prototypes by measuring the baseline water level.

5.5.2 Technical performance of prototypes

Infiltration rates of the Prototype 1 and Prototype 2 during the recharge test are shown in Figure 44 and Figure 45. The experiment was planned for 92 days for both prototypes.

Due to the defect in the pump, the experiment for Prototype 1 and Prototype 2 was run for 80 days and 90.25 days, respectively.

The submersible pump had a maximum capacity of 0.8 bar. At the end of the experiment, it was observed that the pressure dropped to approximately 0.65 bar for both prototypes. The reduction in the pressure could be attributed to friction loss along the water supply system (Provenzano et al., 2016) and pumping capacity reduction. The pressure change was not measured during the experiment. Consequently, identification of the actual time at which the pressure change occurred was difficult.

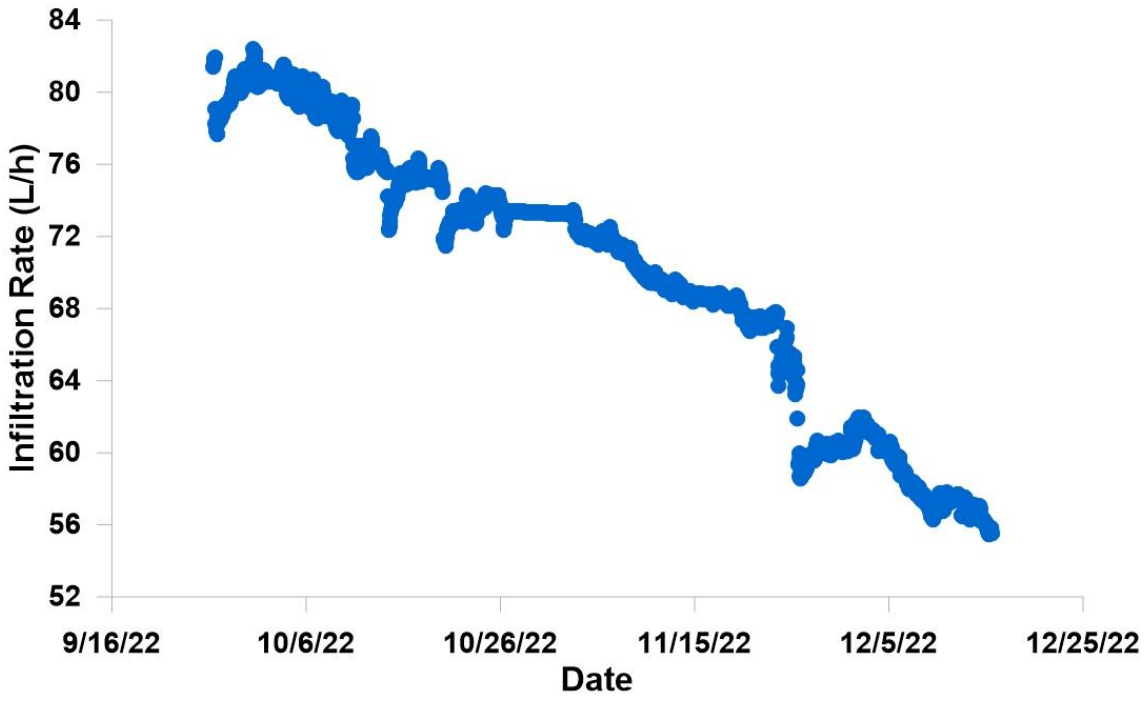

Figure 44 Infiltration rate of Prototype 1.

For Prototype 1 (Figure 44), a decreasing trend of the infiltration rate was observed. During this period, the maximum flow rate was 82.4 L/h, which was reduced to 55.4 L/h at the end of the experiment. The total amount of water infiltrated using Prototype 1 was 1.35×10^5 L in 80 days.

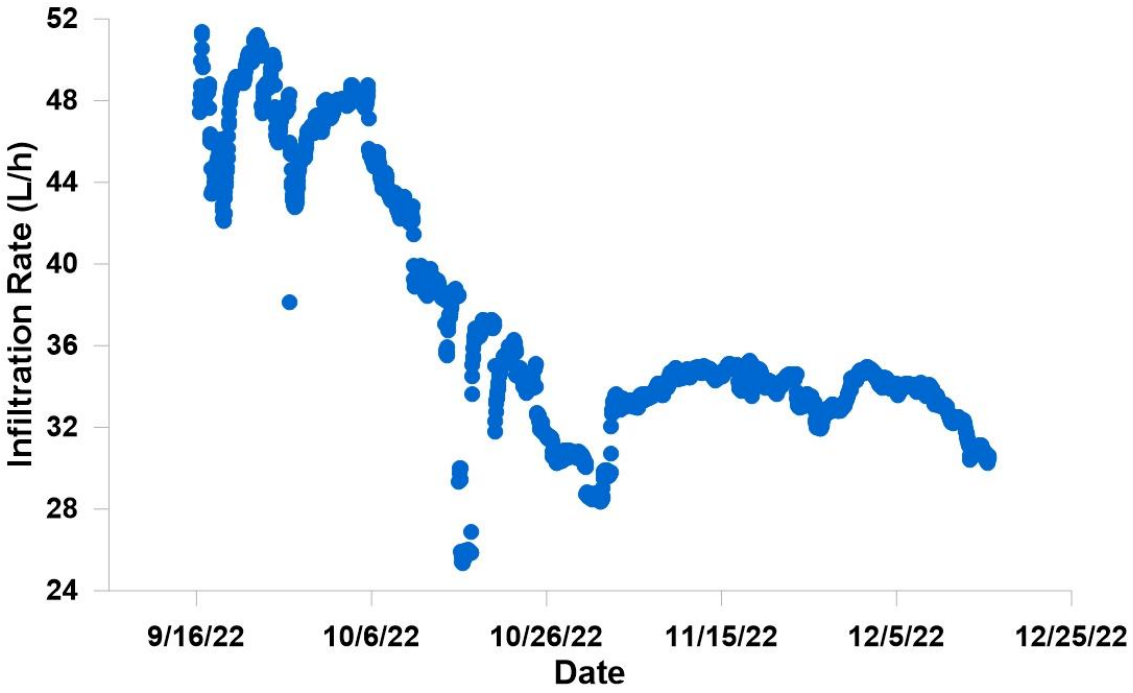

Figure 45 Infiltration rate of Prototype 2.

Prototype 2 infiltration rate also demonstrated a decreasing trend (Figure 45). The maximum flow rate of Prototype 2 was 51.39 L/h. It was reduced to 30.6 L/h at the end of the experiment. The total infiltrated water using Prototype 2 in 90.25 days was 8.1×10^4 L.

The average infiltration rate of both prototypes was approximately 1.8 L/h/m. The reduced infiltration rate in both prototypes can be explained by reduced pressure and clogging. The pressure-discharge characteristics of the SIS indicated that discharge is highly dependent on changes in pressure (Section 4.2.3). Reduction in pressure will decrease the infiltration rate of the prototypes. Studies conducted by Kanda et al., 2018; Makavana, 2018; Qi et al., 2021; and Silva et al. 2021 have also demonstrated the effect of pressure on the discharge characteristics of porous pipes. Wang et al., 2023 further demonstrated in their investigation that the porous pipe infiltration rate was in linear correlation with the pressure head. Soil particles can clog the pore spaces of the porous pipes, influencing the infiltration rate (Hallam & Lahlali, 2021; Kanda et al., 2018). During the experiment, algae formation was also noticed in the water tank, which might be transported by the supplied water to the SIS prototypes, causing the clogging of the SIS pores.

The changes in the groundwater level in three wells were monitored during the experimental period to assess the impact of the prototypes. Figure 46 represents the absolute change in groundwater levels in the wells. The absolute changes are represented here concerning well 3, which was monitored as a reference groundwater level. The figure shows that the infiltration of Prototype 1 does not influence the groundwater level in well 1. There is a maximum increase in groundwater levels of about 2.5 cm at well 2 which is not significant.

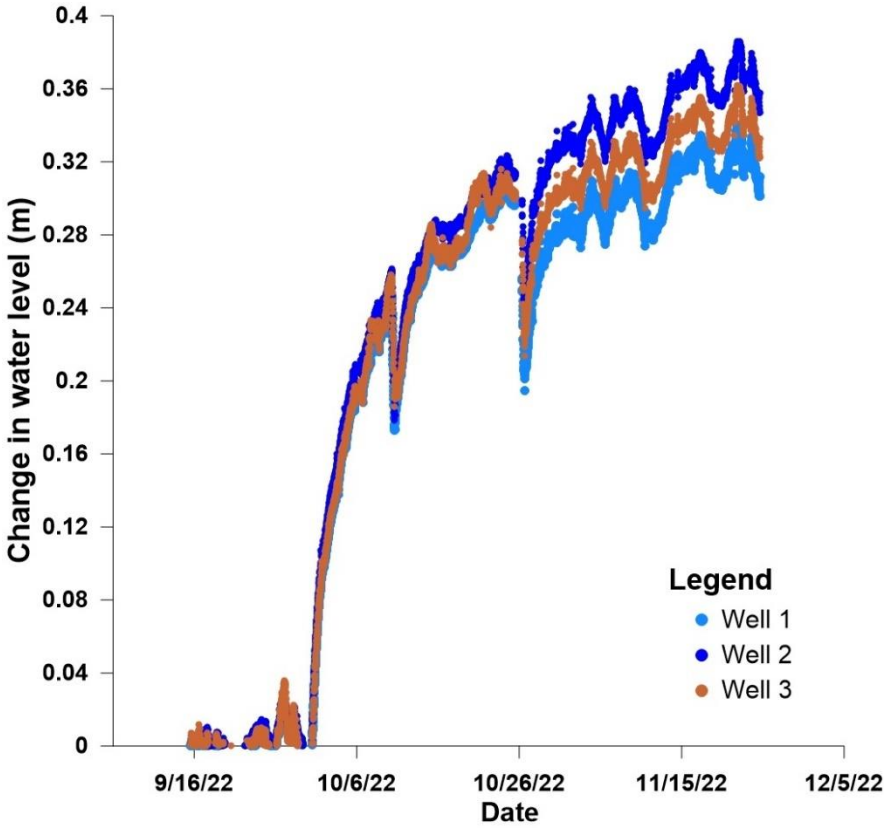

Figure 46 Relative change in groundwater levels in the monitoring wells.

It was also apparent that there was a sudden increase in water level in three wells in early October. It might be because of the termination of pumping activity near the area at the end of September. Further information on groundwater level was unavailable as the logging devices stopped recording data.

5.5.3 Comparison of the observed and simulated technical performance of the prototypes

The simulated cumulative infiltration rate and observed infiltration rate of prototype 1 and prototype 2 at constant 0.8 bar pressure are shown in Figure 47.

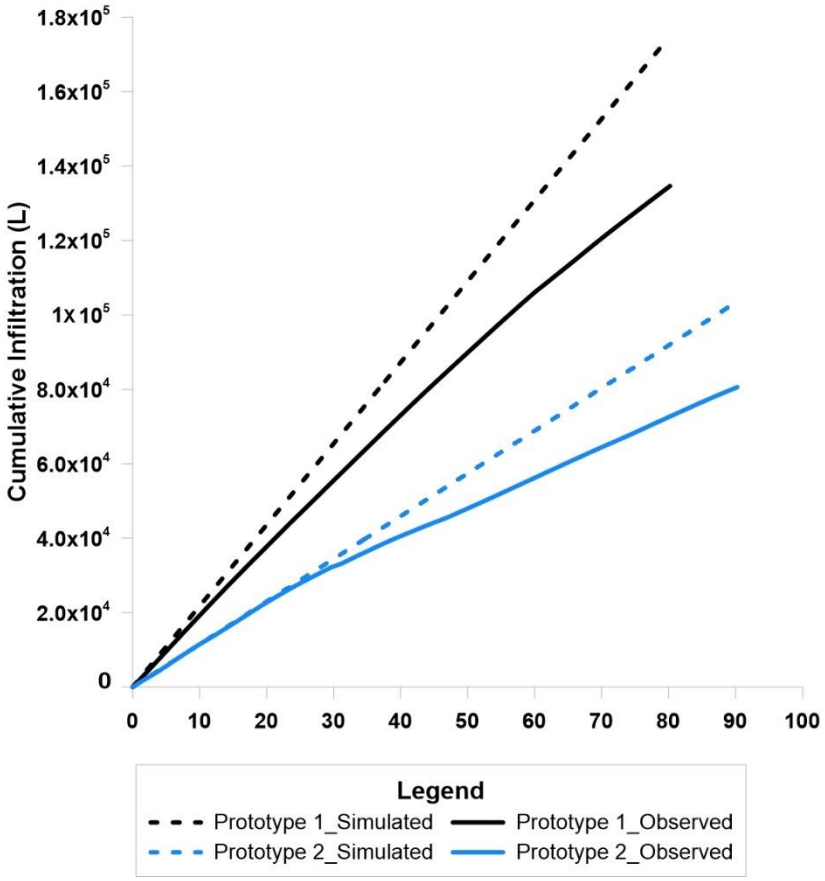

Figure 47 Observed and simulated cumulative infiltration rate of Prototype 1 and Prototype 2 (Constant pressure).

The models overestimated the cumulative infiltration rates of the prototypes. During the model simulation, the operating pressure value was 0.8 bar for the whole duration of the experiment. However, the pressure of the prototypes was not constant for the entire period of the field experiment. Since the operating pressure of the prototypes reduced with time, it could be one of the reasons that there was a difference between simulated and observed infiltration rates. Hence, the model was simulated again to investigate the effect of pressure on the infiltration rate, considering linear pressure change from 0.8 bar

to 0.65 bar. The model dimensions and associated parameters were consistent. The simulated cumulative infiltration rate with linear pressure change compared to the observed cumulative infiltration rate is presented in Figure 48.

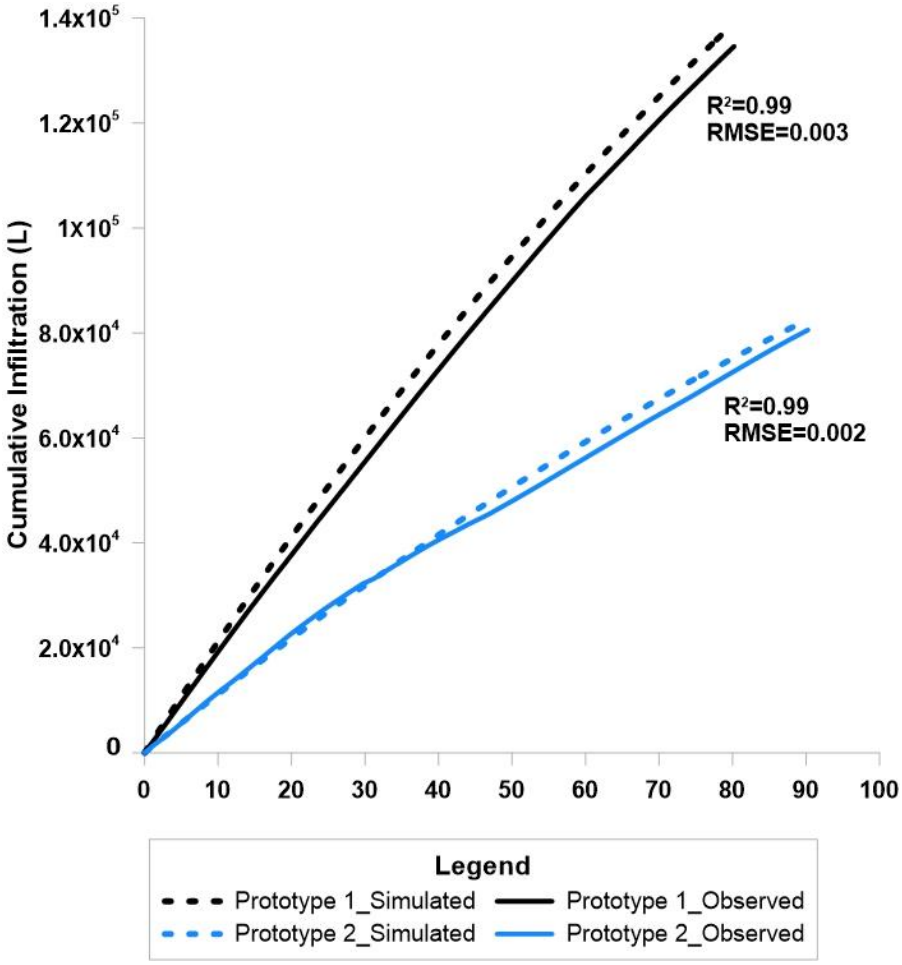

Figure 48 Comparison of simulated and observed cumulative infiltration rate (linear pressure change).

The result showed that the prediction of the model improved with the linear change in pressure, indicating that the main deviation between the observed and simulated result could be explained by the pressure loss. The possible factors contributing to the remaining deviation might be clogging, overburden pressure of soil and soil compaction (Hallam & Lahlali, 2021; Wang et al., 2023). The overburden pressure might have caused a deformation of the SIS from a circular shape towards an ellipsoidal pattern, causing a negative effect on the infiltration (Hills, 1989).

The main objective of these models was to predict the prototypes' overall cumulative infiltration rate and determine the installation depth and the maximum wetting pattern dimension. These parameters were vital for the field experiment design. Both model setups were kept simple to provide a general representation of the field site conditions. It is worth emphasizing that the main aim of this study was not to calibrate these models but to use them as a tool for designing the field recharge experiment.

5.6 Technical potential evaluation of a hypothetical infiltration trench

After assessing the technical performance of the prototypes, the next step was to compare their performance with a surface spreading technique, i.e., infiltration trench. For this purpose, the technical performance of a hypothetical infiltration trench was simulated using the HYDRUS-2D/3D model. The infiltration rate and wetting pattern distribution were predicted based on the geometric properties of infiltration trenches at Schiavon FIA. The trench was represented in a 2D cross-section. Figure 49 illustrates the conceptual representation of the model.

The model domain dimension in this scenario was 10 m × 14.5 m. The trench had a depth of 0.8 m, a top width of 0.8 m, and a bottom width of 0.4 m based on the values mentioned for Schiavon FIA. In the numerical model, one side of the trench was considered the center line, representing a symmetric axis, reducing the time required to perform the simulation. In order to compare the performance of the infiltration trench with SIS, the K_s value of the study area in Guntersblum, 1.6×10^{-04} m/sec, was considered. The model's initial condition and BC were defined similarly to the prototype models.

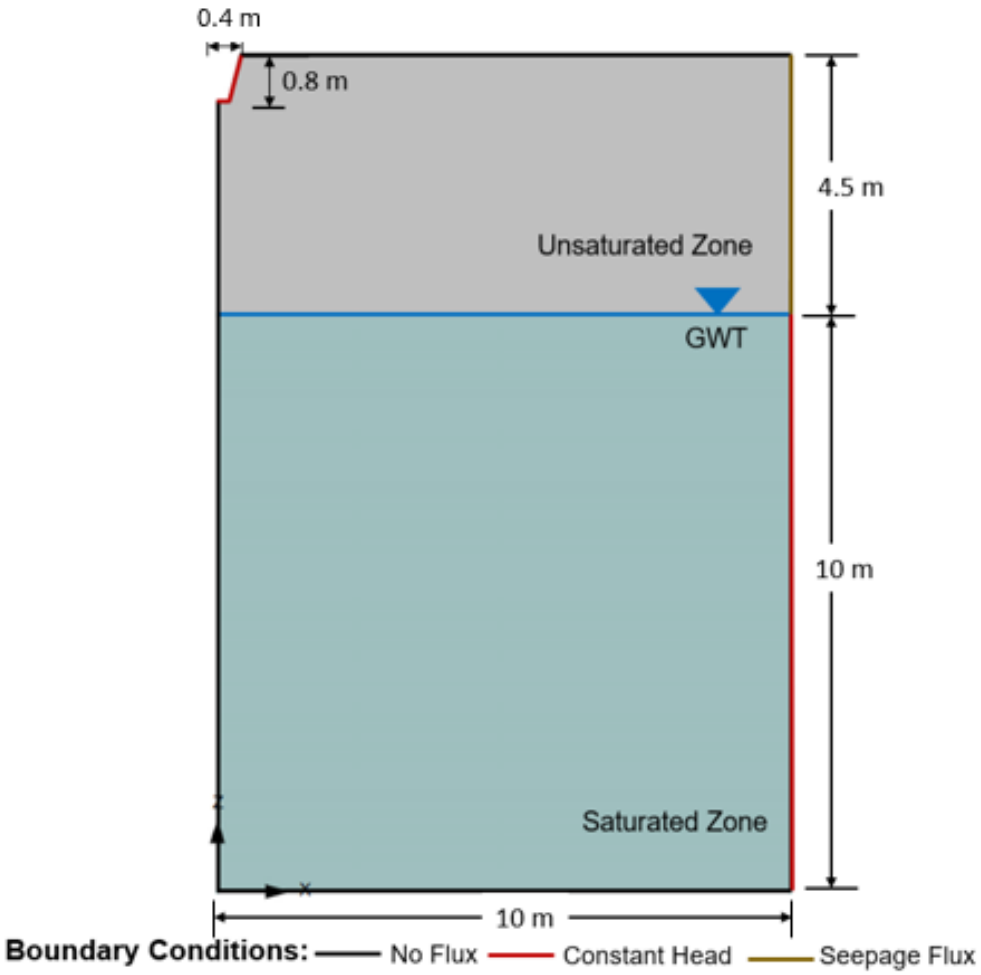

Figure 49 Schematic diagram of the trench symmetric model.

In addition to that, the vertical upper right boundary was set as the seepage face to allow the passage of excess flow. The infiltration from the trench was represented using a constant pressure head of 0.4 m. It should be noted that the BCs used for the trench are simplified representations of the real case scenario. Despite this, the numerical study aimed to demonstrate the behavior of the infiltration trench in its surrounding soil.

Figure 50 shows the simulated cumulative infiltration of one infiltration rate with a length of 162 m. In 92 days, the trench would infiltrate 1.9×10^{8} L of water into the soil. The average infiltration rate of one trench was 2.1×10^{6} L/day.

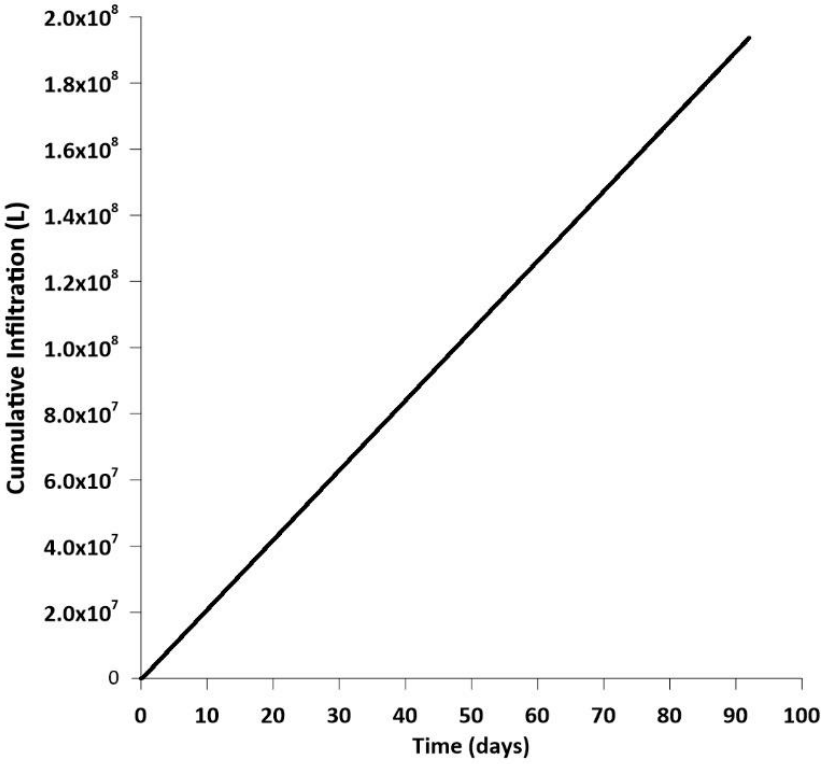

Figure 50 Cumulative infiltration of an infiltration trench.

Figure 51 illustrates the advancement of the wetting front in sand with 0.4 m of water in the trench. The moisture content value of 0.43 represented that saturated flow conditions existed within the wetting front. These figures show how the wetting front moved vertically and laterally away from the edge of the trench. At 2.4 hours, the infiltrated water reached GWT. The water content variation with time demonstrated that water infiltrated through the trench reached GWT faster than infiltrated water through the prototypes.

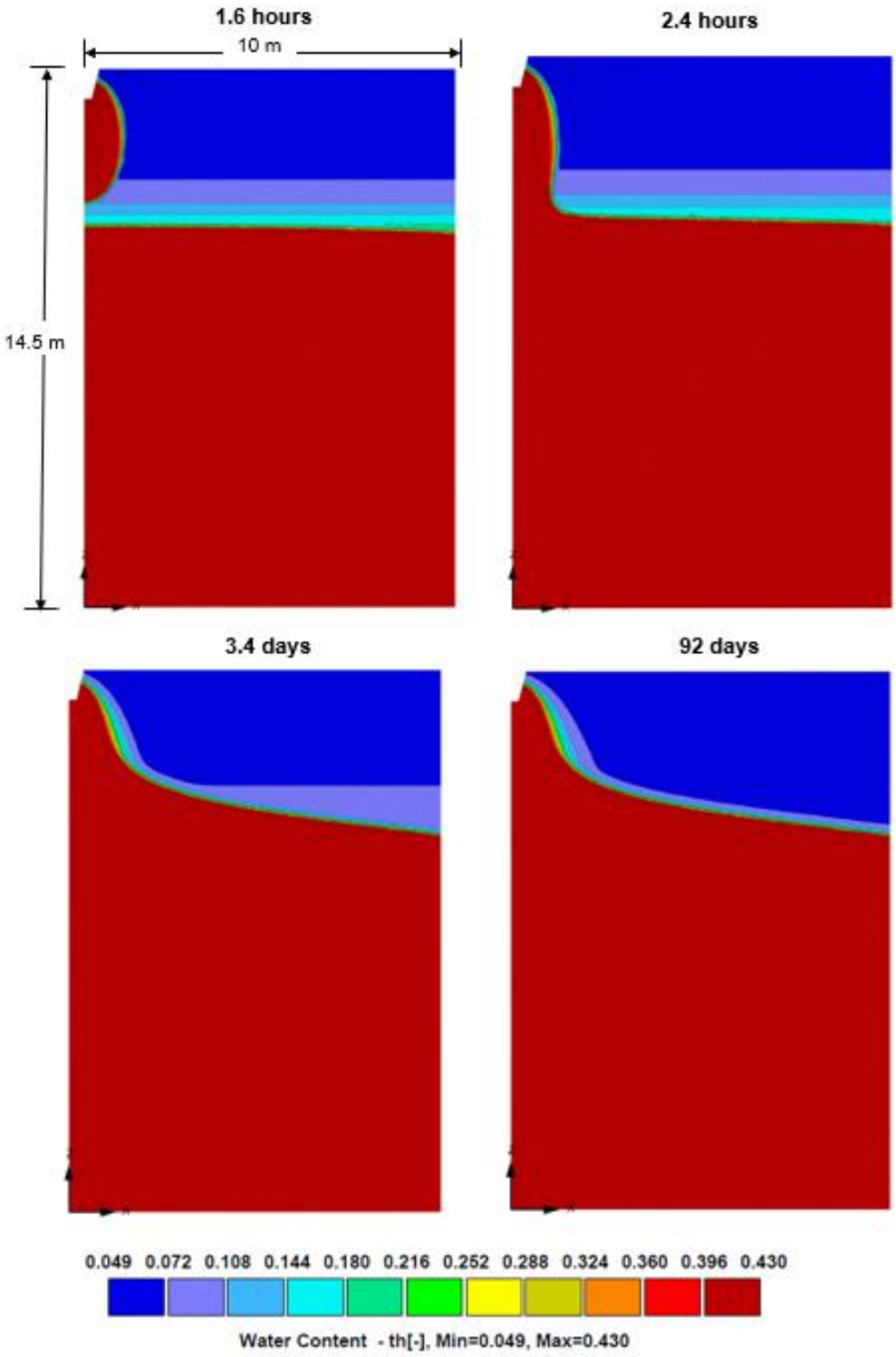

Figure 51 Evolution of water content for infiltration trench after 92 days.

At 3.4 days, the recharge rate stabilized, and the stabilized recharge rate was at 2.11×10^{6} L/day. After the system reached a steady-state condition, the effect of water mounding at

the right boundary was 1 cm, which was almost negligible. Therefore, the distance between the trenches was considered to be 10 m, which would prevent the trenches from interfering with one another.

5.7 Performance of subsurface irrigation system prototypes and infiltration trench under aerial constraints

SIS and trenches were assessed for their infiltration potential based on a limited infiltration area. Figure 52 shows the optimum distributions of the maximum number of prototypes and trenches that can fit within an area of approximately 1.1-hectares. The prototypes and trenches in the hypothetical distribution are distributed in a way to prevent overlap between them, allowing for the computation of cumulative infiltration. The lateral distance between each prototype and infiltration trench is 3 m and 10 m, respectively.

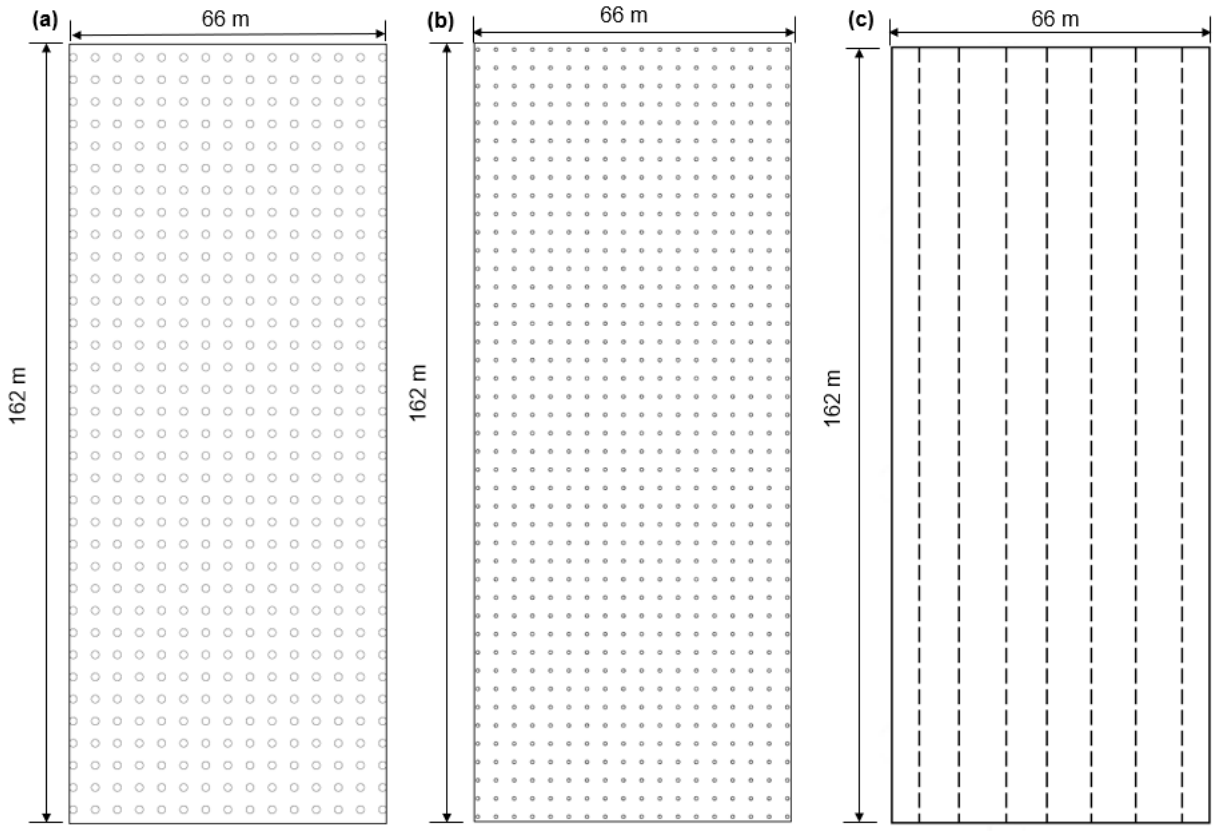

Figure 52 Distribution of the (a) Prototype 1 (b) Prototype 2 (c) Infiltration trench in a hypothetical 1.1-hectare area.

525 Prototype 1 and 774 Prototype 2 can be distributed inside the 1.1-hectare infiltration area. The corresponding daily cumulative recharge for Prototype 1 and 2 is 885 m^3 and 690 m^3, respectively. With a 10 m spacing interval, 7 infiltration trenches can be constructed in a 1.1-hectare area. The combined length of trenches deployed within the area is 1134 m, and the total daily recharge is 1.45×10^4 m^3. The SIS prototype recharge is around 4.81% to 6.13% of the trench recharge. The result indicates that trenches can yield the highest daily cumulative infiltration compared to both prototypes.

5.8 Economic potential of subsurface irrigation system prototypes and infiltration trenches

Table 4 illustrates the computation of construction costs for prototypes to determine whether the proposed approach would be cost-effective at the study site.

Table 4 Typical construction costs in Euro (€ in 2022) and levelized cost in US$ for SIS Prototypes and infiltration trenches. Excavation cost data per m^3 soil volume is provided by Wasserversorgung Rheinhessen-Pfalz GmbH (WVR)

Recharge Techniques	Investment Items	Value (€)	Total Capital Cost (€)	Levelized Cost (US$)
Prototype 1	Excavation cost	140,313.6	285,729.77	0.11
	Removal of soil	49,089.6		
	Backfilling	48,913.2		
	SIS material (21000 m)	21,000		
	Land cost	26,413.37		
Prototype 2	Excavation cost	77,573.4	174,422.30	0.099
	Removal of soil	27,139.5		
	Backfilling	27,042.01		
	SIS material (16254 m)	16,254		
	Land cost	26,413.37		
Infiltration Trenches	Excavation cost	30,307.7	67,324.46	0.003
	Removal of Material	10,603.4		
	Land cost	26,413.37		

The infiltration trenches and prototypes are assumed to have similar operating and maintenance costs. It is necessary to install a central water distribution system to transfer water from available sources to the proposed SIS prototypes and infiltration trenches. It is assumed that the construction costs of the water distribution system for the infiltration trenches and SIS prototypes are similar. Annual operation cost is assumed to be 4,000 euros, and operation life is considered 30 years. Land prices in Germany in 2016 were 22,300 euros per hectare (Silvis & Voskuilen, 2018). The cost was standardized for 2022 by multiplying with a GDP deflator of 1.08 and upscaled for a 1.1-hectare area. The indexed cost of 1.1 hectare of land in 2022 was 26,413.37 euros. Land acquisition cost was considered the same for the prototypes and infiltration trenches implementation. For estimating the levelized cost, 200 days of operation for both the prototypes and infiltration trenches were considered. The annual recharge volume for Prototype 1 is estimated to be 1.8×10^5 m^3, while for Prototype 2 it is expected to be 1.39×10^5 m^3. The infiltration trench is projected to have a recharge volume of 2.89×10^6 m^3. Based on the annual recharge volume, infiltration trenches will cost less than both SIS prototypes. The higher cost of the prototypes is due to the soil excavation, removal and backfilling required to install the prototypes. Despite the higher cost, SIS prototypes will provide multiple land use opportunities, offering additional income and environmental sustainability, which will be discussed in section 6.3.

6 Discussion & conclusion

The results are discussed in the context of the research objectives and the overall goal of promoting the adoption of MAR by developing improved site and infiltration assessment techniques in water scarcity mitigation.

6.1 Evaluation of MAR site suitability by incorporating adaptive site investigation technique enabling optimized infiltration rate assessment and cost-effective implementation of surface spreading techniques

The first objective of this research was to evaluate the MAR site's feasibility by incorporating adaptive site investigation techniques data enabling optimized infiltration rates assessment and cost-effective implementation of surface spreading techniques. The objective was fulfilled by employing adaptive site investigation techniques, including EMI survey, DP EC logging, and soil sampling. The step-by-step method to characterize the MAR site provided an image of the lateral variation in subsurface conditions. It allowed the delineation of different infiltration zones with a quantitative assessment of total infiltration rates of 190.61 l/sec. The delineated individual zones were assumed to be homogeneous in this investigation. This approach may be questioned considering the highly heterogeneous deposits encountered in Schiavon FIA. However, EMI results indicate no significant EC_a variability within the individual zones, only between them – this supports the chosen approach. Furthermore, a strong increase in the number of DP investigations to characterize the low infiltration zone in higher detail would not be financially reasonable as a) the EMI survey does not indicate any high hydraulic conductivity zones and b) even small-scale variations and slight increases of hydraulic conductivity have little effect as the infiltration rate of zone 2 is approximately 2 orders of magnitude lower compared to zones 1 and 3.

The adaptive site investigation technique employed at Schiavon FIA resulted in a theoretical reduction of 77% in the required land area, with a consequent reduction of the uncertainty associated with planning a MAR site. However, our study did not consider the potential requirement for an additional area of land for the conveyance of water. The overall land use reduction could be compromised by the amount of land utilized for the

water transportation facilities essential for operating MAR systems. Therefore, this study should be considered as representing the best-case scenario.

Reducing required land for MAR purposes will increase the profit from cultivation activity, which can be undertaken on the remaining land. Even though the cost of advanced site characterization is 8.5 times greater than that of conventional methods, this approach is expected to minimize the overall levelized cost of the system. The cost of Schiavon FIA was reduced by 58.4% through the advanced site characterization. Ross, 2021; Ross & Hasnain, 2018 and Vanderzalm et al., 2015 reported levelized costs of various MAR projects. The MAR expenses ranged between 0.007 US$ and 2.67 US$, demonstrating the wide variation of MAR costs, which depends on MAR site location, scheme scale, land cost, and implementation strategies. After optimizing the layout, the MAR cost was 0.0012 US$, which deviates from this range. The lower levelized cost is due to the estimated maximum infiltration rate. The infiltration rate was estimated by considering a constant 0.4 m water level in the trenches. Additionally, evaporation loss and clogging effects were not considered which might lead to a higher infiltration rate of Schiavon FIA. Although the levelized cost of the Schiavon FIA project is comparatively lower than other research, the objective of this research was not to compare these costs with other studies. Instead, the main focus was to compare cost differences between the initial and optimized Schiavon FIA layouts.

The approach developed in this research has potential applications in assessing the feasibility of MAR sites, mainly located in complex fluvial deposits. As mentioned by Vogelgesang et al., 2020, the collection of adequate hydrogeological data by traditional approaches is insufficient to accurately characterize the spatial distribution and hydraulic conditions of the alluvial aquifer. Consequently, this often results in inadequate data for model parameterization and uncertainty in MAR planning. The approach developed and applied in this research provides an essential tool for engineers, water planners, scientists, and policymakers, enabling a detailed understanding of MAR sites located in fluvial sediments, thus minimizing MAR planning uncertainty. It will also enhance multiple land use opportunities and increase the cost-effectiveness of the MAR system, ultimately promoting the uptake of MAR in water-scarce regions.

Undoubtedly, the work presented in this work has provided many other directions for future research. The adaptive site investigation can be applied to determine the temporal variation of the subsurface. A feedback system for data collection, analysis, and decision-making should be in place. This will ensure that any changes in hydrogeological conditions can be identified, and MAR operations can be adapted accordingly. Numerical modeling should be performed to simulate and predict the performance of the MAR system under different scenarios using data obtained from the adaptive site investigation. Economic assessment involving stakeholders and using socio-environmental indicators and profitability indices such as net present value (NPV) needs to be discussed. Moreover, the community's willingness to pay the price of water obtained by MAR should also be assessed in future studies.

6.2 Development and assessment of a novel managed aquifer recharge concept by employing a subsurface irrigation system for land use diversification

The second objective of the study was to develop and assess a novel MAR approach by using SIS for diversified land use purposes. The relationship between pressure and discharge was determined as a first step in fulfilling the objective. We conducted laboratory experiments using a 1-meter SIS pipe. The decision to choose a shorter pipe length was to reduce friction loss. Also, with higher pressure, flow irregularities over longer SIS pipe length exist. Hence, operating the SIS pipes at the recommended pressure was essential to ensure uniform flow and prevent irregularities.

Nevertheless, laboratory experiments are recommended to determine discharge uniformity over longer SIS lengths at higher pressures. Kanda et al., 2019 determined a line source emitter's coefficient of variation (CV) under varying pressure. They observed that the average CV was 11.6%, within the acceptable threshold (20%) proposed by Teeluck & Sutton, 1998. Their results showed that the line source emitter could also be operated at pressures ranging from 0.5 to 1.0 bar, with CV values less than 10%. Such experiments will help assess the degree of variation in discharge at different SIS sections and determine the maximum practical length of SIS where higher pressure will have a

significant effect. The evaluation of porous pipe uniformity is also discussed by Salisu et al., 2021; Liang et al., 2009 and Makavana et al., 2018.

In our research, the HYDRUS-2D/3D model was used to predict how SIS infiltrates in sandy soil. The model estimated an infiltration rate of 1.17 L/h/m, which was consistent with the experimental result. The simulated VWC data were also compared with observed VWC and showed good performance with average R^2 and RMSE values of 0.86 and 0.016 respectively. The model result was in accordance with the previous studies by Fan et al., 2018a; Phogat et al., 2012 and Kandelous & Šimůnek, 2010, who experimentally and numerically investigated the VWC distribution of subsurface irrigation system with HYDRUS-2D/3D model and reported that the RMSE value ranged between 0.01 and 0.049. Hence, the evaluated model was used to determine the installation depth and spacing for line-source SIS in a hypothetical scenario.

Understanding the depth plays a role in planning the implementation of SIS, as the installation depth significantly affects the costs involved. Deeper installations require more excavation, leading to higher installation expenses. Determining the depth for SIS installation using a numerical model is also vital in minimizing water loss through evaporation. This comprehensive approach improves this system’s effectiveness. Additionally, the model's ability to simulate different operating conditions allows for assessing SIS performance over time, considering factors like intermittent use and possible interruptions. The insights obtained from this research can serve as a reference for users seeking to optimize their SIS setups regarding technical effectiveness and cost efficiency. This model can further be used for optimizing the layout of SIS for agricultural purposes. In summary, our results demonstrate that this particular SIS model can help optimize MAR planning associated with SIS installation, showcasing its potential as a tool for MAR planning.

The feasibility analysis of the hypothetical scenario indicated that the potential of SIS installation in line configuration is limited to a surface spreading system. It pointed out the relevance of upgrading the SIS's capabilities by altering the installation's concept as one possible solution. Furthermore, in regions where line-source SIS is practiced for crop

production, it may also be used for aquifer recharge during the growing and non-growing seasons. Additional research should be conducted to develop and operate SIS in arable fields to facilitate aquifer recharge in combination with irrigation. Experimental and numerical modeling studies should be carried out to investigate the effect of SIS on aquifer recharge during irrigation, including parameters such as different soil types, water application schedules, and environmental conditions. In addition, the potential for nutrients leaching into groundwater should be investigated in order to improve fertilizer management and technology for minimizing environmental impact.

6.3 Evaluation of the performance and effectiveness of the developed subsurface irrigation system approach for determining its competitiveness with the surface spreading method

The third research objective was to evaluate the performance and effectiveness of the developed SIS approach on a field scale for determining competitiveness with the surface spreading method. In the first step, SIS prototypes were designed based on the geothermal energy basket design to optimize the infiltration rate over a unit area. Subsequently, the prototypes' infiltration rate and wetting pattern dimensions were simulated for a study area in Guntersblum, Germany, to understand the infiltration behavior of the systems, leading to the design of the field experiment.

The numerical simulation predicted the overall infiltration behavior of the SIS prototypes. The model simulated that the average infiltration rate for Prototype 1 and 2 was 2.01×10^5 L and 1.1×10^5 L, respectively, for 92 days. However, there was a significant difference between the observed and simulated flow. When the field experiment started, the operating pressure for the prototypes was 0.8 bar. The reduced submersible pump performance led to a reduction in the working pressure for the SIS prototypes. As the time variation of the pressure value was not measured in the field, it was difficult to determine the accurate timing of pressure change. Therefore, the linear change in pressure value was estimated, and the model was simulated again using the pressure change values. Later, it was observed that the model simulation results improved compared to the

observed value. The remaining deviation can be attributed to the overburdening soil pressure, clogging and bending of the SIS.

Clogging of emitters is a common issue in micro-irrigation systems (Lavanholi et al., 2018). A significant role in emitter clogging is attributed to the water's physical, chemical, and bacteriological characteristics. Different water sources contain varying levels of suspended and dissolved solids and biological contaminants like algae and bacteria, contributing to emitter clogging (Kanda et al., 2019), leading to a reduced infiltration rate. Additional investigation should be performed to assess the clogging characteristics of SIS. Moreover, filters should be used during water supply to the SIS to minimize the clogging effect.

From the field experiment outcomes, it was observed that the average infiltration rate of Prototype 1 and Prototype 2 was 1.8 L/h/m, which was close to the optimum discharge rates of SIS pipes, around 0.6-0.8 bar. It was also noticed that the flow rate of the prototypes had a fluctuating pattern, showing increasing and decreasing infiltration rates and vice versa. Bending may compress the SIS material on the inside of the curvature and expand it on the outside, which can reduce or increase the porosity in various sections of the prototypes. This change in porosity can produce fluctuations in flow rates. Even with the flow irregularities associated with bending, the infiltration rate per unit area could be increased for aquifer recharge. In future research, a more detailed analysis of curvature's effect on SIS's discharge characteristics should be considered to minimize its influence.

In the next step, a numerical simulation of an infiltration trench was performed to determine its infiltration rates for the study area for assessing the competitiveness of the SIS prototypes with infiltration trenches. Finally, the technical performance of these two techniques was compared, which showed that the SIS prototype recharge was approximately 4.81% to 6.13% of the trench recharge. The economic analysis showed that the infiltration trench would have a lower levelized cost compared to the prototypes. Vanderzalm et al., 2015 demonstrated that the levelized cost for MAR schemes varied from 0.04 US$ to 0.36 US$ per m^3 with an annual recharge capacity of 0.6 to 5 Mm^3. The

prototype levelized costs of 0.099 US$ and 0.11 US$ per m^3 are in the range, though the annual recharge capacity varies from 0.14 Mm^3 to 0.18 Mm^3. The estimated levelized cost of infiltration trenches, which is 0.003 US$ per m^3, deviates from the range provided by Vanderzalm et al., 2015. One of the reasons for the trenches low cost is the higher amount of predicted recharge, estimated on the basis of a constant water level in the trenches. Additionally, the clogging effect on the infiltration trench's infiltration rate was not considered in this study. In reality, more factors are involved in the construction cost of an SIS prototype or a trench than the presented estimation in this study. For instance, the excavation costs can vary mainly depending on the geological conditions and the planned setup. The excavation cost of one prototype was upscaled to estimate the total excavation cost in a 1.1-hectare area without considering any discount from the excavation company. Furthermore, the prices employed in the analysis did not consider electricity costs, transmission of data, and site investigation costs. However, the solution derived from this study provides an initial evaluation of the prototypes and infiltration trenches expenditure for comparing the two techniques. The findings show that the levelized cost of SIS prototypes is higher compared to the trenches.

The infiltration capacity of the prototypes must be improved to reduce the levelized cost. Reducing the distance between the SIS line sources distributed in the prototypes can accommodate longer SIS in the basket configuration. It is essential to note that this approach may result in smaller distances between the SIS in the prototypes, which could lead to localized saturation. Experimental or numerical investigations should be carried out in future studies to investigate the effect of the modified design on infiltration rates. Alternatively, the discharge of the SIS at its optimum pressure can be increased. The discharge at a specific pressure depends on the SIS's porosity, which needs to be enhanced to obtain a higher infiltration rate. However, increasing porosity also increases the risk of clogging. Therefore, along with optimized porosity, the diameter of the SIS should also be modified. Such modifications depend on the manufacturing process. The involvement of the manufacturing company is crucial to a better understanding of implementing these changes while maintaining the system's overall efficiency.

Even though the cost per m^3 of recharged water through SIS prototypes is higher with limited infiltration capacity, it has the potential to provide multiple land use opportunities. Obtaining revenue information from multiple land uses can be challenging, which makes it complex to evaluate the profitability of SIS prototypes. After the implementation of SIS prototypes, the land can be rented to farmers for cultivating crops that require minimal or no fertilization. The nominal land rent in western Germany in 2015 was 348 euros per hectare (Plogmann et al., 2018) (Indexed cost for 2022 was 378.24 euros). Additional profit can be earned from the rent. Moreover, farmers can generate revenues by cultivating hay for animal grazing, thereby making additional income from grazed animal products. According to Rebhann et al., 2016, extensive hay production yielded a dried matter biomass of 5.8 t ha^{-1}. $year^{-1}$ in Germany, resulting in total energy production of 16,240 kilowatt-hours of thermal energy annually. The sales revenue from this energy production was 730 € ha^{-1}. $year^{-1}$. Hence, bioenergy can also be produced by the combustion of dried hay, which will provide sales revenue. Besides the traditional feeding of cattle, hay can also be exported to feed horses and pets (Kruse et al., 2023). In addition, grassland plays an essential role in groundwater protection because the run-off of substances from fertilizer and pesticide use into groundwater is significantly reduced on grassland compared to arable land. It also forms the basis of the landscape and contributes significantly to the unique features and attractiveness and the living and recreational quality of these areas (Rösch et al., 2009). There is a great biodiversity in hay meadows, which can lead to an economic value. Hay can also be used in the tourism sector, for example, as a sleeping space for tourists (Kruse et al., 2023). In addition to direct financial returns from land rent and hay cultivation, SIS prototypes have ecological and social benefits, which are challenging to quantify in terms of revenue. Nevertheless, they contribute to environmental sustainability, which can be considered as a form of economic return.

The feasibility of SIS as a tool to enhance MAR uptake depends on its multiple advantages, which have varying applications in developed and developing nations, according to SIS's technical and economic performance assessment. In developing countries, water projects are often competing with other projects that provide social benefits for limited funding (Maliva, 2014). They are usually focused on economically

viable solutions to tackle water scarcity. While the multiple benefits of SIS are widely applicable, the higher capital costs and limited technical potential can present significant implementation barriers in water-scarce developing countries. SIS can be a viable option in developed countries with a focus on sustainable land use practices and aquifer recharge, including the environmental benefits. The income generated by potential land use can offset the increased levelized cost of SIS. In both contexts, the pilot sites using SIS may demonstrate its benefits regarding aquifer recharge and multifunctional land use, encouraging the adoption of this technique.

6.4 Conclusion

MAR sites are becoming increasingly necessary worldwide as the need to balance dwindling groundwater resources with escalating demand intensifies. Improving hydrogeological understanding, economic feasibility, and land use optimization are paramount for augmenting MAR implementation. This study advances the hydrogeological understanding and establishes a new benchmark in optimizing the financial and land use implications of MAR projects through innovative integration of adaptive site investigation techniques. The benefit of the enhanced site investigation approach is its potential to reduce the uncertainties inherent in the conventional approaches applied for hydrogeological characterization of the prospective MAR sites in fluvial deposits. This ensures improved planning, adequate resource allocations, and favorable financial and environmental project outcomes, fostering MAR.

The development and evaluation of a novel MAR technique employing SIS is a significant achievement of this research. Economically, the SIS prototypes are expensive to install and have limited technical potential compared to infiltration trenches. Despite this, the potential benefits of the technology are profound. In contrast to surface spreading methods, SIS prototypes offer the advantage of being installed underground, enabling land use for alternative needs, such as agriculture. In addition, these prototypes can be installed at community sites such as parks or sports facilities, improving the aesthetics of these areas and minimizing the impact of MAR on the surrounding landscape. This approach should be recognized as one aspect of a range of MAR techniques, potentially broadening the acceptance of MAR, notably in developed countries or agriculture-based

regions where land availability is a concern. In conclusion, this research has taken a step towards amplifying the MAR uptake as a solution to water scarcity by integrating enhanced site characterization and infiltration assessment approach and simultaneously expanding the scope for multipurpose land utilization.

7 References

Abdulla, F., Abdulla, C., Eslamian, S., 2021. Concept and Technology of Rainwater Harvesting, in: Handbook of Water Harvesting and Conservation. John Wiley & Sons, Ltd, pp. 1–16. https://doi.org/10.1002/9781119478911.ch1.

Ahmed, K.M., Sultana, S., Chowdhury, T., Islam, R., Delwaruzzaman, M., Alam, S. M. M., Tuinhof, A., Ravenscroft, P., Onabolu, B., Akhter, N., Mahmud, M. N., Rahman, M.S., Ghosh, S.K., Zheng, Y., 2021. Case Study 1: A resilient drinking water supply using aquifer storage and recovery for coastal communities in Batiaghata, Khulna, Bangladesh in: Zheng, Y., Ross, A., Villholth, K.G. and Dillon, P. (Eds.). Managing Aquifer Recharge: A Showcase for Resilience and Sustainability. Paris, UNESCO. https://recharge.iah.org/ ISBN 978-1-3999-2814-4.

Ajjur, S.B., Baalousha, H.M., 2021. A review on implementing managed aquifer recharge in the Middle East and North Africa region: methods, progress and challenges. Water International 46, 578–604. https://doi.org/10.1080/02508060.2021.1889192.

Akter, A., 2022. Groundwater Recharge, in: Akter, A. (Ed.), Rainwater Harvesting—Building a Water Smart City, Springer Water. Springer International Publishing, Cham, pp. 191–214. https://doi.org/10.1007/978-3-030-94643-2_6.

Alam, S., Borthakur, A., Ravi, S., Gebremichael, M., Mohanty, S.K., 2021. Managed aquifer recharge implementation criteria to achieve water sustainability. Science of The Total Environment 768, 144992. https://doi.org/10.1016/j.scitotenv.2021.144992.

Alexandratos, N., Bruinsma, J.,2012. World Agriculture towards 2030/2050: The 2012 Revision. ESA Working Paper No. 12-03, FAO, Rome.

Amin, M.S.M., Lim, C.W., Zakaria, A.A., 1997. Flow Characteristics of a Porous Pipe Irrigation Lateral.

ASTM, 2015. D6282. Standard guide for direct push soil sampling for environmental site characterizations. ASTM International, West Conshohocken, PA. doi: 10.1520/D6282_D6282M-14.

Ashrafi, S., Das Gupta, A., Babel, M., Izumi, N., 2002. Simulation of infiltration from porous clay pipe in subsurface irrigation. Hydrological Sciences Journal 47. https://doi.org/10.1080/02626660209492928.

Bali, K.M., Mohamed, A.Z., Begna, S., Wang, D., Putnam, D., Dahlke, H.E., Eltarabily, M.G., 2023. The use of HYDRUS-2D to simul.ate intermittent Agricultural Managed Aquifer Recharge (Ag-MAR) in Alfalfa in the San Joaquin Valley. Agricultural Water Management 282, 108296. https://doi.org/10.1016/j.agwat.2023.108296.

Baruffi, F., Cisotto, A., Cimolino, A., Ferri, M., Monego, M., Norbiato, D., Cappelletto, M., Bisaglia, M., Pretner, A., Galli, A., Scarinci, A., Marsala, V., Panelli, C., Gualdi, S., Bucchignani, E., Torresan, S., Pasini, S., Critto, A., Marcomini, A., 2012. Climate change impact assessment on Veneto and Friuli plain groundwater. Part I: An integrated modeling approach for hazard scenario construction. Science of The Total Environment, Integrated modelling and monitoring at different river basin scales under global change 440, 154–166. https://doi.org/10.1016/j.scitotenv.2012.07.070.

Becker, M.W., Bauer, B., Hutchinson, A., 2013. Measuring Artificial Recharge with Fiber Optic Distributed Temperature Sensing. Groundwater 51, 670–678. https://doi.org/10.1111/j.1745-6584.2012.01006.x.

Beck, J., Clark, P. J., & Puls, R. W., 2000. Location and characterization of subsurface anomalies using a soil conductivity probe. Ground Water Monitoring and Remediation, 20(2). https://doi.org/10.1111/j.1745-6592.2000.tb00265.x

Beganskas, S., Fisher, A.T., 2017. Coupling distributed stormwater collection and managed

aquifer recharge: Field application and implications., 2017. Journal of Environmental Management 200, 366–379. https://doi.org/10.1016/J.JENVMAN.2017.05.058.

Behroozmand, A.A., Auken, E., Knight, R., 2019. Assessment of Managed Aquifer Recharge Sites Using a New Geophysical Imaging Method. Vadose Zone Journal 18, 180184. https://doi.org/10.2136/vzj2018.10.0184.

Binley, A., Hubbard, S.S., Huisman, J.A., Revil, A., Robinson, D.A., Singha, K., Slater, L.D., 2015. The emergence of hydrogeophysics for improved understanding of subsurface processes over multiple scales. Water Resources Research 51, 3837–3866. https://doi.org/10.1002/2015WR017016.

Bond, N. R., Burrows, R. M., Kennard, M. J., & Bunn, S. E., 2019. Water Scarcity as a Driver of Multiple Stressor Effects. In S. Sabater, A. Elosegi, & R. Ludwig (Eds.), Multiple Stressors in River Ecosystems (pp. 111–129). Elsevier. https://doi.org/10.1016/B978-0-12-811713-2.00006-6.

Boughanmi, H., Lazaar, M., Farhat, A., Guizani, A., 2017. Evaluation of soil thermal potential under Tunisian climate using a new conic basket geothermal heat exchanger: Energy and exergy analysis. Applied Thermal Engineering 113, 912–925. https://doi.org/10.1016/j.applthermaleng.2016.10.204.

Bouwer, H., 2002. Artificial recharge of groundwater: hydrogeology and engineering. Hydrogeology Journal 10, 121–142. https://doi.org/10.1007/s10040-001-0182-4.

Bouwer, H., 1999. Artificial Recharge of Groundwater: Systems, Design, And Management, in: Mays, L.W. (Ed.), Hydraulic Design Handbook. McGraw-Hill Education.

Brand, C.C., 2022. Evaluating the Economics of Managed Aquifer Recharge Systems. Ground Water 60, 602–605. https://doi.org/10.1111/gwat.13176.

Briggs, M., Campbell, S., Nolan, J., Walvoord, M., Ntarlagiannis, D., Day-Lewis, F., Lane, J., 2016. Surface Geophysical Methods for Characterising Frozen Ground in

Transitional Permafrost Landscapes. Permafrost and Periglacial Processes 28. https://doi.org/10.1002/ppp.1893.

Brito, M.M. de, Kuhlicke, C., 2020. Cascading effects of the 2018-2019 German drought: empirical evidence from media reports (No. EGU2020-9499). Presented at the EGU2020, Copernicus Meetings. https://doi.org/10.5194/egusphere-egu2020-9499.

Brunner, N., Starkl, M., Sakthivel, P., Elango, L., Amirthalingam, S., Pratap, C.E., Thirunavukkarasu, M., Parimalarenganayaki, S., 2014. Policy Preferences about Managed Aquifer Recharge for Securing Sustainable Water Supply to Chennai City, India. Water 6, 3739–3757. https://doi.org/10.3390/w6123739.

Butler, J.J., 2002. A simple correction for slug tests in small-diameter wells. Ground Water 40, 303–307. https://doi.org/10.1111/j.1745-6584.2002.tb02658.x.

Cai, Y., Wu, P., Zhang, L., Zhu, D., Wu, S., Zhao, X., Chen, J., Dong, Z., 2018. Prediction of flow characteristics and risk assessment of deep percolation by ceramic emitters in loam. Journal of Hydrology 566, 901–909. https://doi.org/10.1016/j.jhydrol.2018.07.076.

Cai, Y., Zhao, X., Wu, P., Zhang, L., Zhu, D., Chen, J., 2019. Effect of Soil Texture on Water Movement of Porous Ceramic Emitters: A Simulation Study. Water 11, 22. https://doi.org/10.3390/w11010022.

Callegary, J.B., Ferré, T.P.A., Groom, R.W., 2012. Three-Dimensional Sensitivity Distribution and Sample Volume of Low-Induction-Number Electromagnetic-Induction Instruments. Soil Science Society of America Journal 76, 85–91. https://doi.org/10.2136/sssaj2011.0003.

Carsel, R.F., Parrish, R.S., 1988. Developing joint probability distributions of soil water retention characteristics. Water Resources Research 24, 755–769. https://doi.org/10.1029/WR024i005p00755.

Casanova, J., Devau, N., Pettenati, M., 2016. Managed Aquifer Recharge: An Overview of Issues and Options, in: Jakeman, A.J., Barreteau, O., Hunt, R.J., Rinaudo, J.-

D., Ross, A. (Eds.), Integrated Groundwater Management: Concepts, Approaches and Challenges. Springer International Publishing, Cham, pp. 413–434. https://doi.org/10.1007/978-3-319-23576-9_16.

Cherif Taiba, A., Mahmoudi, Y., Hazout, L., Belkhatir, M., Baille, W., 2019. Evaluation of hydraulic conductivity through particle shape and packing density characteristics of sand–silt mixtures. Marine Georesources & Geotechnology 37, 1175–1187. https://doi.org/10.1080/1064119X.2018.1539891.

Crites, R., Middlebrooks, J., Reed, S., 2006. Natural Wastewater Treatment Systems, Natural Wastewater Treatment Systems. https://doi.org/10.1201/9781420026443.

Dara, R., Kettridge, N., Rivett, M.O., Krause, S., Gomez-Ortiz, D., 2019. Identification of floodplain and riverbed sediment heterogeneity in a meandering UK lowland stream by ground penetrating radar. Journal of Applied Geophysics 171, 103863. https://doi.org/10.1016/j.jappgeo.2019.103863.

Darcy, H., 1856. Les Fontaines Publiques de la Ville de Dijon: Exposition et Application des Principes a Suivre et des Formulesa Employer dans les Questions de Distribution d'Eau. Dalmot Paris.

De Carli, A., 2015. Deliverable A.5. Analisi economico-finanziaria delle soluzioni tecniche per il riequilibrio delle falde nell'ambito del progetto AQUOR.

Demanet, D., Renardy, F., Vanneste, K., Jongmans, D., Camelbeeck, T., Meghraoui, M., 2001. The use of geophysical prospecting for imaging active faults in the Roer Graben, Belgium. GEOPHYSICS 66, 78.

DeNicola, E., Aburizaiza, O.S., Siddique, A., Khwaja, H., Carpenter, D.O., 2015. Climate Change and Water Scarcity: The Case of Saudi Arabia. Annals of Global Health, Climate Change, Global Health and Human Rights 81, 342–353. https://doi.org/10.1016/j.aogh.2015.08.005.

De Marsily, Gh., Delay, F., Gonçalvès, J., Renard, Ph., Teles, V., Violette, S., 2005. Dealing with spatial heterogeneity. Hydrogeol J 13, 161–183. https://doi.org/10.1007/s10040-004-0432-3.

Dietrich, P., Leven, C., 2006. Direct Push-Technologies, in: Kirsch, R. (Ed.), Groundwater Geophysics: A Tool for Hydrogeology. Springer, Berlin, Heidelberg, pp. 321–340. https://doi.org/10.1007/3-540-29387-6_11.

Dillon, Pat, Pavelic, P., Page, D., Beringen, H., Ward, J., 2009. Managed aquifer recharge: an introduction. Waterlines Report Series no. 13, February 2009, National Water Commisssion, Canberra. Australia.

Dillon, P., Stuyfzand, P., Grischek, T., Lluria, M., Pyne, R.D.G., Jain, R.C., Bear, J., Schwarz, J., Wang, W., Fernandez, E., Stefan, C., Pettenati, M., van der Gun, J., Sprenger, C., Massmann, G., Scanlon, B.R., Xanke, J., Jokela, P., Zheng, Y., Rossetto, R., Shamrukh, M., Pavelic, P., Murray, E., Ross, A., Bonilla Valverde, J.P., Palma Nava, A., Ansems, N., Posavec, K., Ha, K., Martin, R., Sapiano, M., 2019. Sixty years of global progress in managed aquifer recharge. Hydrogeol J 27, 1–30. https://doi.org/10.1007/s10040-018-1841-z.

Dirwai, T.L., Senzanje, A., Mabhaudhi, T., 2021. Development and Validation of a Model for Soil Wetting Geometry Under Moistube Irrigation. https://doi.org/10.21203/rs.3.rs-710106/v1.

Doolittle, J.A., Brevik, E.C., 2014. The use of electromagnetic induction techniques in soils studies. Geoderma 223–225, 33–45. https://doi.org/10.1016/j.geoderma.2014.01.027

Eltarabily, M.G., Berndtsson, R., Abdou, N.M., El-Rawy, M., Selim, T., 2021. A Comparative Analysis of Root Growth Modules in HYDRUS for SWC of Rice under Deficit Drip Irrigation. Water 13, 1892. https://doi.org/10.3390/w13141892.

EPA, 1997. Expedited site assessment tools for underground storage tank sites - A guideline for regulators. Office of Solid Waste and Emergency Response. U.S Goverment Printing Office, Pittsburgh.

Eurostat, 2017. Agricultural land prices by region. https://ec.europa.eu/eurostat/databrowser/view/APRI_LPRC/default/table?lang=en&category=agr.apri.apri_lpr.

Fan, Y., Zhao, T., Bai, G., & Liu, W., 2018a. HYDRUS-2D simulation of soil wetting pattern with horizontal moistube-irrigation and analysis of its influencing factors. Transactions of the Chinese Society of Agricultural Engineering, 34(4), 115–124.

Fan, Y.-W., Huang, N., Zhang, J., Zhao, T., 2018b. Simulation of Soil Wetting Pattern of Vertical Moistube-Irrigation. Water 10, 601. https://doi.org/10.3390/w10050601.

Fares, A., Polyakov, V., 2006. Advances in Crop Water Management Using Capacitive Water Sensors, in: Advances in Agronomy. Academic Press, pp. 43–77. https://doi.org/10.1016/S0065-2113(06)90002-9.

Fathi, S., Hagen, J.S., Matanó, A., Nogueira, G.E.H., 2021. Review of GIS Multi-Criteria Decision Analysis for Managed Aquifer Recharge in Semi-Arid Regions, in: Pande, C.B., Moharir, K.N. (Eds.), Groundwater Resources Development and Planning in the Semi-Arid Region. Springer International Publishing, Cham, pp. 19–52. https://doi.org/10.1007/978-3-030-68124-1_2.

Filippi, E., Marcala,V., Ferri,M., Cisotto, A.,Vienken,T., Kofakis, P., 2016. Deliverable 7.1. MAR through forested infiltration in the River Brenta Catchment, Vicenza, Italy. FP7 MARSOL (Demonstrating Managed Aquifer Recharge as a Solution to Water Scarcity and Drought).

Gale, I., Neumann, I., Calow, R., Moench, M., 2002. The effectiveness of artificial recharge of groundwater: a review. URL https://nora.nerc.ac.uk/id/eprint/527471/ (accessed 7.12.22).

Gammie, G., Bievre, B.D., 2015. Assessing Green Interventions for the Water Supply of Lima, Peru. Forest Trends. URL https://www.forest-trends.org/publications/assessing-green-interventions-for-the-water-supply-of-lima-peru/ (accessed 10.4.23).

Ganot, Y., Dahlke, H.E., 2021. A model for estimating Ag-MAR flooding duration based on crop tolerance, root depth, and soil texture data. Agricultural Water Management 255, 107031. https://doi.org/10.1016/j.agwat.2021.107031.

Ganot, Y., Holtzman, R., Weisbrod, N., Nitzan, I., Katz, Y., Kurtzman, D., 2017. Monitoring and modeling infiltration–recharge dynamics of managed aquifer recharge with desalinated seawater. Hydrology and Earth System Sciences 21, 4479–4493. https://doi.org/10.5194/hess-21-4479-2017.

Geoprobe, 2019. Geoprobe® Optical Image Profiler (OIP): Standard operating procedure. Kejr, Inc., Salina.www.geoprobe.com.

Ghanbarian, B., Hunt, A.G., Ewing, R.P., Sahimi, M., 2013. Tortuosity in Porous Media: A Critical Review. Soil Science Society of America Journal 77, 1461–1477. https://doi.org/10.2136/sssaj2012.0435.

Ghodeif, K., Grischek, T., Bartak, R., Wahaab, R., Herlitzius, J., 2016. Potential of river bank filtration (RBF) in Egypt. Environ Earth Sci 75, 671. https://doi.org/10.1007/s12665-016-5454-3.

Gobert, J., Rudolf, F., 2023. Rhine low water crisis: From individual adaptation possibilities to strategical pathways. Frontiers in Climate 4.

Gupta, A.D., Babel, M.S., Ashrafi, S., 2009. Effect of soil texture on the emission characteristics of porous clay pipe for subsurface irrigation. Irrig Sci 27, 201–208. https://doi.org/10.1007/s00271-008-0129-9.

Hallam, J., Lahlali, M., 2021. Nano-irrigation: Hydraulic characteristics of the line-source emitters as a function of pressure heads under different soil types and bulk densities 100–115. https://doi.org/10.34874/IMIST.PRSM/afrimed-i133.31267.

Halytsia, O., Vrachioli, M., Janik, K., Sitek, S., Wojtal, G., Imig, A., Rein, A., Sauer, J., 2022. Assessing Economic Feasibility of Managed Aquifer Recharge Schemes: Evidence from Cost-benefit Analysis in Poland. Water Resour Manage 36, 5241–5258. https://doi.org/10.1007/s11269-022-03303-0.

Hardie, M., Lisson, S., Doyle, R., Cotching, W., 2013. Determining the frequency, depth and velocity of preferential flow by high frequency soil moisture monitoring. Journal of Contaminant Hydrology 144, 66–77. https://doi.org/10.1016/j.jconhyd.2012.10.008.

Hasan, M.B., Driessen, P.P.J., Majumder, S., Zoomers, A., van Laerhoven, F., 2019. Factors Affecting Consumption of Water from a Newly Introduced Safe Drinking Water System: The Case of Managed Aquifer Recharge (MAR) Systems in Bangladesh. Water 11, 2459. https://doi.org/10.3390/w11122459.

Heilweil, V. M., & Watt, D. E., 2011. Trench infiltration for managed aquifer recharge to permeable bedrock. Hydrological Processes, 25(1), 141–151. https://doi.org/10.1002/hyp.7833.

Heil, K., Schmidhalter, U., 2012. Characterisation of soil texture variability using the apparent soil electrical conductivity at a highly variable site. Computers & Geosciences 39, 98–110. https://doi.org/10.1016/j.cageo.2011.06.017.

Hellauer, K., Karakurt, S., Sperlich, A., Burke, V., Massmann, G., Hübner, U., Drewes, J.E., 2018. Establishing sequential managed aquifer recharge technology (SMART) for enhanced removal of trace organic chemicals: Experiences from field studies in Berlin, Germany. Journal of Hydrology 563, 1161–1168. https://doi.org/10.1016/j.jhydrol.2017.09.044.

Hiscock, K.M., Grischek, T., 2002. Attenuation of groundwater pollution by bank filtration. Journal of Hydrology 266, 139–144. https://doi.org/10.1016/S0022-1694(02)00158-0.

Hills, D J., Tajrishy, M., Gu, Y.,1989. Hydraulic Considerations for Compressed Subsurface Drip-tape. Transactions of the ASABE. 32. p. 1197–201.

Hausmann, J., Zielhofer, C., Werther, L., Berg-Hobohm, S., Dietrich, P., Heymann, R., & Werban, U., 2018. Direct push sensing in wetland (geo)archaeology: High-resolution reconstruction of buried canal structures (Fossa Carolina, Germany). Quaternary International, 473, 21–36. https://doi.org/10.1016/j.quaint.2017.02.008.

Hutchinson, A., Rodriguez, G., Woodside, G., & Milczarek, M., 2017. Maximizing Infiltration Rates by Removing Suspended Solids: Results of Demonstration Testing of Riverbed Filtration in Orange County, California †. *Water*, *9*, 119. https://doi.org/10.3390/w9020119.

IGRAC, 2007. Artificial Recharge of Groundwater in the World. https://www.un-igrac.org/resource/igrac-global-mar-inventory-report.

Ingrao, C., Strippoli, R., Lagioia, G., Huisingh, D., 2023. Water scarcity in agriculture: An overview of causes, impacts and approaches for reducing the risks. Heliyon 9, e18507. https://doi.org/10.1016/j.heliyon.2023.e18507.

Itani, N., Harik, G., Alameddine, I., & El-Fadel, M., 2022. Managed aquifer recharge in karstic systems:Site suitability mapping by coupling multi-criteria decision analysis with remote sensing and hydrologic modeling. Journal of Environmental Management, 322, 116162. https://doi.org/10.1016/j.jenvman.2022.116162.

Jackisch, C., Germer, K., Graeff, T., Andrä, I., Schulz, K., Schiedung, M., Haller-Jans, J., Schneider, J., Jaquemotte, J., Helmer, P., Lotz, L., Bauer, A., Hahn, I., Šanda, M., Kumpan, M., Dorner, J., de Rooij, G., Wessel-Bothe, S., Kottmann, L., Schittenhelm, S., Durner, W., 2020. Soil moisture and matric potential – an open field comparison of sensor systems. Earth System Science Data 12, 683–697. https://doi.org/10.5194/essd-12-683-2020.

Jakeman, A.J., Barreteau, O., Hunt, R.J., Rinaudo, J.-D., Ross, A., Arshad, M., Hamilton, S., 2016. Integrated Groundwater Management: An Overview of Concepts and Challenges, in: Jakeman, A.J., Barreteau, O., Hunt, R.J., Rinaudo, J.-D., Ross, A. (Eds.), Integrated Groundwater Management: Concepts, Approaches and Challenges. Springer International Publishing, Cham, pp. 3–20. https://doi.org/10.1007/978-3-319-23576-9_1

Javadi, S., Saatsaz, M., Hashemy Shahdany, S.M., Neshat, A., Ghordoyee Milan, S., Akbari, S., 2021. A new hybrid framework of site selection for groundwater recharge. Geoscience Frontiers 12, 101144. https://doi.org/10.1016/j.gsf.2021.101144.

Kalbus, E., Reinstorf, F., Schirmer, M., 2006. Measuring methods for groundwater & surface water interactions: a review. Hydrology and Earth System Sciences 10, 873–887. https://doi.org/10.5194/hess-10-873-2006.

Kanda, E.K., Mabhaudhi, T., Senzanje, A., 2018. Hydraulic and clogging characteristics of Moistube irrigation as influenced by water quality. Journal of Water Supply: Research and Technology-Aqua 67, 438–446. https://doi.org/10.2166/aqua.2018.166.

Kanda, E.K., Senzanje, A., Mabhaudhi, T., 2020. Soil water dynamics under Moistube irrigation. Physics and Chemistry of the Earth, Parts A/B/C 115, 102836. https://doi.org/10.1016/j.pce.2020.102836.

Kandelous, M.M., Šimůnek, J., 2010. Numerical simulations of water movement in a subsurface drip irrigation system under field and laboratory conditions using HYDRUS-2D. Agricultural Water Management 97, 1070–1076. https://doi.org/10.1016/j.agwat.2010.02.012.

Kanso, T., Gromaire, M.-C., Ramier, D., Dubois, P., Chebbo, G., 2020. An Investigation of the Accuracy of EC5 and 5TE Capacitance Sensors for Soil Moisture Monitoring in Urban Soils-Laboratory and Field Calibration. Sensors 20, 6510. https://doi.org/10.3390/s20226510.

Kästner, M., Braeckevelt, M., Döberl, G., Cassiani, G., Petrangeli Papini, M., Leven-Pfister, C., van Ree, D. (eds), 2012. Model-driven soil probing, site assessment and evaluation. Sapienza Università Editrice, Rome, 307 pp.

Kirkham, M.B., 2014. Chapter 8 - Time Domain Reflectometry, in: Kirkham, M.B. (Ed.), Principles of Soil and Plant Water Relations (Second Edition). Academic Press, Boston, pp. 103–122. https://doi.org/10.1016/B978-0-12-420022-7.00008-2.

Kitchen, N.R., Sudduth, K.A., Drummond, S.T., 1999. Soil Electrical Conductivity as a Crop Productivity Measure for Claypan Soils. Journal of Production Agriculture 12, 607–617. https://doi.org/10.2134/jpa1999.0607.

Koltermann, C.E., Gorelick, S.M., 1996. Heterogeneity in Sedimentary Deposits: A Review of Structure-Imitating, Process-Imitating, and Descriptive Approaches. Water Resources Research 32, 2617–2658. https://doi.org/10.1029/96WR00025.

Kruse, A., Špulerova, J., Centeri, C., Eiter, S., Ferrario, V., Jurgens, S., Kladnik, D., Kučera, Z., Marusca, T., Neculai, D., Renes, H., Sickel, H., Sigura, M., Slámová, M., Stensgaard, K., & Strasser, P., 2023. Country Perspectives on Hay-Making Landscapes as Part of the European Agricultural Heritage. Land, 12(9), Article 9. https://doi.org/10.3390/land12091694.

Lasage, R., Aerts, J., Mutiso, G.-C.M., de Vries, A., 2008. Potential for community based adaptation to droughts: Sand dams in Kitui, Kenya. Physics and Chemistry of the Earth, Parts A/B/C, Hydrological Assessment and Integrated Water Resources Management with Special Focus on Developing Countries 33, 67–73. https://doi.org/10.1016/j.pce.2007.04.009.

Laukka, V., Katko, T.S., Peltonen, L., Rajala, R., 2021. Creating collaboration for contentious projects on managed aquifer recharge: two cases from Finland. Hydrogeol J 29, 1369–1378. https://doi.org/10.1007/s10040-021-02334-y.

Lavanholi, R., Oliveira, F. C., Camargo, A. P. de, Frizzone, J. A., Molle, B., Ait-Mouheb, N., & Tomas, S., 2018. Methodology to Evaluate Dripper Sensitivity to Clogging due to Solid Particles: An Assessment. The Scientific World Journal, 2018, e7697458. https://doi.org/10.1155/2018/7697458.

Lazarovitch, N., Šimůnek, J., Shani, U., 2005. System-Dependent Boundary Condition for Water Flow from Subsurface Source. Soil Science Society of America Journal 69, 46–50. https://doi.org/10.2136/sssaj2005.0046.

Levintal, E., Kniffin, M.L., Ganot, Y., Marwaha, N., Murphy, N.P., Dahlke, H.E., 2023. Agricultural managed aquifer recharge (Ag-MAR)—a method for sustainable groundwater management: A review. Critical Reviews in Environmental Science and Technology 53, 291–314. https://doi.org/10.1080/10643389.2022.2050160.

Liang, H., Liu, Z., Shu, Q., Yin, G., 2009. Effects of operating pressure on the discharge characteristics of porous pipes as micro-irrigation laterals 25, 1–5.

Liao, R., Zhang, S., Zhang, X., Wang, M., Wu, H., Zhangzhong, L., 2021. Development of smart irrigation systems based on real-time soil moisture data in a greenhouse: Proof of concept. Agricultural Water Management 245, 106632. https://doi.org/10.1016/j.agwat.2020.106632.

Loaiciga, H.A., Doh, R., 2023. Groundwater for people and the environment: a globally threatened resource. Groundwater. https://doi.org/10.1111/gwat.13376.

Makavana, J., Deraari, J., Mashru, H., 2018. Pressure Variation Effect on Discharge Characteristics of Porous Pipe (1st ed.). LAP LAMBERT Academic Publishing. Retrieved from https://www.perlego.com/book/3442095/pressure-variation-effect-on-discharge-characteristics-of-porous-pipe-develop-the-pressure-discharge-relationship-of-porous-pipe-pdf.

Maliva, R.G., 2016. Aquifer Characterization Techniques: Schlumberger Methods in Water Resources Evaluation Series No. 4, 1st ed. 2016 edition. ed. Springer, New York, NY.

Maliva, R.G., Herrmann, R., Coulibaly, K., 2015. Advanced aquifer characterization for optimization of managed aquifer recharge. Environ Earth Sci **73**, 7759–7767. https://doi.org/10.1007/s12665-014-3167-z.

Maliva, R.G., 2014. Economics of Managed Aquifer Recharge. Water 6, 1257–1279. https://doi.org/10.3390/w6051257.

Maliva, R.G., Guo, W., Missimer, T.M., 2006. Aquifer Storage and Recovery: Recent Hydrogeological Advances and System Performance. Water Environment Research 78, 2428–2435. https://doi.org/10.2175/106143006X123102.

Maples, S.R., Foglia, L., Fogg, G.E., Maxwell, R.M., 2020. Sensitivity of hydrologic and geologic parameters on recharge processes in a highly heterogeneous, semi-

confined aquifer system. Hydrology and Earth System Sciences 24, 2437–2456. https://doi.org/10.5194/hess-24-2437-2020.

Maréchal, J.-C., Bouzit, M., Rinaudo, J.-D., Moiroux, F., Desprats, J.-F., Caballero, Y., 2020. Mapping Economic Feasibility of Managed Aquifer Recharge. Water 12, 680. https://doi.org/10.3390/w12030680.

Mastrocicco, M., Colombani, N., Salemi, E., Boz, B., Gumiero, B., 2015. Managed aquifer recharge via infiltration ditches in short rotation afforested areas. Ecohydrology 9, 167-178.

Mawer, C., Parsekian, A., Pidlisecky, A., Knight, R., 2016. Characterizing Heterogeneity in Infiltration Rates During Managed Aquifer Recharge. Ground Water 54, 818–829. https://doi.org/10.1111/gwat.12423.

Mawer, C., 2014. Characterization and Monitoring of Managed Aquifer Recharge (Doctoral dissertation). https://stacks.stanford.edu/file/druid:hd273hn5235/ThesisFinalB-augmented.pdf.

Martín Civantos, J.M., 2010. Las aguas del río Alhama de Guadix y el sistema de careos de Sierra Nevada (Granada) en época medieval. In: El paisaje y su dimensión arqueológica. Estudios sobre el Sur de la Península Ibérica en la Edad Media, Granada, Alhulia, pp. 79–111.

McCall, W., 2011. Application of the Geoprobe® HPT Logging System for Geo-Environmental Investigations 36.

McCall, W., Christy, T.M., 2020. The Hydraulic Profiling Tool for Hydrogeologic Investigation of Unconsolidated Formations. Groundwater Monitoring & Remediation 40, 89–103. https://doi.org/10.1111/gwmr.12399.

McCall, W., Christy, T.M., Christopherson, T., Issacs, H., 2009. Application of Direct Push Methods to Investigate Uranium Distribution in an Alluvial Aquifer. Groundwater Monitoring & Remediation 29, 65–76. https://doi.org/10.1111/j.1745-6592.2009.01258.x.

McCall, W., Christy, T.M., Pipp, D., Terkelsen, M., Christensen, A., Weber, K., Engelsen, P., 2014. Field Application of the Combined Membrane-Interface Probe and Hydraulic Profiling Tool (MiHpt). Groundwater Monitoring & Remediation 34, 85–95. https://doi.org/10.1111/gwmr.12051.

McCall, W., Christy, T.M., Pipp, D.A., Jaster, B., White, J., Goodrich, J., Fontana, J., Doxtader, S., 2018. Evaluation and application of the optical image profiler (OIP) a direct push probe for photo-logging UV-induced fluorescence of petroleum hydrocarbons. Environ Earth Sci 77, 374. https://doi.org/10.1007/s12665-018-7442-2.

McDowell, P.W., Barker, R.D., Butcher, A.P., Culshaw, M.G., Jackson, P.D., McCann, D.M., Skipp, B.O., Matthews, S.L., Arthur, J.C.R., 2002. Geophysics in engineering investigations. Geological Society of London. https://doi.org/10.1144/GSL.ENG.2002.019.

McNeill, J., 1980. Electromagnetic Terrain Conductivity Measurement at Low Induction Numbers. https://ufdc.ufl.edu/WL00000277/00001 (accessed 11.12.21).

Medina, R., Pham, C., Plumlee, M.H., Hutchinson, A., Becker, M.W., O'Connell, P.J., 2020. Distributed Temperature Sensing to Measure Infiltration Rates Across a Groundwater Recharge Basin. Groundwater 58, 913–923. https://doi.org/10.1111/gwat.13007.

Mendieta-Mendoza, A., Hanson, R.T., Renteria-Villalobos, M., 2021. Potential adverse impacts on vulnerability and availability of groundwater from climate-change and land use. Journal of Hydrology 594, 125978. https://doi.org/10.1016/j.jhydrol.2021.125978.

METER Group AG.,2016: KSAT operation manual. URL: http://library.metergroup.com/Manuals/UMS/KSAT_Manual.pdf

Minsley, B.J., Ajo-Franklin, J., Mukhopadhyay, A., Morgan, F.D., 2011. Hydrogeophysical Methods for Analyzing Aquifer Storage and Recovery Systems. Groundwater 49, 250–269. https://doi.org/10.1111/j.1745-6584.2010.00676.x

Mishra, B.K., Kumar, P., Saraswat, C., Chakraborty, S., Gautam, A., 2021. Water Security in a Changing Environment: Concept, Challenges and Solutions. Water 13, 490. https://doi.org/10.3390/w13040490.

Mochizuki, H., Sakaguchi, I., 2023. In-situ Simple Rapid Calibration Method for the EC-5 Moisture Sensor. Japan Agricultural Research Quarterly: JARQ 57, 131–137. https://doi.org/10.6090/jarq.57.131.

Morgan, J.H., 1996. Sampling Environmental Media, ASTM STP 1282. ASTM.

Mozzi, G., Pavelic, P., Alam, M.F., Stefan, C., Villholth, K.G., 2021. Hydrologic Assessment of Check Dam Performances in Semi-Arid Areas: A Case Study From Gujarat, India. Frontiers in Water 3.

Mualem, Y., 1976. A new model for predicting the hydraulic conductivity of unsaturated porous media. Water Resources Research 12, 513–522. https://doi.org/10.1029/WR012i003p00513.

Mukherjee, A., Scanlon, B.R., Aureli, A., Langan, S., Guo, H., McKenzie, A., 2021. Chapter 1 - Global groundwater: from scarcity to security through sustainability and solutions, in: Mukherjee, A., Scanlon, B.R., Aureli, A., Langan, S., Guo, H., McKenzie, A.A. (Eds.), Global Groundwater. Elsevier, pp. 3–20. https://doi.org/10.1016/B978-0-12-818172-0.00001-3.

Murray, R., Tredoux, G., 1998. Artificial recharge: A technology for sustainable water resource development. Water Research Commission Pretoria, South Africa.

Nabighian, M.N., Macnae, J.C., 1991. 6. Time Domain Electromagnetic Prospecting Methods, in: Electromagnetic Methods in Applied Geophysics: Volume 2, Application, Parts A and B, Investigations in Geophysics. Society of Exploration Geophysicists, pp. 427–520. https://doi.org/10.1190/1.9781560802686.ch6.

Naik, P.K., Mojica, M., Ahmed, F., Al-Mannai, S., 2017. Storm water injection in Bahrain: pilot studies. Arab J Geosci 10, 452. https://doi.org/10.1007/s12517-017-3232-5.

National Research Council, 1994. Ground Water Recharge Using Waters of Impaired Quality. National Academies Press, Washington, D.C. https://doi.org/10.17226/4780.

O'Geen, A., Saal, M., Dahlke, H., Doll, D., Elkins, R., Fulton, A., Fogg, G., Harter, T., Hopmans, J., Ingels, C., Niederholzer, F., Sandoval Solis, S., Verdegaal, P., Walkinshaw, M., 2015. Soil suitability index identifies potential areas for groundwater banking on agricultural lands. California Agriculture 69, 75–84.

Palma Nava, A., Parker, T.K., Carmona Paredes, R.B., 2022. Challenges and Experiences of Managed Aquifer Recharge in the Mexico City Metropolitan Area. Ground Water 60, 675–684. https://doi.org/10.1111/gwat.13237.

Parimalarenganayaki, S., 2021. Managed Aquifer Recharge in the Gulf Countries: A Review and Selection Criteria. Arab J Sci Eng 46, 1–15. https://doi.org/10.1007/s13369-020-05060-x.

Parker, T.K., Jansen, J., Behroozmand, A.-A., Halkjaer, M., Thorn, P., 2022. Applied Geophysics for Managed Aquifer Recharge. Groundwater 60, 606–618. https://doi.org/10.1111/gwat.13235.

Parsons, L.R., Bandaranayake, W.M., 2009. Performance of a New Capacitance Soil Moisture Probe in a Sandy Soil. Soil Science Society of America Journal 73, 1378–1385. https://doi.org/10.2136/sssaj2008.0264.

Passadore, G., Monego, M., Altissimo, L. et al., 2012. Alternative conceptual models and the robustness of groundwater management scenarios in the multi-aquifer system of the Central Veneto Basin, Italy. Hydrogeol J **20**, 419–433. https://doi.org/10.1007/s10040-011-0818-y.

Pasini, S., Torresan, S., Rizzi, J., Zabeo, A., Critto, A., Marcomini, A., 2012. Climate change impact assessment in Veneto and Friuli Plain groundwater. Part II: A spatially resolved regional risk assessment. Science of The Total Environment, Integrated modelling and monitoring at different river basin scales under global change 440, 219–235. https://doi.org/10.1016/j.scitotenv.2012.06.096.

Patel, G.R., Ghaghada, R.H., Chalodia, A.L., 2011. Hydraulics performance evaluation of porous pipe (sub surface) irrigation system. International Journal of Agricultural Engineering.

Peng, J., Liu, T., Chen, J., Li, Z., Ling, Y., De Wulf, A., De Maeyer, P., 2023. The conflicts of agricultural water supply and demand under climate change in a typical arid land watershed of Central Asia. Journal of Hydrology: Regional Studies 47, 101384. https://doi.org/10.1016/j.ejrh.2023.101384.

Petronici, F., Pujades, E., Jurado, A., Marcaccio, M., Borgatti, L., 2019. Numerical Modelling of the Mulino Delle Vene Aquifer (Northern Italy) as a Tool for Predicting the Hydrogeological System Behavior under Different Recharge Conditions. Water 11, 2505. https://doi.org/10.3390/w11122505.

Philipp, W., Kraljevic, A., 2015. The imported risk: Germany's water risks in times of globalisation, WWF study. WWF Deutschland, Berlin, Germany.

Phogat, V., Mahadevan, M., Skewes, M., & Cox, J. W., 2012. Modelling soil water and salt dynamics under pulsed and continuous surface drip irrigation of almond and implications of system design. Irrigation Science, 30(4), 315–333. https://doi.org/10.1007/s00271-011-0284-2.

Plogmann, J., Mußhoff, O., Odening, M., Ritter, M., 2018. What moves the German land market? A decomposition of the land rent-price ratio (Working Paper No. 05 (2018)). FORLand-Working Paper. https://doi.org/10.18452/19486.2.

Portmann, F.T., Döll, P., Eisner, S., Flörke, M., 2013. Impact of climate change on renewable groundwater resources: assessing the benefits of avoided greenhouse gas emissions using selected CMIP5 climate projections. Environ. Res. Lett. 8, 024023. https://doi.org/10.1088/1748-9326/8/2/024023.

Post, V.E.A., Zhou, T., Neukum, C., Koeniger, P., Houben, G.J., Lamparter, A., Šimůnek, J., 2022. Estimation of groundwater recharge rates using soil-water isotope

profiles: a case study of two contrasting dune types on Langeoog Island, Germany. Hydrogeol J 30, 797–812. https://doi.org/10.1007/s10040-022-02471-y.

Provenzano, G., Alagna, V., Autovino, D., Juarez, J.M., Rallo, G., 2016. Analysis of Geometrical Relationships and Friction Losses in Small-Diameter Lay-Flat Polyethylene Pipes. Journal of Irrigation and Drainage Engineering 142, 04015041. https://doi.org/10.1061/(ASCE)IR.1943-4774.0000958.

Pyne, R.D.G., 2005. Aquifer storage recovery: a guide to groundwater recharge through wells, 2nd ed. ed. ASR Systems, Gainesville, Florida.

Qi, W., Zhang, Z., Wang, C., Huang, M., 2021. Prediction of infiltration behaviors and evaluation of irrigation efficiency in clay loam soil under Moistube® irrigation. Agricultural Water Management 248, 106756. https://doi.org/10.1016/j.agwat.2021.106756.

Racz, A.J., Fisher, A.T., Schmidt, C.M., Lockwood, B.S., Los Huertos, M., 2012. Spatial and temporal infiltration dynamics during managed aquifer recharge. Ground Water 50, 562–570. https://doi.org/10.1111/j.1745-6584.2011.00875.x.

Ray, C., Jasperse, J., Grischek, T., 2011. Bank Filtration as Natural Filtration, in: Ray, C., Jain, R. (Eds.), Drinking Water Treatment: Focusing on Appropriate Technology and Sustainability, Strategies for Sustainability. Springer Netherlands, Dordrecht, pp. 93–158. https://doi.org/10.1007/978-94-007-1104-4_5.

Rebhann, M., Karatay, Y.N., Filler, G., Prochnow, A., 2016. Profitability of Management Systems on German Fenlands. Sustainability 8, 1103. https://doi.org/10.3390/su8111103.

Reischer, M., Christensen, A.G., De Weirdt, F., Bruns, S., Dideriksen, K., 2020. Capabilities of an optical direct push probe for 2D-subsurface imaging. Journal of Contaminant Hydrology 232, 103636. https://doi.org/10.1016/j.jconhyd.2020.103636

Richards, L.A., 2004. Capillary Conduction of Liquids Through Porous Mediums. Physics 1, 318–333. https://doi.org/10.1063/1.1745010.

Ringleb, J., Sallwey, J., Stefan, C., 2016. Assessment of Managed Aquifer Recharge through Modeling—A Review. Water 8, 579. https://doi.org/10.3390/w8120579.

Ritchie, H. and Roser, M., 2018. Water use and stress. OurWorldInData.org. ourworldindata.org/water-use-stress.

Rösch, C., Skarka, J., Raab, K., Stelzer, V., 2009. Energy production from grassland – Assessing the sustainability of different process chains under German conditions. Biomass and Bioenergy 33, 689–700. https://doi.org/10.1016/j.biombioe.2008.10.008.

Ross, A., 2022. Benefits and Costs of Managed Aquifer Recharge: Further Evidence. Water 14, 3257. https://doi.org/10.3390/w14203257.

Ross, A., 2021. Economic costs and benefits of Managed Aquifer Recharge Case Studies, in: Zheng, Y., Ross, A., Villholth, K.G. and Dillon, P. (Eds.). Managing Aquifer Recharge: A Showcase for Resilience and Sustainability. Paris, UNESCO. https://recharge.iah.org/ ISBN 978-1-3999-2814-4.

Ross, A., Hasnain, S., 2018. Factors affecting the cost of managed aquifer recharge (MAR) schemes. Sustain. Water Resour. Manag. 4, 179–190. https://doi.org/10.1007/s40899-017-0210-8.

Rossetto, R., Barbagli, A., De Filippis, G., Marchina, C., Vienken, T., Mazzanti, G., 2020. Importance of the Induced Recharge Term in Riverbank Filtration: Hydrodynamics, Hydrochemical, and Numerical Modelling Investigations. Hydrology 7, 96. https://doi.org/10.3390/hydrology7040096.

Russo, T.A., Fisher, A.T., Lockwood, B.S., 2015. Assessment of Managed Aquifer Recharge Site Suitability Using a GIS and Modeling. Groundwater 53, 389–400. https://doi.org/10.1111/gwat.12213.

Saey, T., Simpson, D., Vermeersch, H., Cockx, L., Van Meirvenne, M., 2009. Comparing the EM38DD and DUALEM-21S Sensors for Depth-to-Clay Mapping. Soil Science Society of America Journal 73, 7–12. https://doi.org/10.2136/sssaj2008.0079.

Salisu, A., Wayayok, A., Abdallah, A. F., & Kamal, R. M., 2021. Discharge Characterization and Variability Determination along Shorter Sections of Soaker Hose Pipe for Soil Column Experiment. Basrah Journal of Agricultural Sciences, 34, 92–99. https://doi.org/10.37077/25200860.2021.34.sp1.10.

Sales, N., Remédios, O., Arsenio, A., 2015. Wireless sensor and actuator system for smart irrigation on the cloud, in: 2015 IEEE 2nd World Forum on Internet of Things (WF-IoT). Presented at the 2015 IEEE 2nd World Forum on Internet of Things (WF-IoT), pp. 693–698. https://doi.org/10.1109/WF-IoT.2015.7389138.

Sasidharan, S., Bradford, S.A., Šimůnek, J., Kraemer, S.R., 2021. Comparison of recharge from drywells and infiltration basins: A modeling study. Journal of Hydrology 594, 125720. https://doi.org/10.1016/j.jhydrol.2020.125720.

Schijven, J., Berger, P., 2003. Removal of Pathogens, Surrogates, Indicators, and Toxins Using Riverbank Filtration. pp. 73–116. https://doi.org/10.1007/0-306-48154-5_7.

Schmidt, J., Rabiger-Völlmer, J., Werther, L., Werban, U., Dietrich, P., Berg, S., Ettel, P., Linzen, S., Stele, A., Schneider, B., & Zielhofer, C., 2019. 3D-Modelling of Charlemagne's Summit Canal (Southern Germany)—Merging Remote Sensing and Geoarchaeological Subsurface Data. Remote Sensing, 11(9), Article 9. https://doi.org/10.3390/rs11091111.

Schuetze, C., Vienken, T., Werban, U., Dietrich, P., Finizola, A., Leven, C., 2012. Joint application of geophysical methods and Direct Push-soil gas surveys for the improved delineation of buried fault zones. J. Appl. Geophys. 82. https://doi.org/10.1016/j.jappgeo.2012.03.002

Schulmeister, M. k., Butler Jr., J. j., Healey, J. m., Zheng, L., Wysocki, D. a., McCall, G. w., 2003. Direct-Push Electrical Conductivity Logging for High-Resolution Hydrostratigraphic Characterization. Groundwater Monitoring & Remediation 23, 52–62. https://doi.org/10.1111/j.1745-6592.2003.tb00683.x.

Seidl, C., Wheeler, S.A., Page, D., 2024. Understanding the global success criteria for managed aquifer recharge schemes. Journal of Hydrology 628, 130469. https://doi.org/10.1016/j.jhydrol.2023.130469.

Sellwood, S.M., Healey, J.M., Birk, S., Butler, J.J., 2005. Direct-push hydrostratigraphic profiling: coupling electrical logging and slug tests. Ground Water 43, 19–29. https://doi.org/10.1111/j.1745-6584.2005.tb02282.x.

Shan, V., Singh, S.K., Haritash, A.K., 2020. Water Crisis in the Asian Countries: Status and Future Trends, in: Kumar, M., Munoz-Arriola, F., Furumai, H., Chaminda, T. (Eds.), Resilience, Response, and Risk in Water Systems: Shifting Management and Natural Forcings Paradigms, Springer Transactions in Civil and Environmental Engineering. Springer, Singapore, pp. 173–194. https://doi.org/10.1007/978-981-15-4668-6_10.

Sharma, V., 2018. Methods and techniques for soil moisture monitoring. https://wyoextension.org/publications/html/B1331/ (accessed 11.10.23).

Silva, B.P.C., Tassinari, D., Silva, M.L.N., Silva, B.M., Curi, N., Rocha, H.R. da, 2021. Nonlinear models for soil moisture sensor calibration in tropical mountainous soils. Sci. agric. (Piracicaba, Braz.) 79, e20200253. https://doi.org/10.1590/1678-992X-2020-0253.

Silvis, H., Voskuilen, M., 2018. Agricultural land prices in the EU in 2016. Wageningen Economic Research. https://edepot.wur.nl/446327.

Simunek, J., Jirka, M., S., M., T.V.G., 2012. HYDRUS technical manual, version 2. Software Package for Simulating the Two-and Three-Dimensional Movement of Water, Heat and Multiple Solutes in Variably-Saturated Media.

Šimůnek, J., van Genuchten, M.Th., Šejna, M., 2016. Recent Developments and Applications of the HYDRUS Computer Software Packages. Vadose Zone Journal 15, vzj2016.04.0033. https://doi.org/10.2136/vzj2016.04.0033.

Siyal, A.A., van Genuchten, M.T., Skaggs, T.H., 2009. Performance of Pitcher Irrigation System. Soil Science 174, 312–320. https://doi.org/10.1097/SS.0b013e3181a97532.

Siyal, A.A., van Genuchten, M.Th., Skaggs, T.H., 2013. Solute transport in a loamy soil under subsurface porous clay pipe irrigation. Agricultural Water Management 121, 73–80. https://doi.org/10.1016/j.agwat.2013.01.005.

Skaggs, T.H., Trout, T.J., Rothfuss, Y., 2010. Drip Irrigation Water Distribution Patterns: Effects of Emitter Rate, Pulsing, and Antecedent Water. Soil Science Soc of Amer J 74, 1886–1896. https://doi.org/10.2136/sssaj2009.0341.

Sottani, A., Bertoldo, S., Campagnolo, F., Altissimo, L., Gusmaroli, G., Muraro, T., 2014. Esperienze di MAR con sistemi disperdenti a largo diametro: primo bilancio di attività sperimentali nell'alta pianura vicentina (Italia Settentrionale). Acque Sotterranee. https://doi.org/10.7343/AS-082-14-0108.

Sprenger, C., Hartog, N., Hernández, M., Vilanova, E., Grützmacher, G., Scheibler, F., Hannappel, S., 2017. Inventory of managed aquifer recharge sites in Europe: historical development, current situation and perspectives. Hydrogeol J 25, 1909–1922. https://doi.org/10.1007/s10040-017-1554-8.

Standen, K., Costa, L.R.D., Monteiro, J.-P., 2020. In-Channel Managed Aquifer Recharge: A Review of Current Development Worldwide and Future Potential in Europe. Water 12, 3099. https://doi.org/10.3390/w12113099.

Statistica, 2021. Prices for Tap Water in Selected Cities in the United States in 2021.

Swain, S., Taloor, A.K., Dhal, L., Sahoo, S., Al-Ansari, N., 2022. Impact of climate change on groundwater hydrology: a comprehensive review and current status of the Indian hydrogeology. Appl Water Sci 12, 120. https://doi.org/10.1007/s13201-022-01652-0.

Swamee, P.K., Mishra, G.C., Chahar, B.R., 2000. Design of minimum seepage loss canal sections. 6. J. Irrig. and Drain. Engrg., ASCE 126(1), 28-32.

Teeluck, M., & Sutton, B. G., 1998. Discharge characteristics of a porous pipe microirrigation lateral. Agricultural Water Management, 38(2), 123–134. Scopus. https://doi.org/10.1016/S0378-3774(98)00060-2.

Thompson, R.B., Gallardo, M., Valdez, L.C., Fernández, M.D., 2007. Using plant water status to define threshold values for irrigation management of vegetable crops using soil moisture sensors. Agricultural Water Management 88, 147–158. https://doi.org/10.1016/j.agwat.2006.10.007.

Topp, G.C., Davis, J.L., Annan, A.P., 1980. Electromagnetic determination of soil water content: Measurements in coaxial transmission lines. Water Resources Research 16, 574–582. https://doi.org/10.1029/WR016i003p00574.

Uhlemann, S., Ulrich, C., Newcomer, M., Fiske, P., Kim, J., Pope, J., 2022. 3D hydrogeophysical characterization of managed aquifer recharge basins. Frontiers in Earth Science 10.

Ulibarri, N., Escobedo Garcia, N., Nelson, R.L., Cravens, A.E., McCarty, R.J., 2021. Assessing the Feasibility of Managed Aquifer Recharge in California. Water Resources Research 57, e2020WR029292. https://doi.org/10.1029/2020WR029292

UN Water, 2022. Groundwater making the invisible visible, The United Nations world water development report. UNESCO, Paris.

UN-Water, 2018. Nature-based Solutions for Water 2018: The United Nations World Water Development Report 2018. https://wedocs.unep.org/20.500.11822/32857.

UN, 2015. Transforming Our World: The 2030 Agenda for Sustainable Development. Resolution Adopted by the General Assembly on 25 September 2015, 42809, 1-13.

Utom, A.U., 2019. Observation-Based Conceptual Site Modeling Framework Combining Surface Geophysical, Direct Push-Based, Hydrogeochemical and Stable Isotope Methods. https://doi.org/10.15496/publikation-30454.

Van Genuchten, M.Th., 1980. A Closed-form Equation for Predicting the Hydraulic Conductivity of Unsaturated Soils. Soil Science Society of America Journal 44, 892–898. https://doi.org/10.2136/sssaj1980.03615995004400050002x.

Vanderzalm, J., Dillon, P., Tapsuwan, S., Pickering, P., Arold, N., Bekele, E., Barry, K., Donn, M., Hepburn, P., McFarlane, D., 2015. Economics and experiences of managed aquifer recharge (MAR) with recycled water in Australia. Australian Water Recycling Centre of Excellence.

Vanderzalm, J., Page, D., Dillon, P., Gonzalez, D., Petheram, C., 2022. Assessing the costs of Managed Aquifer Recharge options to support agricultural development. Agricultural Water Management 263, 107437. https://doi.org/10.1016/j.agwat.2021.107437.

Verhegge, J., Delvoie, S., 2021. Direct push, in situ video imaging of buried prehistoric landscapes in soft soils: First results in the polders, coversands, and loess belt of Belgium. Geomorphology 373, 107483. https://doi.org/10.1016/j.geomorph.2020.107483

Vienken, T., Dietrich, P., 2011. Field evaluation of methods for determining hydraulic conductivity from grain size data. Journal of Hydrology - J HYDROL 400, 58–71. https://doi.org/10.1016/j.jhydrol.2011.01.022.

Vitharana, U.W.A., Van Meirvenne, M., Cockx, L., Bourgeois, J., 2006. Identifying potential management zones in a layered soil using several sources of ancillary information. Soil Use and Management 22, 405–413. https://doi.org/10.1111/j.1475-2743.2006.00052.x

Vogelgesang, J.A., Holt, N., Schilling, K.E., Gannon, M., Tassier-Surine, S., 2020. Using high-resolution electrical resistivity to estimate hydraulic conductivity and improve characterization of alluvial aquifers. Journal of Hydrology 580, 123992. https://doi.org/10.1016/j.jhydrol.2019.123992.

Vollmer, D., Harrison, I.J., 2021. H2O ≠ CO2: framing and responding to the global water crisis. Environ. Res. Lett. 16, 011005. https://doi.org/10.1088/1748-9326/abd6aa

Walters, D., 2019. North vs. South and farm vs. City conflicts continue to roil California's

water politics, San Diego, CA: Times of San Diego. Retrieved from https://timesofsandiego.com/politics/2019/05/18/north-south-and-farm-city-conflicts-continue-to-roil-californias-water-politics/.

Wang, C., Ye, J., Zhai, Y., Kurexi, W., Xing, D., Feng, G., Zhang, Q., Zhang, Z., 2023. Dynamics of Moistube discharge, soil-water redistribution and wetting morphology in response to regulated working pressure heads. Agricultural Water Management 282, 108285. https://doi.org/10.1016/j.agwat.2023.108285.

Wang, W., Zhao, J., Duan, L., 2021. Simulation of irrigation-induced groundwater recharge in an arid area of China. Hydrogeol J 29, 525–540. https://doi.org/10.1007/s10040-020-02270-3.

Wang, W., Zhou, Y., Sun, X., & Wang, W., 2014. Development of Managed Aquifer Recharge in China. Boletin Geologico y Minero, 125(2), 227-233.

White, C., 2014. Understanding water scarcity: Definitions and measurements. https://doi.org/10.22459/GW.05.2014.28

Wriedt, G., 2019. Grundwasserbericht Niedersachsen - Sonderausgabe zur Grundwasserstandssituation im Trockenjahr 2018. Niedersächsischer Landesbetrieb für Wasserwirtschaft, Küsten- und Naturschutz (NLWKN).

Zetland, D., 2021. The role of prices in managing water scarcity. Water Security 12, 100081. https://doi.org/10.1016/j.wasec.2020.100081.

Zhang, H., Xu, Y., Kanyerere, T., 2020. A review of the managed aquifer recharge: Historical development, current situation and perspectives. Physics and Chemistry of the Earth, Parts A/B/C, Integrated Water Resources Development and Management: Leaving No One Behind for Water Security in Eastern and Southern Africa. 118–119, 102887. https://doi.org/10.1016/j.pce.2020.102887.

Zhao, Z., Luo, N., Illman, W.A., 2023. Geostatistical analysis of high-resolution hydraulic conductivity estimates from the hydraulic profiling tool and integration with

hydraulic tomography at a highly heterogeneous field site. Journal of Hydrology 617, 129060. https://doi.org/10.1016/j.jhydrol.2023.129060.

Zheng, Y., Vanderzalm, J., Hartog, N., Escalante, E.F., Stefan, C., 2023. The 21st century water quality challenges for managed aquifer recharge: towards a risk-based regulatory approach. Hydrogeol J 31, 31–34. https://doi.org/10.1007/s10040-022-02543-z.